

An investigation into noble metal free catalysts for
diesel particulate filters using combinatorial
chemistry and high throughput technology

Dissertation

zur Erlangung des Grades des Doktors der Ingenieurwissenschaften
der Naturwissenschaftlich-Technischen Fakultät III
Chemie, Pharmazie, Bio- und Werkstoffwissenschaften
der Universität des Saarlandes

von

Dipl.-Ing. Kristina Pokorná

Saarbrücken

2008

Tag des Kolloquiums: 19.09.2008

Dekan: Prof. Dr. Uli Müller

Berichterstatter: Prof. Dr. Wilhelm F. Maier
Prof. Dr. Gerhard Wenz

“Knowing is not enough; we must apply.

Willing is not enough; we must do.”

JOHANN WOLFGANG von GOETHE

The present work has been accomplished at the Robert Bosch GmbH research center in Stuttgart, in Germany under the direction of Prof. Dr. W. F. Maier of the university Saarbrücken department of technical chemistry in Germany.

I wish to express special thanks to Prof. Dr. W. F. Maier for the opportunity to work on such an exciting research topic. I appreciate the freedom in working practices which he afforded me, the worthwhile discussions, and his excellent encouragement, as well as his helpful and thoughtful advice respectively.

I would like to thank Prof. Dr. G. Wenz for the kind acceptance of the supplementary report, for his time and interest in this work.

I thank Dr. J. Jockel for the opportunity to perform this research work at Robert Bosch GmbH and for providing excellent working conditions and his support.

I thank N. Olong for the cooperation and the sharing of our experiences. I would like to thank Prof. W. F. Maier's research working group for the helpful discussions of technical items. In addition to that, the group members showed me e.g. special sights of Saarbrücken and on the other hand I had the possibility to guide them through lovely Prague – we had a great time enjoying these events. This gave me a very close connection to the research group in spite of working mainly at a location which is not nearby.

The workshop at Robert Bosch GmbH built the reactor under the direction of J. Hülzinger. My thanks go to him for his support in technical design and practical knowledge. I also thank Dr. J. Scheidtmann for his technical support in terms of software questions during development of measurement setup.

At the university Saarbrücken I thank Dr. G. Frenzer for pore size analysis. I thank S. Tenhagen for performing the elemental analysis, H. Weis for the SEM micrographs and Dr. T. Köhler for the X-ray diffraction analysis at Robert Bosch GmbH. And I also thank Dr. M. Noyong for SEM micrographs and Dr. P. Müller for X-ray diffraction analysis at RWTH Aachen.

I would like to thank to all my colleagues in the chemical processes and technology department at Robert Bosch GmbH for their continual assistance, comfortable working atmosphere and good collaboration, especially to H. Potthast, H. Magenau and Dr. B. Cramer.

Finally I would like to heartily thank my parents and my sister Dagmar for their love and support. I wish also to thanks to Jens for his love and keeping me a good mood even in the most difficult moments. Last but not least my thanks go to all my friends for giving me motivation all the time.

ABSTRACT

This study is focused on combinatorial chemistry in order to prepare noble metal free catalysts for diesel particulate filters (DPF) and to test them using high throughput technology (HTT). Both methods play an important role in heterogeneous catalysis, since the impending stringent diesel emissions limits must be met and therefore the application of new catalytic coat for DPF is required. In this thesis three different syntheses were studied resulting in the sol-gel process using a commercially available pipetting robot, which is the most applicable for the catalysts' preparation. Composition spreads of Co, Ce and Mn based mixed oxide have been prepared and simultaneously tested for their relative activity by emissivity corrected infrared thermography (ecIRT), which is an efficient method to indicate potentially good catalyst candidates. The results have been confirmed by thermogravimetric and differential thermal analysis (TG-DTA). The combination of HTT and conventional measurement is excellent, since HTT is a fast method for the discovery and evaluation of soot combustion catalysts and the conventional measurement gives more precise information about the catalytic activity. From 250 prepared catalysts which were tested by ecIRT the compositions of Co/La, Ca/Mn and Ag/Ce were shown to be highly active with regards to soot oxidation. The proper determination by TG-DTA resulted in $\text{La}_5\text{Co}_{95}\text{O}_x$, $\text{Ca}_5\text{Mn}_{95}\text{O}_x$ and $\text{Ce}_y\text{Ag}_{100}\text{O}_x$ ($y = 45-55$) each reducing the combustion temperature to approx. 400 °C. All of these tests were conducted in loose contact mode in order to simulate practical conditions. The investigation of different soot deposition techniques results in the conclusion that contact between soot and catalyst is crucial in the catalytic soot oxidation.

ZUSAMMENFASSUNG

Das Hauptaugenmerk dieser Arbeit richtet sich auf die kombinatorische Chemie für die Herstellung von edelmetallfreien Katalysatoren für Dieselpartikelfilter (DPF) und das Testen dieser mittels Hochdurchsatz-Verfahren. Beide Methoden spielen eine wichtige Rolle in der heterogenen Katalyse, da die ständig verminderten Dieselemissionsgrenzen erreicht werden müssen und daher die Anwendung neuer katalytischer Beschichtungen für DPF erforderlich ist. In dieser Arbeit stellte sich von den drei untersuchten Präparationsmethoden der Sol-Gel Prozess für die Katalysatorherstellung als am geeignetsten heraus. Binärer composition spread von Mischoxiden auf Co-, Ce- und Mn-Basis wurden präpariert und parallel auf ihre katalytische Aktivität mittels emissivitätskorrigierter infrarot Thermographie (ecIRT) getestet. Dieses Hochdurchsatz-Verfahren ist sehr effizient um Katalysatoren mit hoher Aktivität schnell zu detektieren und wurde mittels Thermogravimetrie-Differenzthermoanalyse (TG-DTA) bestätigt. Die Kombination von Hochdurchsatz-Screening und konventioneller Untersuchung hat sich bewährt, da Hochdurchsatz-Screening ein sehr schnelles Verfahren für die Entdeckung und Evaluierung von Rußverbrennungs-Katalysatoren ist. Dagegen liefert die konventionelle Messung genauere Informationen hinsichtlich der katalytischen Aktivität. Von den 250 getesteten Katalysatoren weisen Mischoxide von Co/La, Ca/Mn und Ag/Ce hohe Aktivität bei der Rußoxidation auf. $\text{La}_5\text{Co}_{95}\text{O}_x$, $\text{Ca}_5\text{Mn}_{95}\text{O}_x$ und $\text{Ce}_y\text{Ag}_{100}\text{O}_x$ ($y = 45-55$) senken die Verbrennungstemperatur bis auf ca. 400 °C. Um praktische Bedingungen zu simulieren wurden alle Versuche in „loose“ Kontakt durchgeführt. Die Untersuchungen von unterschiedlichen Rußablage-Verfahren haben gezeigt, dass der Kontakt zwischen Ruß und Katalysator für die katalytische Rußoxidation entscheidend ist.

Content

1. Introduction.....	1
1.1 Diesel emission	1
1.1.1 Diesel particulate matter	2
1.1.2 DPM size distribution	3
1.1.3 Health effect of diesel particulate matter	6
1.1.4 Legislation	7
1.2 Reduction of diesel particulate matter	8
1.3 Mechanism of catalytic soot oxidation	9
1.4 Catalyst coated DPF.....	12
1.4.1 Catalysts containing base metals	13
1.4.2 Catalysts containing noble metals.....	18
1.5 Combinatorial approach in automotive exhaust aftertreatment.....	20
1.6 Sol-gel process.....	22
2. Scientific objective	27
3. Results and discussions.....	29
3.1 IR thermography setup.....	29
3.1.1 Reactor design.....	29
3.1.2 Reactor setup.....	30
3.1.3 Reactor flow profile	34
3.1.4 Reactor temperature profile	36
3.2 Synthesis evaluation	38
3.2.1 Paste synthesis	38
3.2.2 Impregnation.....	41
3.2.3 Sol-gel synthesis	41
3.2.4 Discussion.....	42
3.3 High throughput technology	43
3.3.1 Automated soot deposition	43
3.3.2 Soot and catalyst mixture by spatula	45

3.3.3	Evaluation of high throughput technology	48
3.3.4	Discussion.....	50
3.4	Characterization of alumina support.....	51
3.4.1	Pore structure and surface area	52
3.4.2	X-ray diffraction analysis	54
3.4.3	Structure characteristics.....	55
3.4.4	Concentration influence on combustion temperature.....	57
3.4.5	Elemental composition of catalyst.....	59
3.4.6	Discussion.....	61
3.5	Soot characterization.....	62
3.6	High throughput design of experiments.....	64
3.6.1	Synthesis design.....	64
3.6.2	Screening design.....	65
3.7	Catalysts development	68
3.7.1	Ce, Mn and Co based catalysts	68
3.7.2	Pt doped binary catalysts	74
3.7.3	Discussion.....	77
3.8	Catalysts characterization	78
3.8.1	Catalysts deactivation	78
3.8.2	X-ray diffraction analysis and structure characteristics.....	81
3.8.3	Discussion.....	87
4.	Experimental setup	89
4.1	High throughput screening of catalysts	89
4.1.1	IR thermography setup.....	89
4.1.2	Test procedure.....	94
4.1.3	Soot coating system	95
4.2	Thermogravimetric and differential thermal analysis.....	97
4.3	Preparation methods of catalysts	100
4.3.1	Sol-gel synthesis	100
4.3.2	Impregnation.....	103
4.3.3	Paste synthesis	105
4.4	Characterization methods	107
4.4.1	Catalysts deactivation	107

4.4.2	Inductively coupled plasma optical emission spectrometry	107
4.4.3	X-ray diffraction analysis	108
4.4.4	Specific surface area determination	108
4.4.5	Ultra fine particle analyzer	108
4.4.6	Rheological properties determination	109
5.	Summary and outlook	111
5.1	Summary	111
5.2	Outlook	115
6.	Bibliography	117
7.	Appendix	134
7.1	Nomenclature	134
7.2	Chemical list	136
7.3	Compound composition	137
7.4	SEM micrographs	141

Chapter 1

1. Introduction

1.1 Diesel emission

The high performance of diesel cars associated with their low revolutions and high torque leads to enjoyable driving, and makes diesel passenger cars very attractive. The fuel economy and the durability of diesel engines also contribute to their advantages compared to gasoline cars, and the diesel car market increases continuously. For instance, in 2000 diesel passenger cars accounted for over 30% of the European Union market, compared to only about 15% in the previous year [1]. Diesel engines are used world-wide, and thus belong to an important transport sector, including trucks, buses and ships. Diesel exhaust emissions have therefore become more important and their environmental and health effects have attracted attention. Diesel fuel is a mixture of HCs and produces CO₂ and water vapor during complete ideal fuel combustion (Equation 1.1).



CO₂ is indeed a nontoxic gas to human beings, however it contributes to the green house effect. Diesel pollutants are formed when incomplete fuel combustion occurs, including carbon monoxide (CO), unburned hydrocarbons (HC), nitrogen oxide (NO_x) and particulate matter (PM), also referred to as diesel particulate matter (DPM). Their concentration depends on the engine operation and fuel composition. In particular two diesel pollutants PM and NO_x are the most harmful and therefore emissions control technologies are focused on these in order to meet increasingly strict emissions limits.

Diesel engines operate by injecting fuel into a cylinder filled with high temperature compressed air achieving high combustion temperatures, which are responsible for the thermal formation of NO_x. In contrast, the uneven air-to-fuel mixture which is

dependent on current conditions results in the formation of PM. When NO_x emissions are reduced in the engine cylinder, the particulate emissions increase and vice versa. This effect is referred to as the NO_x –PM trade-off which is illustrated in Figure 1.1. NO_x emissions are higher than those from gasoline engines equipped with a three-way catalyst (TWC) but lower than gasoline emissions when no catalyst is used. However, the real drawback of diesel engines is PM emission formation, which is negligible in gasoline engines.

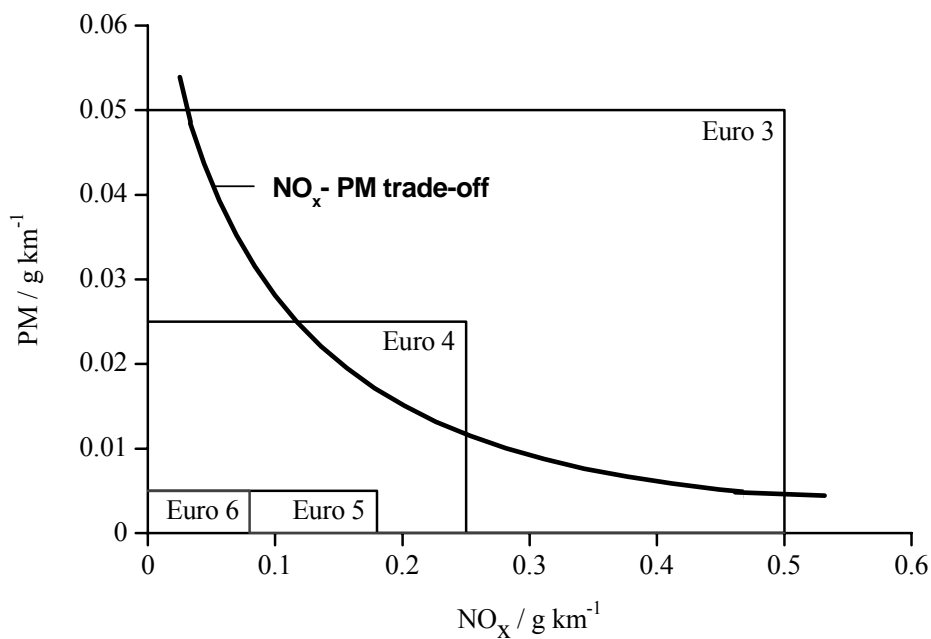


Figure 1.1 Effect of NO_x – PM trade-off and emission control for diesel engines. From [2]

1.1.1 Diesel particulate matter

DPM is a very complex diesel pollutant consisting of solid and liquid substances. Their formation, chemical characteristics and human health effects are not completely understood. The different combustion conditions, fuel quality, loss of oil control and cold starts all result in PM formation.

The composition of DPM is depicted in Figure 1.2. The DPM is subdivided into solid fraction (SF), soluble organic fraction (SOF) including HCs and finally SO_4^{2-} containing H_2SO_4 and H_2O . The main elements present in the solid fraction of PM are elemental carbon and ash, which includes several components. The carbonaceous matter is produced during the heterogeneous combustion process in the engine. The primary carbon particles are nearly spherical in shape, and agglomerate into chain-like structures with undefined shape and diameter. HCs are derived from engine lubricating oil and from fuel adsorbing onto the carbon surface which oxidizes to CO_2 and H_2O , or forms aldehydes or ketones.

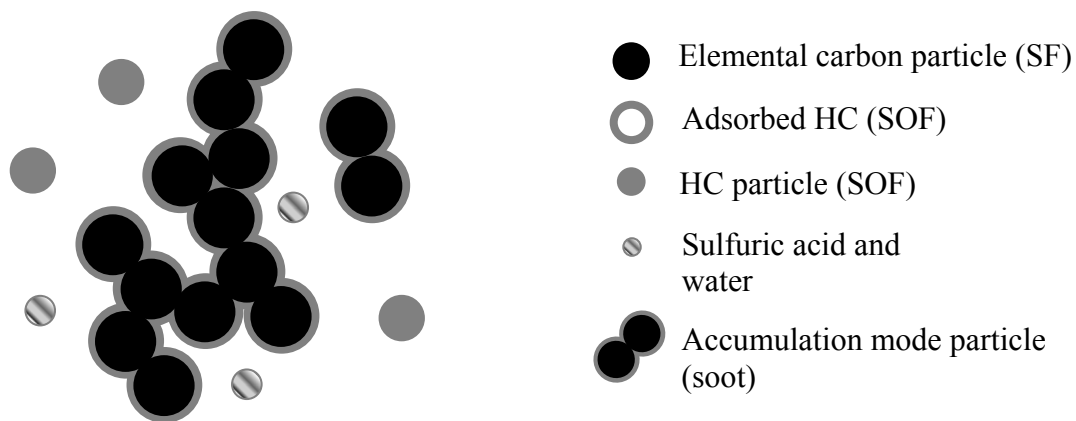


Figure 1.2 Schematic of DPM composition. From [2]

Due to the presence of S in the fuel and in lube oil, SO_4^{2-} formation occurs. The composition of PM varies depending on the combustion process, the condition of the engine operation, on the composition of the fuel used, which may differ in S content. For instance Ålander and coworkers [3] showed that the diesel particles produced were considerably affected by the fuel composition and engine operation.

1.1.2 DPM size distribution

The permanent development of various aftertreatment technologies such as particulate traps, oxidation catalyst converters or exhaust gas recirculation (EGR), and the development of engines with high pressure injection or turbo-charging systems have

contributed to the reduction of PM emissions [4]. While efficient diesel engines and after treatments result in the reduction of diesel particulate mass, the number of nanoparticles, however, is increased [5, 6].

The DPM have a typical bimodal size distribution including the nuclei mode and accumulation mode. The nuclei mode is the beginning of the particulate formation followed by agglomeration of the nuclei particles. The most common particles are found in the nuclei mode of low mass, while on the other hand most of the particle mass is found in the accumulation mode, which includes lower numbers of particles (Figure 1.3). The coarse mode is a small fraction of diesel particles above 1 μm in diameter, containing up to 20% of the total mass but nearly no particle number [6]. In contrast more than 90% of the total particles are in nuclei mode, but these only account for less than 10% of the particle mass [6].

The diesel particle size distribution depends for instance on engine operation parameters and fuel aftertreatment design, as well as on other factors such as environmental conditions. The PM size is divided into nanoparticles below 50 nm diameter, ultrafine particles up to 100 nm and fine particles less than 2.5 μm diameter. Ålander et al. [3] determined the particle size distribution between 10 and 480 nm depended on engine operation parameters, engine type and fuel reformulation. Virtanen et al. [7] found that the quantity of diesel particles and their structure is affected by engine load. Kim et al. [8] analyzed particle size distribution from different light and heavy-duty diesel engines, and while both exhibit similar particle size distribution, the heavy-duty engines emitted much higher PM amount. About 70% of particles produced by the light-duty diesel engines and heavy-duty engines equipped with turbo charger were less than 100 nm in size.

The DPM concentration in the atmosphere varies according to location, for instance urban areas with high traffic density feature higher than average DPM exposure. Particle size distribution and DPM concentration at different locations in a tunnel and in the ambient air was analyzed by Sturm and coworkers [9]. The team demonstrated that the PM concentration and the particle size distribution, as a function of time of travel and day of the week (working days, weekend) were strongly affected by traffic density.

The particle size distribution in the tunnel approached that of ambient air as the traffic volume in the tunnel decreased. Conversely increased traffic led to particle size distribution changes due to coagulation of the ultrafine particles. Fewer particles of nucleation mode were detected in the urban background compared to the roadside. The diesel particle size distribution is depicted in Figure 1.3. Particles of a diameter below $10\ \mu\text{m}$ are so-called PM_{10} , those smaller than $2.5\ \mu\text{m}$ are fine particles also referred to as $\text{PM}_{2.5}$, particles of a diameter below $100\ \text{nm}$ are ultrafine particles, and nanoparticles are characterized by a diameter of less than $50\ \text{nm}$.

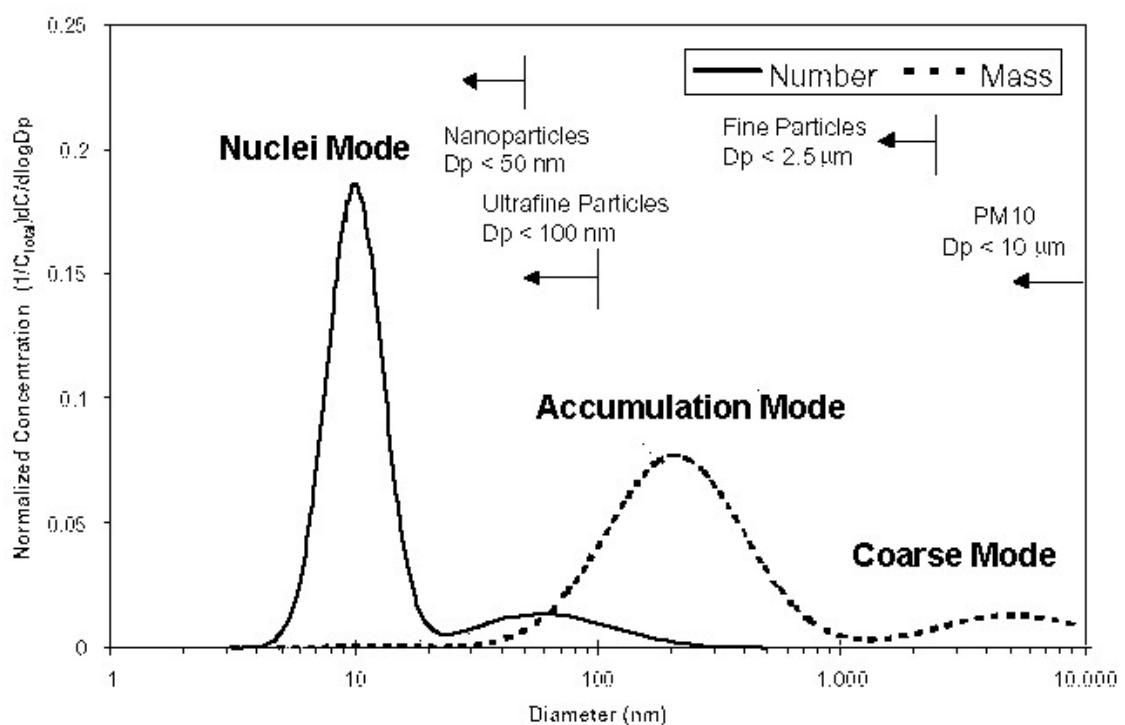


Figure 1.3 Diesel particle size distribution. From [6]

The formation of diesel particles is highly affected by the temperature in the combustion chamber. Mathis et al. [10] described how the diameter of primary diesel particles decreased with increased flame temperature of diesel fuel. The authors also studied the influence of injection pressure (IP) on primary soot particles and found that increased IP did not increase the primary particle diameter, but a decrease in particle size with increased IP was observed. The IP also has a significant influence on particle concentration. For example, changing the pressure from 500 to 1400 bar caused an estimated tenfold drop in particle numbers. Direct injection engines produce less PM

emissions in comparison to indirect injection engines and besides for direct injection engines particle mass distribution shows maximum at higher particle size [11].

1.1.3 Health effect of diesel particulate matter

Variation in the particle size and composition of the DPM have become more important due to their effects on human health, in ways which are not yet well understood. Other non-diesel particles of similar size are also present in the environment, making it difficult to determine which particles are causing any given effect on health. The well-known and widely studied compounds forming toxic gases contained in diesel engine exhausts are CO, NO, NO₂ and SO₂. The DPM contains several compounds, which may also cause harm to human health, even though their quantities are small. For instance many aldehydes are toxic and some of them, such as formaldehydes, are classified as carcinogens.

The penetration of particles into human respiratory tracts is dependent on particle size. The smaller the particles the more likely they are to penetrate deeper into the respiratory system, and the interaction of small particles with cells in the lung is more likely than with larger particles. Smaller particles are also present in higher numbers, although their total mass is lower, and some researchers believe that the majority of toxicity is caused by ultrafine particles [12]. Nemmar et al. [13] reported ultrafine carbon particles that may diffuse into the systemic circulation creating particle translocation from the lungs into the blood followed by its distribution to other parts of the body. The ultrafine particles may also target the central nervous system as reported by Oberdörster et al. [14].

The inhalation effect of ultrafine particles was investigated with laboratory animals such as mice and rats [15] and demonstrated that ultrafine particles of carbon black caused cancer in rats. Animal studies of the carcinogen effect of diesel particulates are summarized by the National institute for occupational safety and health (NIOSCH) [16] and draw conclusion that animals exhibit lung symptoms such as inflammation and fibrosis at high diesel particle concentration following extended exposure. Somer et al. [17] demonstrated that air pollution exposure added to heritable mutations

in mice. These findings contribute to evidence that PM may exhibit both a genetic and a higher disease risk to humans.

1.1.4 Legislation

Air pollution legislation began in 1967 with the Clean Air Act (CAA) introduced in the USA [18]. Emission standards, based on tailpipe emissions from gasoline passenger cars, were introduced first, which resulted in the application and development of catalyst technologies for treatment of gasoline passenger car emissions.

Emission limits have been established worldwide for more than two decades in the United States, the European Union (EU), and several other countries, in order to reduce diesel pollutants due to their severe effects on human health and the environment. The EU emission standards for diesel passenger cars are summarized in Table 1.1. To meet such stringent future emission limits, the additional application of diesel particulate emission control is essential. The diesel particulate filter (DPF) is one of the required methods of trapping the soot, and thereby reducing the diesel particulates emission and the associated risks.

Table 1.1 EU emission standards for diesel passenger cars (g km^{-1}). From [19]

	Date	CO	HC + NO _x	NO _x	PM
Euro 1	07/ 1992	2.72	0.97	-	0.14
Euro 2	01/ 1996	1.00	0.90	-	0.10
Euro 3	01/ 2000	0.64	0.56	0.50	0.05
Euro 4	01/ 2005	0.50	0.30	0.25	0.025
Euro 5*	09/ 2009	0.50	0.23	0.18	0.005
Euro 6*	09/ 2014	0.50	0.17	0.08	0.005

* proposed

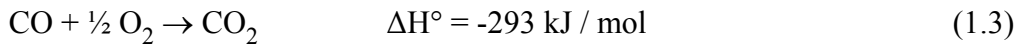
1.2 Reduction of diesel particulate matter

Initially, engine technologies, improved fuel content and properties, charge air control and lube oil consumption were studied in order to reduce the diesel emissions. Diesel exhaust particulates are trapped by DPF. The requirements for diesel filter material are high filtration efficiency, use of high operating temperature, high soot load capacity, low thermal expansion, resistance to thermal shock, low pressure drop, chemical stability, long life, low weight and low cost.

Wall-flow monoliths are the most common trap of diesel filter substrate and consist of numerous parallel channels like honeycombs, which are open on one side and plugged on the other alternately in order to force the diesel exhaust flow through the walls of the channels. The monoliths are made of a porous ceramic such as cordierite or SiC. Cordierite is composed of Si, Al and Mg oxide ($2\text{MgO}-2\text{Al}_2\text{O}_3-5\text{SiO}_2$) and it is characterized by low cost, by a low thermal expansion coefficient, and exhibits good mechanical strength. In contrast SiC exhibits high thermal expansion, long term thermal durability and higher cost. However, SiC features lower pressure drop at even higher quantities of trapped soot in comparison to cordierite [20, 21].

The mechanism of soot collection is based on the combination of surface filtration also referred to as cake filtration, and of a deep-bed filtration in these channel walls. This type of deep filtration features low efficiency and low pressure drop. During the surface filtration a layer of soot is accumulated inside the open inlet channels resulting in high efficiency and also the pressure drop rises in the filter as the soot layer increases. Diesel filters exhibit high filtration efficiencies for the solid fractions of diesel particulates of between 95% and 99.9% depending on the wall thickness and mean pore diameter. However the maximum soot collection is usually limited by the high temperatures occurring during uncontrolled regeneration. Different materials feature different temperatures during uncontrolled regeneration at the same soot loadings [22]. In any case the temperature is limited by the maximum soot loading and the increased load results in a temperature rise. With the increasing filter soot load the pressure drop rises and causes higher fuel consumption. Reducing the pressure drop may have consequences on the engine operation, the trapped soot has to be removed by a process

known as filter regeneration, to restore the filter capacity. The regeneration is done by oxidizing captured soot. The carbon is oxidized sequentially as shown in Equations 1.2 and 1.3 and the reactions take place at the carbon surface. The rate of oxidation is limited by the kinetics, with a slower soot oxidation rate at lower temperatures [23].



The soot is oxidized at temperatures of about 600 °C quickly and completely. The thermal oxidation of carbon by oxygen has been widely studied whereas the reaction mechanism was proposed by Moulijn research group [24, 25]. The oxidation rate changes with the soot amount, at the beginning when the soot mass is higher the oxidation rate is higher and with the soot mass decrease the oxidation rate declines. The diesel filter is regenerated faster when the soot loading is higher however the pressure drop increases.

1.3 Mechanism of catalytic soot oxidation

The mechanism of catalytic soot oxidation is not completely understood. Two mechanisms at the atomic scale have been proposed. On the one hand the electron transfer [26], which has never been experimentally confirmed and on the other hand the oxygen transfer proposed earlier by Neumann and coworkers [27] and accepted as being a general mechanism for the catalytic carbon oxidation [28]. In the first case the theory is based on a redistribution of π electrons in the carbon sheet which are thus more susceptible to oxidation in contrast to the oxygen transfer based on redox mechanism.

Most catalysts required physical contact with the carbon, resulting in acceleration of oxidation. There are two modes of catalytic oxidation mechanism, channeling and edge recession [29], represented in Figure 1.4, however the second mechanism uses the catalyst most efficient [30]. A distinction is drawn between monolayer channeling through a single graphite layer and deep channeling through multiple carbon sheets. Whichever channeling mode takes place depends on the rate-limiting step during

oxidation and also varies between different catalysts [31]. The catalyst affects the mode which depends on the interaction between catalyst and the carbon edge atom [30].

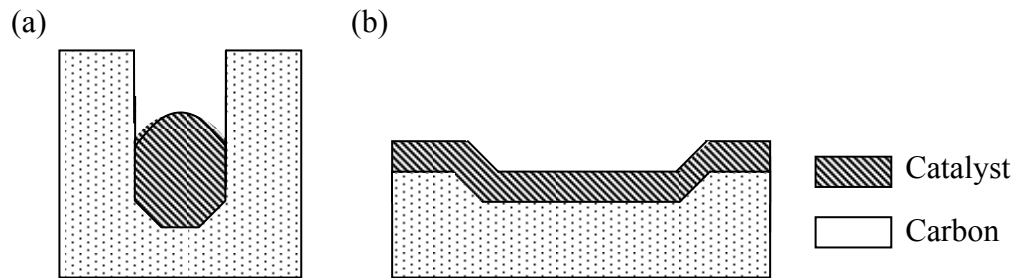


Figure 1.4 Catalytic attacks on carbon sheets; channeling (a) and edge recession (b). From Setten [32]

It was confirmed by several authors that the contact is of critical importance in the catalytic soot combustion [33-35]. The contact occurs in the gas phase between gas molecules and the active center of a solid catalyst. The addition of catalysts to fuel, referred to as soluble catalysts, provides better contact between the catalysts, whereas the mechanism of regeneration of particulate filters is similar to that of catalyst coated filters. Many studies determined different catalytic fuel additives such as Ce, Fe and Cu [36, 37], but there is still little known about the interaction between the additives and diesel particulates and the mechanism is not yet understood, whereas only few studies have used additive doped fuel to investigate the oxidation of soot collected from diesel engines [38, 39]. A review of metal additives is given by Howard and Kausch [40]. The authors described three mechanisms using alkali or alkaline earth additives which form ions. In the first mechanism the so-called ionic mechanism, the nucleation or coagulation rate of soot decreases or smaller particle size distribution is obtained resulting in faster burn out. In the second mechanism the soot precursors are removed by formed hydroxyl radicals and the last mechanism is an acceleration of the oxidation rate at a late phase of the soot formation process.

The synergetic effect of a Pt additive in a combination of Ce, Cu, Fe additives was analyzed by Jelles and coworkers [41] using Pt impregnated filters. The authors observed a reduction of combustion temperature up to approx. 330 °C, when Pt/Ce fuel additives were utilized in the following procedure. The Pt coated onto monolith substrate oxidizes NO to NO₂ which subsequently reacts with the catalyzed soot from

the Pt/Ce fuel additives. The enhanced catalytic oxidation was caused by what is assumed to be multiple NO_x reactions. The postulated reaction scheme of the oxidation mechanism of soot using Pt/Ce fuel additives is shown in Figure 1.5. It has to be noticed that the Pt catalyst is only effective when NO is present in the gas phase.

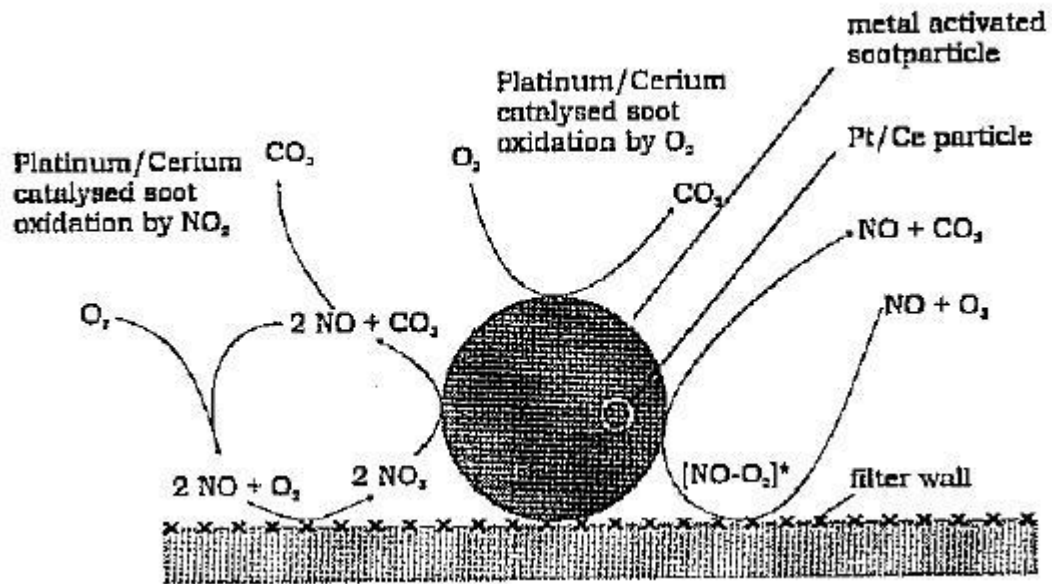


Figure 1.5 Oxidation mechanism of soot in the presence of NO_x and O_2 catalyzed by Pt/Ce fuel additives. From Jelles [41]

Although the regeneration method using fuel additives is effective the metal is emitted from the engine in the form of a metal oxide referred to as ash. This accumulates on the filter contributing to an increase of pressure drop. However this process needs an additional additive tank and a control unit to dose the quantity resulting in a more complex and expensive system.

Studies on catalysts' mobility were performed in relation to carbon and graphite oxidation. Early studies of Baker [42] showed the Fe particles become mobile on the graphite surface investigated by controlled atmosphere electron microscopy. Later, Baker [43, 44] observed the mobility of particles at the nanoscale (10nm) of different metals and oxides in the oxidation of graphite. He discovered a correlation with the melting point of the respective material studied, as depicted in Figure 1.6. The temperature at which the mobility of catalyst particles was determined corresponds to the Tammann temperature of the materials, approx. the half bulk melting point. Also

other scientists like McKee and coworkers found low combustion temperatures to be associated with low melting points of the catalysts.

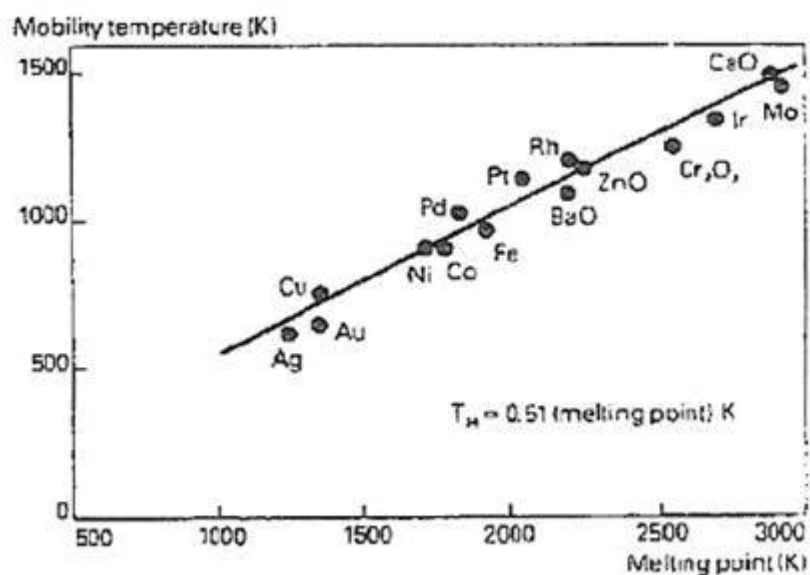


Figure 1.6 Relationship between mobility temperature and bulk melting point, particles of 10 nm supported on graphite. From Baker [44]

1.4 Catalyst coated DPF

There are several catalyst application technologies for the oxidation of soot in diesel exhaust, such as catalytic coatings or catalytic fuel additives. The regeneration of diesel particle filters is usually performed by coating the monolithic wall-flow substrate with a catalyst. In the 1980s catalyst coated filters were developed with their commercial implementation in Mercedes cars sold in California in 1985 [45]. The catalyst should be characterized by life durability, high activity and selectivity, thermal stability, resistance to S poisoning, high surface area, no formation of secondary emissions, no interaction with the filter material and low cost.

The soot is oxidized at temperatures of about 600 °C while the exhaust gas only reaches temperatures up to 400 °C depending on the driving conditions and engines. Such low exhaust temperatures, in some cases below 300 °C [46], are insufficient to oxidize the trapped diesel soot. The main objective of this catalyst is DPM oxidation under exhaust gas temperatures. A number of soot oxidation catalysts have been studied and

developed which can be classified into noble and base metal groups, as described in the following paragraphs.

Most studies on catalytic soot oxidation were executed on a laboratory scale, and the direct comparison of the catalytic activities between studies is difficult, as the experimental conditions vary greatly from each other. It is challenging to simulate in model studies the conditions which occur in particulate traps such as the composition of soot and diesel exhaust, gas flow rate and deposition of particulates on the catalyst layer. Care must be taken when comparing catalytic activities between studies since their definition varies. For instance, the catalytic activity can be expressed as temperature T_{ign} which is the soot ignition temperature, or as temperature T_{50} at which 50% of the soot is converted, or as T_f or T_m . T_f represents the temperature at which the soot combustion is completed and T_m is defined as a temperature of the maximum in the DTA curve. Also the catalyst to soot ratio, the carbon material selection, and oxygen concentration are important factors significantly affecting the catalytic activity.

The contact between soot and catalyst is one of the most important parameters in soot oxidation and it is critical for the reaction rate, depending mainly on the surface characteristics of the catalyst layer. Neeft [47] and van Setten [48] classified the contact between catalyst and soot into “loose” and “tight”. Loose contact mode is defined by mixing the catalyst and soot by spatula, shaking the mixture in a bottle, trapping the soot on catalytic filters or the catalytic filter is dipped into soot dispersion. Conversely, tight contact mode is achieved by the mechanical milling of the catalyst and soot mixture. Under practical conditions in a diesel particulate filter the loose contact mode is present.

1.4.1 Catalysts containing base metals

A number of studies of base metal as single and multi-compound catalysts also combined with noble metal for the soot and graphite oxidation have been carried out. The base metals, in comparison to noble metals, feature lower activity in promoting filter regeneration and are less active for the oxidation of CO and HC. On the other hand their advantages are that there is no formation of sulfate particulate and low cost.

McKee [49, 50] studied the catalytic activity of numerous metal oxides for the oxidation of graphite by thermogravimetric analysis (TGA) and explained the catalytic activity based on the heat formation of the redox reactions. He found PbO was the most active metal oxide investigated. 0.5 wt% of V₂O₅ decreased the ignition temperature by about 250 °C and oxides of Mn and Co were also active catalysts for the combustion of graphite.

Neeft and coworkers [34, 35] studied catalytic activity of various metal oxides in tight and loose contact mode and found Co₃O₄, V₂O₅, Fe₂O₃, La₂O₃ and MnO₂ were highly active in tight contact but exhibited hardly any activity in loose contact with soot, compared to MoO₃, which showed activity in loose contact similar to the activity in tight contact.

Ahlström and Odenbrandt [51] dispersed catalytic material on γ -Al₂O₃ and found high activity for V₂O₅ at higher temperatures and also for CuO, MnO₂, Cr₂O₃, Ag and Pt at relatively low temperatures, whereas oxides of Co, Fe, Mo and Pb showed hardly any activity for the combustion of diesel soot. Furthermore the activity of Ag, Pt, MnO₂ and CuO decreased by SiO₂ deactivation. V₂O₅ was the most active catalyst with the highest combustion rate, expressed as a ratio between the combustion rate in the presence of the catalyst and the mixture of soot and Al₂O₃.

Hoffman and Rieckmann [52] studied the combustion rates of several metal oxides coated by the impregnation method onto different filter materials and reported that V₂O₅ is the most active catalyst when coated with any combination of all tested filter materials with the exception of Al₂O₃ and sintered ceramic named as Ind (63% SiO₂, 30% Al₂O₃, 1% TiO₂, 2% K₂O and other oxide of amount < 1%), whereas in both cases Cu oxide showed to be most active when coated on these filter materials. Oxides of Ca and Zn also exhibited high catalytic activity. The authors confirm that the soot oxidation activity is more strongly affected by the filter material and the performance of the filter than by the catalytic materials.

Van Doorn et al. [53] studied the influence of several support materials on the soot combustion and found La₂O₃, CeO₂ and V₂O₅ to be active soot oxidation catalysts whereas Al₂O₃ and SiO₂ showed no catalytic effect. The activity of La₂O₃ and V₂O₅ did

not change even after SO₂ poisoning in contrast to CeO₂, which was deactivated. McKee [54] interpreted the high activity of V₂O₅ as being due to the high mobility of the V species associated with a low melting point (690 °C). Ahlström and Odenbrand [55] combined V₂O₅ with CuO and found their optimal catalytic activity at a molar ratio of 9:1. The addition of small amounts of Pt 0.01 wt% contributed to a further increase in catalytic soot combustion. However, no rise in catalytic activity was measured when the Pt content was above 0.1 wt%, indicative of special dispersion effects.

The influence of different loadings of V₂O₅ and MoO₃ on catalytic activity and CO₂ selectivity was investigated by Leocadio et al. [56]. The catalysts were deposited onto Al₂O₃ by thermal spreading and the results show that the catalytic soot combustion decreased by 60 °C with an increased quantity of Mo compared to non catalyzed soot combustion. MoO₃ features higher CO₂ selectivity, 75%, compared to V₂O₅, exhibiting 57%, and to a non-catalyzed sample exhibiting CO₂ selectivity of only 30%. The authors described the reaction path of Mo and V oxide related to redox mechanism.

Ciambelli and coworkers [57, 58, 33, 59-61] studied intensively the combination of Cu/K/V and reduced the combustion temperature by 300 °C compared to non catalytic soot combustion. The same combination of Cu, K and V was also examined by Badini et al. [62] and by Serra et al. [63]. The authors reported the rising K content in the catalyst composition increased the catalytic activity and the most active catalyst Cu/K/V at atomic ratio of 2:2:1 decreased the combustion temperature by 230 °C. The activity was expressed as peak combustion temperature. All authors used Cu and K chlorine precursors to prepare a catalyst, α -Al₂O₃ was then impregnated with this catalyst. Also the combination of Cu/K/Mo/Cl catalysts exhibited high catalytic activity reported by Moulijn's research group [64, 65]. The high activity of these catalysts is likely according to volatile compounds contained in the composition. The authors found that the loss of the catalysts' mass caused a decrease in catalytic activity.

Neri and coworkers [66] studied V oxide promoted with alkali chloride and several metal chlorides supported on Al₂O₃. The temperature T_{ox} was expressed as a temperature at the maximum of CO₂ formation. The most active catalyst was Cu/K/V showing a soot combustion temperature of about 300 °C while pure V oxide exhibited

a higher combustion temperature by 200 °C. The authors suggested that the activity correlated with their reducibility.

Ce oxide with oxygen storage capacity (OSC) is known to be active in soot combustion [67] and is used as a promoter of exhaust catalysts [68]. However when treated with S its storage properties are deactivated [69, 70] due to the formation of bulk sulfates, mainly at temperatures above 200 °C in the presence of O₂ [71]. According to Flouty and coworkers the resistance to S poisoning can be improved by the addition of Mo to Ce oxide [69]. These authors studied the combination of Mo/Ce at various atomic ratios and found that only a low Mo loading showed high catalytic activity for soot oxidation in the range between 400 and 450 °C and 100% CO₂ selectivity. Also Tikhomirov et al. [72] investigated various molar ratios of MnO_x-CeO₂ mixed oxides. The catalytic activity of these mixtures does not significantly differ, however the soot oxidation temperature was found to be lower than for the individual metal oxide indicating their synergetic effect. Conversely K doped Ce promoted the catalytic activity of soot oxidation [73]. The authors found the optimum K content to be about 7 wt% showing catalytic activity at 369 °C. The further addition of Ba, a known catalyst for NO_x storage capacity, to K/Ce did not effectively increase the catalytic activity, which was extensively studied in TWC by Fridell et al. [74-76].

The combinations of Co and K supported on Mg, La and Ce oxide have been widely studied by Querini and coworkers [77, 73, 78-80]. The authors found Co/K/CeO₂ and K/CeO₂ to be the most active catalysts oxidizing soot at temperatures lower than 400 °C while the combination of K/MgO was inactive for soot combustion. Co supported on MgO exhibited high activity for soot oxidation however the addition of K notably increases the activity and its optimum loading was found to be 4.5 wt%. Higher K content caused a decrease of catalytic activity in this composition. K also promotes the activity of ZrO₂ supported Cu catalyst [81]. While K up to 1.1 wt% increases the catalytic activity for soot oxidation significantly, its higher content enhances the activity only slightly. The same observation was confirmed by McGinn's research group [82]. The authors studied K/Cu catalysts and found that the onset temperature decreases with increased K content and is relatively constant after any further rise in K content. Also Milt et al. [83] examined different K loadings but supported on La₂O₃ and found the maximum combustion rates between 350 and 400 °C to be determined by temperature

programmed oxidation (TPO). The catalytic activity rose with increased K content. However 10 wt% of K shifted the activity to higher temperatures. The authors demonstrated that the soot combustion is affected by the catalyst ratio. Yuan and coworkers [84] found that K increases the catalytic activity for the soot combustion over TiO₂ supported Cu catalyst due to its interaction with the support resulting in the reduction of sintering of small TiO₂ particles and thereby increasing the surface area of the catalyst.

Saracco, Badini and coworkers [85, 86] studied several catalysts based on potassium vanadate combined with alkali chlorides supported on α -Al₂O₃. The CsCl-KVO₃ catalyst showed the highest activity whereas the RbCl-KVO₃ material exhibited the best thermal stability in contrast to CsVO₃-KCl catalyst which featured the relatively high activity in combination with high stability. The process involved the formation of eutectic liquids that enable better surface migration contact between catalyst and soot than between two solids. McKee [54, 87] had already shown that the eutectic phase provided good contact between the catalyst and carbon. The low melting eutectics of the alkali halides showed higher catalytic activity toward graphite oxidation in comparison to pure salt components. Saracco et al. [88] studied single vanadate as well as pyrovanadates of K and Cs and found that Cs₄V₂O₇ was already exhibiting high catalytic activity at about 300 °C. Van Setten and coworkers [89-93] extensively studied other groups of molten salts catalysts based on eutectic mixtures of Cs₂O, V₂O₅ and MoO₃. The catalysts were dispersed on several supports. CsVO₃-MoO₃ and Cs₂MoO₄-V₂O₅ catalysts showed high activity for soot oxidation resulting also from liquid-phase mobility of the catalysts. Indeed the CsVO₃-MoO₃ catalyst is not water resistant, up to 50% of the quantity was soluble. The catalysts showed low hydrothermal stability and also the formation of secondary emissions was likely.

Fino et al. [94] studied the catalytic activity of soot oxidation catalysts based on Cs and V oxides. The higher Cs content in the catalysts the higher is the catalytic activity. The authors found a decrease in catalytic activity in the range Cs₃VO₄ > Cs₂O > Cs₄V₂O₇ > Cs₂O·V₂O₅ > CsVO₃ > CsV₄O₁₁ > V₂O₅.

Several authors studied the activity of alkali metal chlorides and found soot oxidation catalysts to be active. For instance Watebe and coworkers [95] using SiO₂-Al₂O₃

supported catalysts reduced the temperature T_{50} by up to 180 °C in the range $\text{CsCl} > \text{LiCl} > \text{KCl} > \text{NaCl}$. The authors also studied TiO_2 supported catalysts composed of two or three metal salts and found that the composition of CuCl_2 -KCl is very active toward soot oxidation however the catalyst vaporized at elevated temperatures of 600 °C. Its combination with V and with Mo resulted in stability up to 900 °C, lowering the temperature T_{50} by 300 °C.

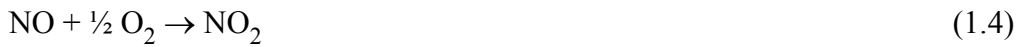
There have been several studies carried out on the catalytic activity of various metal chloride catalysts and the CuCl_2 was reported to be the most active catalyst toward soot combustion. For instance Murphy and coworkers [96] found that low concentration of metal chlorides increase the soot oxidation rates. Hillenbrand and Trayser [97] reported that the addition of NaCl to CuCl_2 reduced the combustion temperature by 50 °C, the ignition temperature was lower than 400°C. Mul et al. [98, 99] studied several metal chlorides and also reported that CuCl_2 was a very active catalyst which decreased the combustion temperature by 200-275 °C compared to a non catalytic reference. The catalytic activity of the tested catalysts correlates with the melting point. The authors noted that due to the decomposition of active species or high vapor pressure their application for the soot oxidation is not recommended.

1.4.2 Catalysts containing noble metals

Various scientific studies of noble metals such as Pt, Pd, Rh, Ru were performed, however, these are found predominantly in the patent literature [100-102]. The most commercial and most active noble metal based filter uses Pt, usually combined with promoters, known to be active to oxidize CO and HC. The disadvantages of Pt are its high cost and production of sulfate particulates. Therefore its application is limited when using fuels containing high S contamination.

Cooper and Thoss [103] observed and reported Pt promoting soot oxidation indirectly. The combustion mechanism involved a two step process in which the NO present in exhaust gas is converted into the active oxidant NO_2 (Equation 1.4) over the Pt catalyst. This NO_2 subsequently oxidizes soot (Equation 1.5) [103] at a temperature of about

280 to 480 °C [104]. This reaction exhibits a higher oxidation rate than the oxidation via O₂.



The authors showed that the contact between soot and Pt placed upstream of the particulate trap is not a precondition. Neri et al. [105] reported that the high activity of Pt supported on $\gamma\text{-Al}_2\text{O}_3$ in air, even at low loadings of the noble metal, was explained by the spillover effect. The authors determined the catalytic activity by means of TPO. The engine soot and catalyst were milled together to achieve so-called tight contact, resulting in catalytic soot oxidation in air.

Pt features high activity for oxidation of SO₂ to H₂SO₄, which is a drawback. The addition of Pd to Pt significantly reduces the selectivity, and tests on Rh, Ir, and Ru exhibit selectivity near zero, due to their poor NO oxidation activity [103]. An example of a Pt loaded catalyst developed by Engelhard consists of 5-150 g ft⁻³ Pt/Rh at 5:1 weight ratio and of 30-1500 g ft⁻³ MgO support [106]. The regeneration temperature of a filter coated with the catalyst lay between 375 and 400 °C. The addition of Rh reduced SO₂ oxidation. Whereas 51% of SO₂ is converted to SO₃ by 100% Pt, only 13% conversion is achieved by a combination of Pt/Pd at a weight ratio of 5:1. However, although Pd effectively reduces the SO₂ oxidation, the addition of Rh to Pt significantly increases the filter regeneration temperature [103]. The total DPM emissions can be controlled by a catalyst with high Pt loading, only when ultra low S fuel is used, therefore, in order to obtain high PM conversion efficiency in the Pt catalyzed filter the S content has to be minimized while NO oxidation should be maximized. In contrast some authors reported a slightly increased soot oxidation rate in the presence of SO₂ for the Pt catalyst [104, 107].

The effect of a Pt supported catalysts on soot oxidation was intensively studied by Uchisawa and coworkers [107-111]. The catalytic activity was estimated using TPO by detecting the temperature of the CO₂ signal maximum. Numerous support metal oxides [110] were impregnated with different Pt precursors [107] to determine the catalytic

activity. $\text{Pt}(\text{NH}_3)_4(\text{OH})_2/\text{MO}_x/\text{SiC}$ ($\text{MO}_x = \text{TiO}_2, \text{ZrO}_2$ and Al_2O_3) showed relatively high oxidation activity and durability at high temperatures and with exposure to sulfate. The authors suggested that the supports with low basicity had reduced the affinity toward SO_3 .

The effect of V on Pt based catalysts for the reduction of diesel emissions was studied under SO_2 conditions, for example by Kim et al. [112] and Liu et al. [113]. V is known to reduce the sulphate in diesel oxidation catalysts. Kim and coworkers found that SO_2 molecules adsorb onto the hydroxyl groups of TiO_2 , and are promoted by V_2O_5 [112]. The SO_2 migrate to Pt particles and react with oxygen adsorbed onto them. Another example of using the combination of Pt and V is the catalysts developed by Süd-Chemie [114]. They applied a Pt/Mg/V catalyst coated onto a W doped TiO_2 washcoat. The Pt/V catalyst may reduce sulphate, due to the effect of V as a sulphate suppressant. Regeneration of the soot loaded filter took place at a temperature of 350 °C. The TiO_2 washcoat was favoured over Al_2O_3 to avoid interaction between Mg and Al_2O_3 , resulting in a loss of surface area and catalyst deactivation. Davies and coworkers [115] found that washcoat selection is most important for the catalytic activities of supported Pt and Pd.

1.5 Combinatorial approach in automotive exhaust aftertreatment

Combinatorial chemistry has been used successfully for many years in the pharmaceutical industry [116, 117] and biotechnology [118, 119] in the search for new active ingredients. High throughput methods are increasingly established for the development and improvement of the activity of existing catalysts [120, 121] and for the search for still unknown elemental compositions [122, 123]. The aim of these approaches is the systematic combination of elements in order to prepare and to test a large variety of chemically and/or physically different compositions as a so-called library [124], hence the preparation and determination is carried out automatically. Such methods accelerate the effective discovery of more active materials in a shorter time, which would normally have taken months or years by manual synthesis and analysis methods.

A great number of catalysts have been tested for the automotive exhaust aftertreatment. These include diesel oxidation catalysts (DOC) [125] which reduce PM emissions, CO and HC, selective catalytic reduction (SCR₁) with ammonia [126], or application of SCR₁ with HCs referred to as DeNO_x or as lean NO_x catalysts [127] to reduce NO_x and the simultaneous conversion of HC, CO and NO_x by TWC [128, 129]. Such catalysts were produced manually and studied individually or in low numbers. However, there are few studies reporting the application of the combinatorial approach and high throughput screening to exhaust gas aftertreatment.

The combinatorial screening approach used for the development of diesel soot oxidation catalysts was employed by the McGinn research group [82]. A polymerizable-complex method (PCM) of powder processing based on the Pechini method was used. Libraries of 16 wells containing combinations of Ce-O, Cu-O and alkali metals were prepared by means of a drop-on-demand inject printer and the soot dispersion was deposited manually with a pipette in order to achieve loose contact. The authors investigated the relative catalytic activity using infrared (IR) thermography in a temperature range between 340 and 400 °C in increments of 5 °C. Thermal images were taken while pure oxygen flowed through the reactor. The thermal difference images showed temperature changes of 1.5 to 2 °C. Although the parallel IR thermography screening presents a fast approach in comparison, for instance, to conventional analysis, the authors did not pursue the measurement approach further, since the IR thermography design requires a higher resolution.

The same research group carried out further development of soot oxidation catalysts using a combinatorial approach [130, 131]. PCM was used to synthesize oxide powder of CuFe₂O₄ and CoFe₂O₄ doped with alkali metals (Li, Na, K and Cs). The catalytic activity of the mixtures of soot and catalysts was analyzed serially in an auto-loading high resolution modulated TGA. The catalytic solution was dispensed automatically by drop-on-demand printer directly into crucibles slightly taller than the one usually used in the TGA. This method allows the preparation of up to 55 samples. The soot dispersion was deposited in the same manner as mentioned above; pipetted manually. K exhibits the most catalytic activity towards soot oxidation of all the alkali-metal doped systems showing a soot combustion temperature T₅₀ approx. 300 °C. The authors noted evidence of K loss in temperature range between 500 and 700 °C.

The combinatorial chemistry and high throughput experiments (HTE) were also applied in the study of DeNO_x catalysts. Richter and coworkers [132] developed a parallel 64-channel microreactor to test catalysts under lean conditions. The reactor was connected to an automated time-of-flight mass spectrometer (TOF-MS) coupled with fast gas chromatography (GC), which allowed the sequential analysis of each reaction channel stream. The combinatorial synthesis of In, Ag, Co and Cu compositions was prepared using the incipient wetness method, and carried out by a dispensing robot. The test showed that the highest NO_x conversion was achieved by In_{0.2}Ag_{0.8} at 450 °C.

Schmitz et al. [133] developed a high throughput approach for the automated design, synthesis, screening, and statistical analysis of Pt supported catalysts for NO oxidation, applicable to automotive emissions aftertreatment technologies. The catalysts were prepared via the incipient wetness method using a pipette robot and the screening was performed in a 10-channel flow reactor.

1.6 Sol-gel process

The sol-gel process is a method for the preparation of glass and ceramic materials and coatings which has attracted increasing research interest in recent years because of its application in sensor materials [134], in catalysis [135] as catalysts with adjustable surface polarity [136] and formselective catalysis [137].

Generally the sol-gel process allows the controlled preparation of tailored inorganic or organic-inorganic materials [138] at the nanoscale resulting in new chemical or physical properties which can also be used in catalysis. The precursors, usually metal salts or metal alkoxides [139], are transferred by hydrolysis and condensation to new phases referred to as a loose network of oligomers (sol), followed by further polymerization leading to formation of a gel. In a sol colloidal particles are dispersed in a liquid, which are suspended by Brownian motions. In contrast, a gel consists of a three-dimensional network with homogenous distribution of the elements whose pores are filled with liquid. The gel is dried and calcinated afterwards as the pore liquid is evaporated from the network. Due to the drying method aerogels or xerogels differ. An aerogel is formed

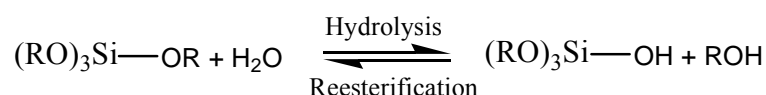
by means of supercritical drying technology placed in an autoclave, whereas xerogels are obtained using conventional drying methods [140].

The synthesis of materials using the sol-gel process is advantageous as it is prepared at low temperatures, and achieves narrow particle size distributions at the nanoscale resulting in high surface area. The pore volume and pore size distribution can be controlled. The sol-gel process is an attractive procedure, as several components can be introduced into the solution in a single step, and therefore it is suitable for the preparation of binary or multicomponent catalysts, also with dopants which can be present even in small amounts giving variable qualitative and quantitative elemental compositions. The samples feature high surface area, large pore volume and textural stability. The materials can be obtained with specific characteristic [141] in different physical forms. Due to this variability their technical application has been established, such as in films [142], fibers [143] and polymers [144].

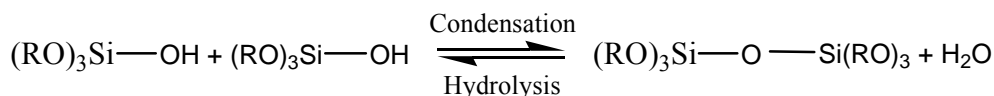
Tetraethyl orthosilicate (TEOS) is the most extensively studied precursor in sol-gel chemistry [145]. The hydrolysis and condensation is affected by the pH value, the temperature, the ratio of water to alkoxy group and the kind of solvent and precursor. Many scientists studied the influence of the modification of these parameters on the physico-chemical characteristic [146, 147]. The hydrolysis can be catalyzed either with base (OH^-) or acid (H^+), which has an important influence on the network formation [148]. Under acidic conditions hydrolysis is favored resulting in linear polymer-like gels with narrow pore size distribution. In contrast, under base conditions condensation is favored forming a network with large spherical particles featuring a wide pore size distribution.

The chemical reaction which occurs during the sol-gel process of tetraalkoxysilanes is generally described by three equations. Initially an alkoxides group (OR) is replaced by a hydroxyl group (OH) during hydrolysis reaction (Figure 1.7 a). The subsequent linking of the Si–O–Si bond can take place both by splitting off water (Figure 1.7 b) and by splitting off alcohol (Figure 1.7 c). The reactions do not run sequentially.

(a)



(b)



(c)

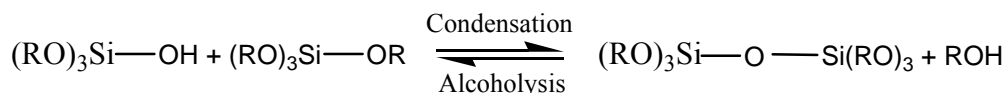
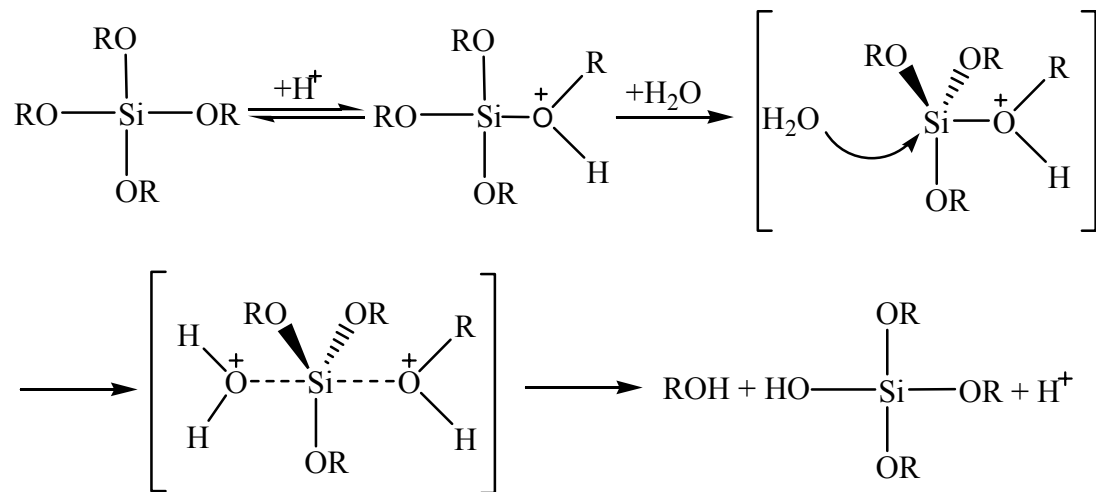


Figure 1.7 Main mechanism of sol-gel process; hydrolysis (a), water condensation (b) and alcohol condensation (c)

The condensation begins even before the tetraalkoxysilanes are completely hydrolyzed [149], thus the condensation and hydrolysis proceed in parallel during the sol-gel process containing simultaneously Si-OR and Si-OH groups. A silane alkoxide is firstly protonated during acid catalysis on the oxygen of the alkoxides group, followed by nucleophil substitution among addition by water or alcohol attack of the silicon atom. The mechanism of the acid catalyzed sol-gel process is shown in Figure 1.8. Under base conditions the nucleophilic hydroxide ion reacts with the silicon of the alkoxysilane by elimination of an alkoxide anion.

The network of pure and mixed metal oxides gels is formed in similar way to silica gels. Precursors of metal alkoxides such as titanium, zirconium, tin or aluminum have to be stabilized because they are much more reactive towards hydrolysis than alkoxysilanes, resulting in the formation of precipitates. The lower electronegativity of the transition metals causes them to be more electrophilic and hence less stable towards hydrolysis [150]. For this reason in base catalysis the undesirable formation of precipitates of hydroxides can occur. The hydroxide ion acts as an attacking reagent resulting in the acceleration of both hydrolysis and condensation. The hydroxide ion directly attacks the metal ion. The more electropositive ions cause the formation of oxide domain and consequently undesired phase separation, wherein the nanoparticles are formed. Since the reactivity towards hydrolysis is too high for many alkoxides, in order to avoid the precipitates of the precursors the sol-gel process has to be proceeded in acid catalysis.

(a)



(b)

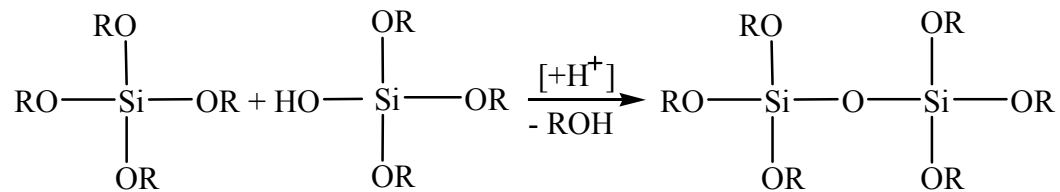


Figure 1.8 Mechanism of acid catalyzed sol-gel process; hydrolysis (a) and condensation (b)

Under acid conditions the differences in electronegativity of the metal ions affect the electron density of the anionic oxygen atoms less. This means that the protons do not differentiate between single metal ions. They particularly attack the alkoxides or anionic oxygen bound to the metal ions. Thus, the formation of mixed metal oxides with homogeneous distribution of the metals in the network is promoted only under acid reaction conditions but not under base reaction conditions. The addition of, for example, acetic acid to the precursor solution is most common. In addition to acidic reaction conditions a complexing agent, for instance, β -diketon like acetylaceton, 4-hydroxy-4-methyl-2-pentanone and others, can be added in order to avoid the precipitation or formation of single oxides. [151]. Thus, on the one hand the reactivity of the metal alkoxides precursors is decreased, and on the other hand the concentration of water is controlled.

To conclude, in the literature there are several descriptions of the sol-gel process of mixed metal oxides [152, 153], many publications [140, 154] and also the monograph [150] for a detailed insight into sol-gel is recommended.

Chapter 2

2. Scientific objective

To develop and optimize the catalysts for diesel particulate filters (DPF) using the combinatorial preparation of samples and their parallel screening revealing which materials are suitable to reduce the soot oxidation temperature is required. The investigation of the new materials by conventional application of thermogravimetric analysis (TGA) is time consuming and therefore less effective. Both the combinatorial approach and high throughput technology (HTT) can allow for a raise in the number of prepared and measured samples and therefore the amount of information obtained.

The aim of this work was to analyze a high throughput syntheses as well as a HTT to the development of low temperature noble metal free catalysts for DPF. From this objective the following single tasks were established:

- (i) The requirements of the catalysts were: catalytic activity at a temperature of approx. 400 °C, constant activity after long time periods of thermal and hydrothermal aging, and high stability toward S poisoning. The most active catalysts should be Pt doped raising the question how will their activity be affected?
- (ii) The combinatorial preparation of the oxidation catalysts should be carried out using different high throughput syntheses and thus should be determined and compared to each other with same aspects further studied by HTT.
- (iii) For the high throughput experiments (HTE) two different soot deposition methods should be studied, however the contact between soot and catalyst should be in loose mode in order to be close to practical conditions. Also for the HTE a reactor should be designed and built, in which up to 144 samples should be simultaneously measured by emissivity corrected infrared thermography (ecIRT). The HTT should be verified by a conventional synthesis method for the reliability of its screening and both

technologies should be compared to each other in terms of whether the ecIRT is a fast and suitable screening approach for the evaluation of soot catalysts development.

Chapter 3

3. Results and discussions

3.1 IR thermography setup

The main focus of this chapter is the reactor constructed for the parallel measurement of relative activity of soot oxidation catalysts. The emissivity corrected infrared thermography (ecIRT) device consists of the reactor, together with a gas supply, a control unit, and an IR camera head. The reactor design and its requirements as well as the reactor setup, and its flow and temperature profile are described in detail. The particular reactor features are discussed in terms of the high throughput screening. Among other things, alternative material for the slate plate library was investigated and evaluated for its use in ecIRT.

3.1.1 Reactor design

The reactor was designed and built at the in-house workshop at Robert Bosch GmbH in cooperation with J. Hilzinger.

The following requirements had to be satisfied:

- The temperature should be kept constant over the entire sample plates in order to achieve the same reaction velocity in each area.
- The temperature limit should be up to 700 °C.
- The view of the entire reaction chamber should not be obstructed.
- The gas should flow evenly into the reactor to give a uniform gas diffusion rate.
- The gas volume within the reaction chamber should be as small as possible in order to avoid heat radiation which has an influence on the measured intensity.

- The volume of the reaction chamber should be also as small as possible to give a gas stream as close to laminar as possible.
- No reflection from the reaction chamber should take place, therefore a suitable plate for the IR thermography is required.

It has to be kept in mind that during the setup of measurement other technical requirements also have to be considered. For instance, the gas flow controller was connected to the GPIB using 24-pin connectors, and among other things the selection of the cable length plays an important role. E.g. if the cable is too long, the signal to noise ratio increases and no signal can be detected.

3.1.2 Reactor setup

The reactor is composed of a reactor lid, a reactor body, a gas distribution frame and cartridge heaters. A schematic view of its setup can be found in Figure 3.1. The reactor lid consists of upper and lower parts, attached together with sapphire glass placed in between, making a leak-proof seal between the sapphire glass and the lid. In order to change the library plates it was only necessary to lift the reactor lid, which was screwed to the reactor body by four hexagonal nuts and headless pins. This saved a great deal of the operator's time and the efficient changing of the library plates was achieved.

Sapphire glass is very well suited to IR thermography of oxidation catalysts, due to its superior mechanical and chemical properties compared to other IR glass materials and its high IR transparency up to 6.5 μm . At temperatures above 400 $^{\circ}\text{C}$ the detector was saturated due to high IR brightness, so an IR attenuating borosilicate glass plate was situated in the front of the camera head lens to prevent further saturation. The glass plate absorbed a part of the IR radiation and enabled measurements to be performed at higher temperatures.

The gas distribution frame was designed in such way that it can be placed into the reactor chamber without affecting the fixed input and output of the gas. Homogenous gas distribution in the reaction chamber was achieved by an array of 40 equidistant bore

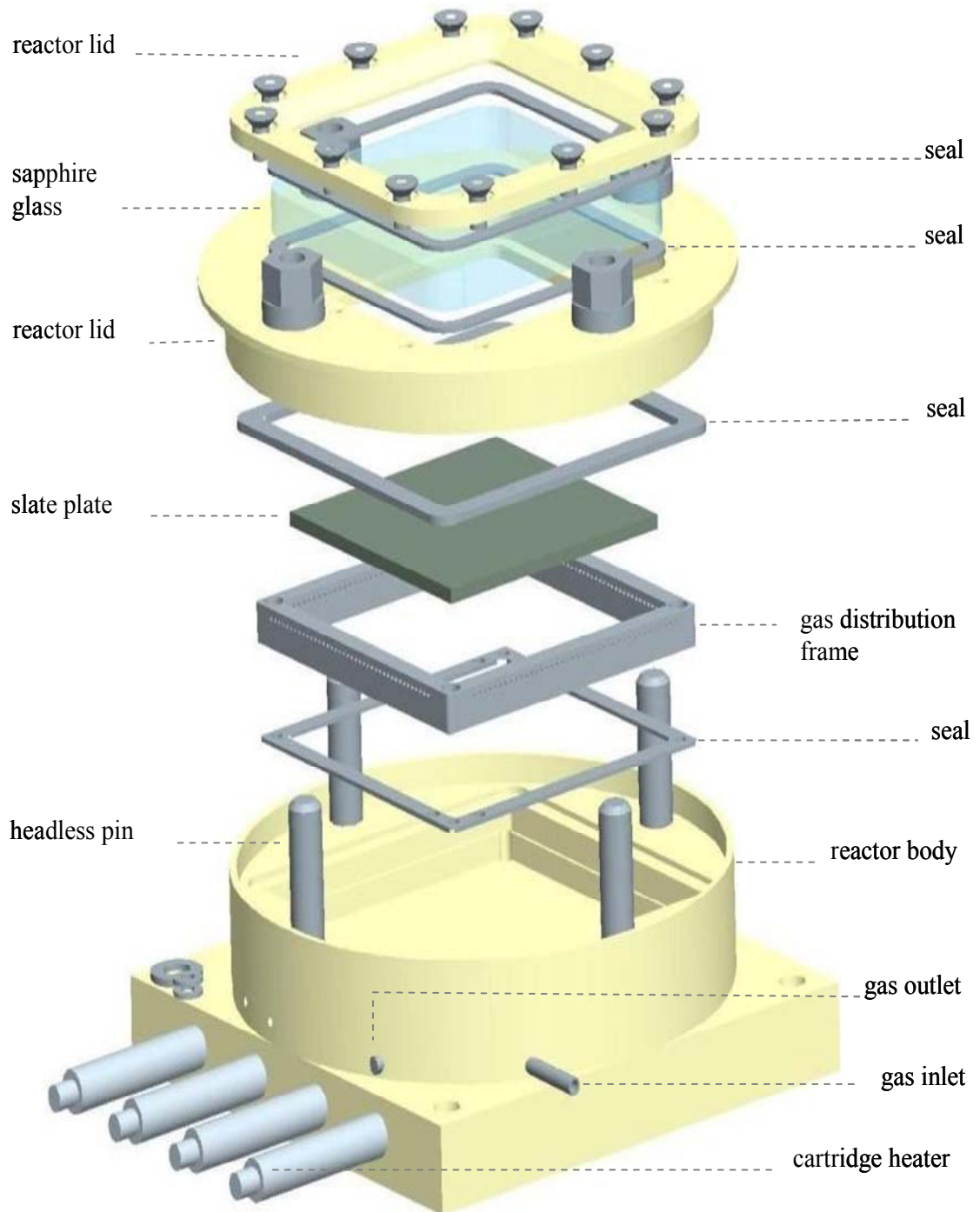


Figure 3.1 Exploded view of reactor

holes on each side. In order to distribute the gas before streaming it into the reactor, deep longitudinal slots were milled within the gas distribution frame. The gas flowed in through two adjacent sides of the reactor and was expelled through the other two sides. The view of the gas flow within the gas distribution frame is presented in Figure 3.4. Finally a pressure regulating valve was connected to the gas outlet. This chamber design ensured homogenous gas distribution within the reaction area.

Investigation into library material

In order to test other library material a steel library of identical size to the slate plate library was produced. The objective was to find alternatives to the slate library plates which are difficult to handle as the material is brittle and besides the processing time of steel library plates is about five times lower than of slate plates.

A steel cover of 0.5 mm thickness was made to fit exactly over the library with holes drilled precisely in alignment with the library wells. It was sprayed with black high-temperature paint named Pyromark series 2500 (Helling GmbH, Heidgraben) and afterwards treated according to the manufacturer's instructions. This paint is characterized by temperature stability up to 1093 °C, its reflectivity is negligible, it features a high emissivity (0.98) and is suitable for application on metal surfaces that are subjected to high temperatures.

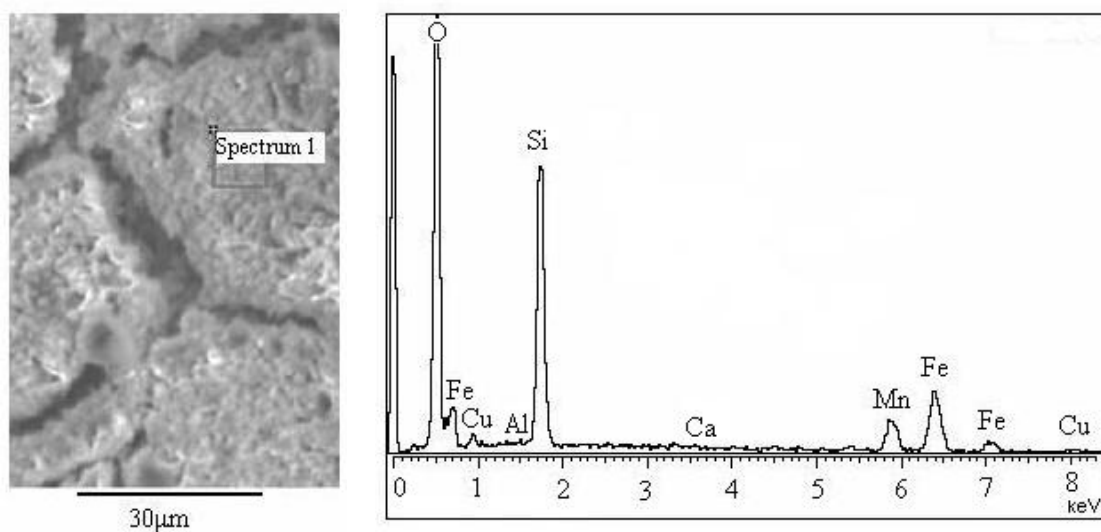


Figure 3.2 EDS spectra of coating film surface

The surface of the paint was firstly analyzed using SEM (Leo 1450VP) equipped with energy dispersive spectroscopy (EDS) with an acceleration voltage of 15 kV to ensure that the elements in the coat of lacquer were not catalytic, see the schematic view of EDS analysis in Figure 3.2. The coating film exhibited partial structural cracks and contained predominantly O and Si, some Fe and Mn as well as low amounts of Cu and it is assumed that minute traces of Al and Ca are also present.

To determine its potential application, steel libraries covered by the painted steel sheets were placed into the reactor and a measurement was carried out by means of ecIRT at 450°C. The IR thermography results showed that the film surface is changed during the process of the experiment suggesting chemical surface modification. Hence the high-temperature paint cannot be applied in high throughput screening and thus is not acceptable for use in this study. Therefore the library plates were made of slate showing very favourable IR properties, in that it absorbs IR radiation and does not strongly reflect IR radiation. Moreover the surface stays unvaried during the entire series of experiments.

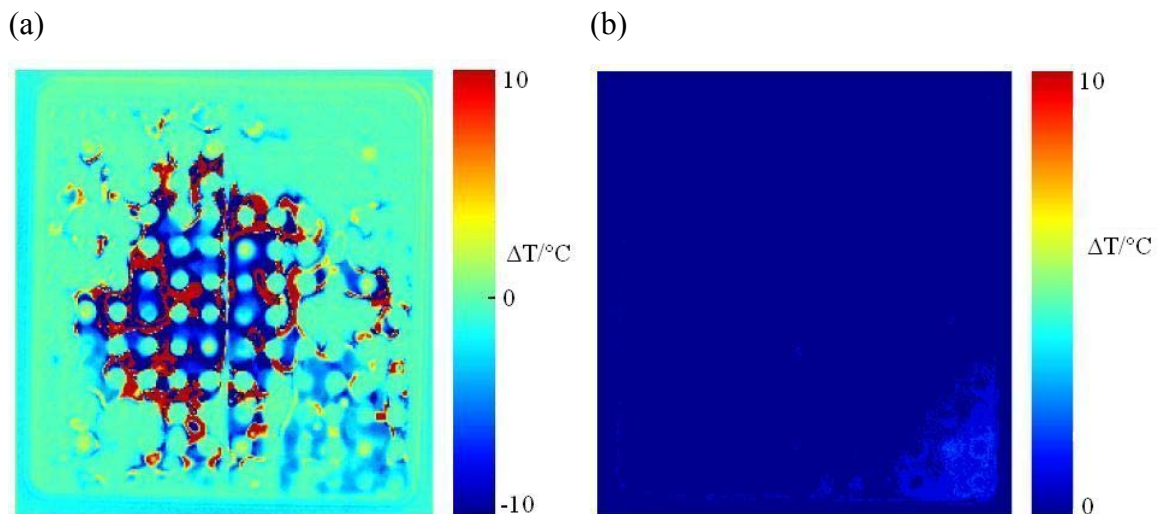


Figure 3.3 ecIRT image of steel cover coated with black high-temperature paint (a) and of slate plates (b) at a temperature of 450 °C

3.1.3 Reactor flow profile

To determine the gas flow profile within the reactor the wells of the slate plates were fully filled with zeolite beta H-Form and placed inside the reactor chamber. N_2 flowed through a wash bottle (100 ml min^{-1}) filled with concentrated liquid ammonia and the ammonia rich mixture was streamed over the samples. The heat of adsorption of ammonia by the zeolite could be easily recorded and conveyed by the IR camera, as seen in Figure 3.5.

There is a fully developed velocity distribution within the reactor chamber. The gas starts to flow from the lower right corner (Figure 3.5 b) and is split into the longitudinal slots milled inside the gas distribution frame, see Figure 3.4. From here, gas flows into the reactor chamber from two directions, progressing evenly across the surface (Figure 3.5 c-e) and finally filling the complete chamber (Figure 3.5 f). The samples nearest to the lower right corner are reached first, while the upper left area, where the gas outlet is situated, is reached last. Before the gas leaves the reactor it flows through the upper and the left lateral longitudinal slots.

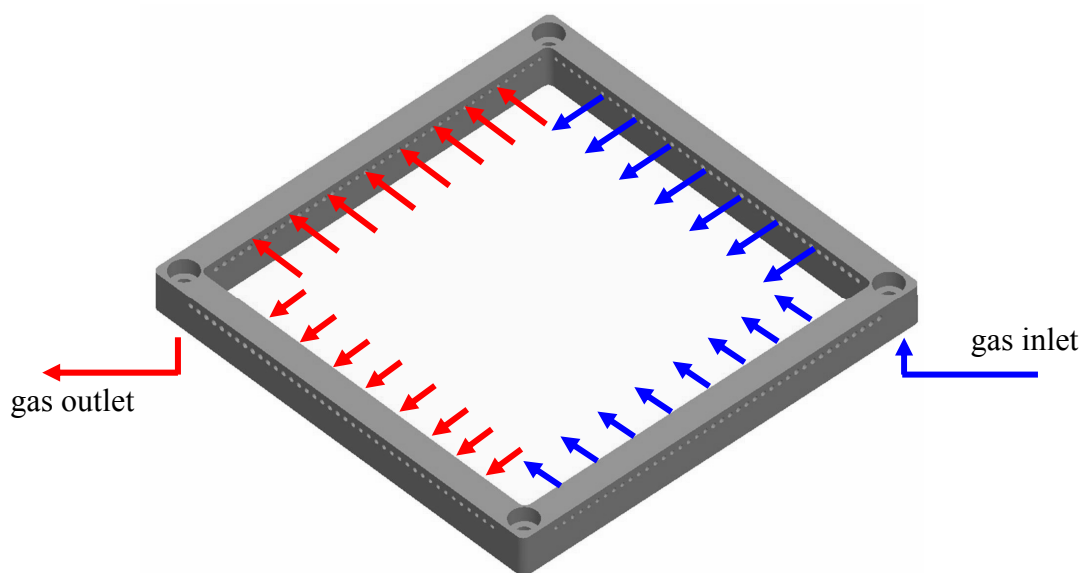


Figure 3.4 Schematic of gas flow within gas distribution frame

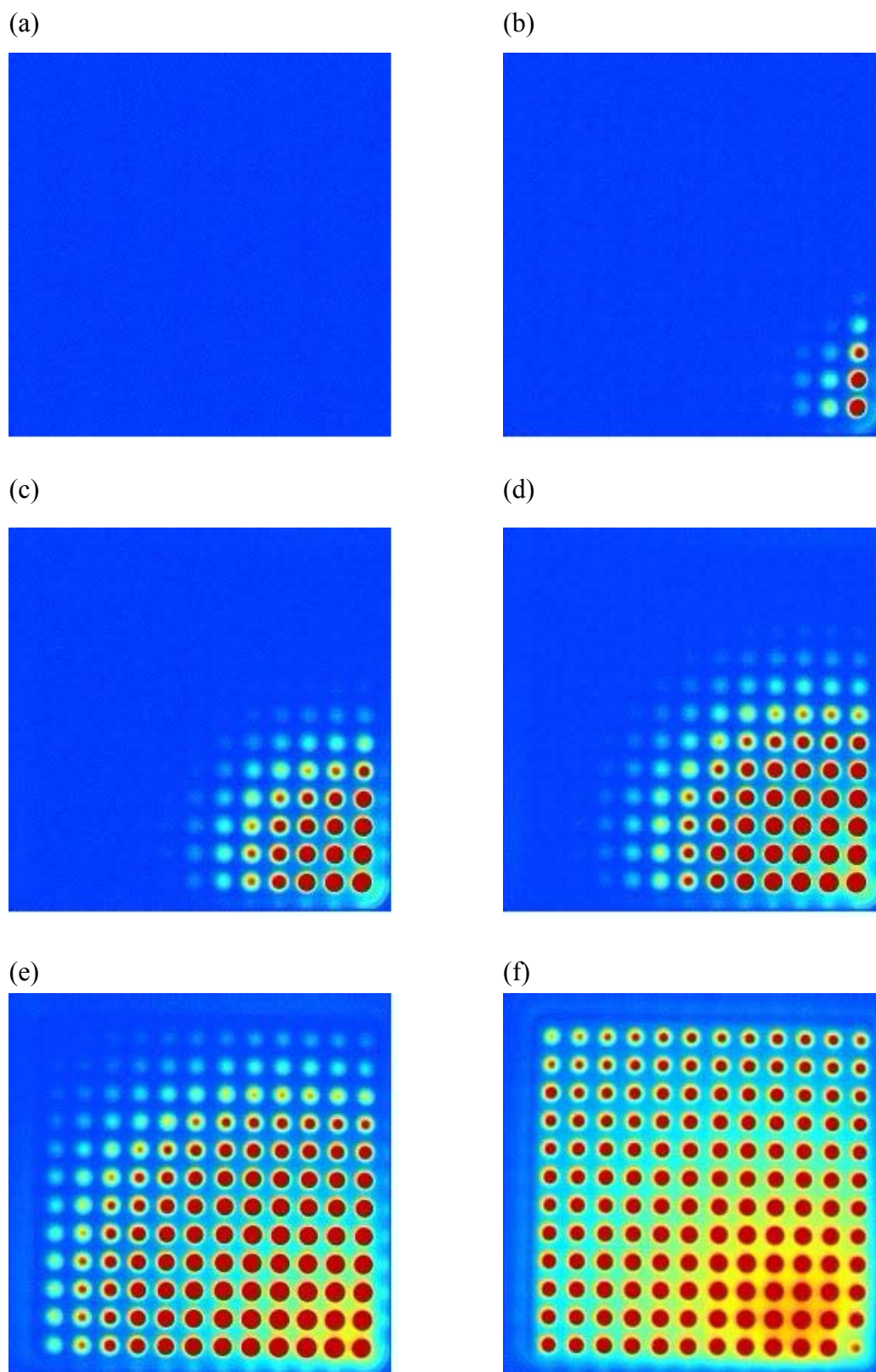


Figure 3.5 Reactor flow profile taken at 1 s (a) and at intervals of 3 s (b-f). Zeolite beta H-Form is shown with a concentrated ammonia N_2 mixture flowing over it from the lower right corner toward upper left corner at ambient temp. Red (warm) represents the ammonia adsorption on the zeolite, and the blue (cold) area shows where no reaction occurred yet. The images above (f) showed the samples fully covered by the reaction gas.

The soot oxidation tests showed that the catalysts positioned in any substrate wells display nearly identical relative activity (Figure 3.10). This allowed us to conclude that the design of the reactor and the gas flow profile was suitable and demonstrated high gas flow homogeneity.

3.1.4 Reactor temperature profile

The temperature was controlled by a thermocouple placed in the lower part of the reactor. A temperature difference was observed between the target and the current temperature within the reactor chamber, where the samples were located. The temperature difference on the substrate surface and the reactor depends on the operating temperature (Figure 3.6). At a set temperature of 450 °C a difference of 80 °C was observed, while at a set temperature of 400 °C a 70 °C difference was detected.

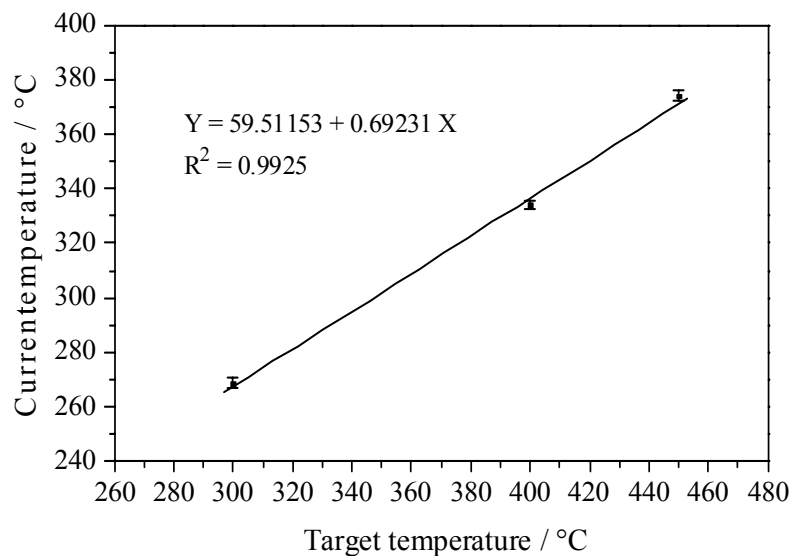
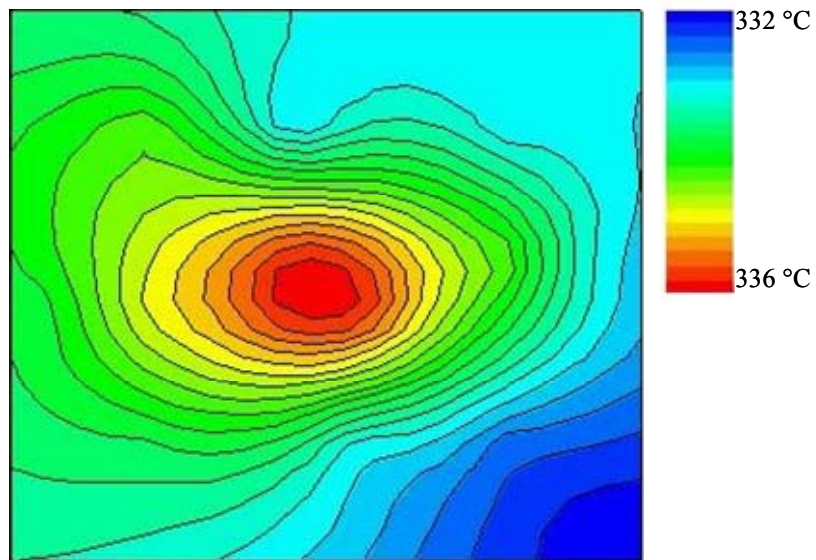


Figure 3.6 Linear regression of current temperature as a function of target temperature and its standard deviation

The temperature distribution in the reactor is presented in Figure 3.7. The temperature of the slate plate surface decreases from the centre to the periphery by approx. 4 °C at an operating temperature of 400 °C, and by approx. 6 °C at 450 °C. The thermocouple was positioned nearly 10 mm to the left of the reactor centre which slightly affected the temperature distribution in the reactor. As a result the hottest spot was found to be slightly off-centre and the lowest temperature area was asymmetric on the right side.

This temperature profile was considered acceptable for the combinatorial soot oxidation catalysts screening experiments.

(a)



(b)

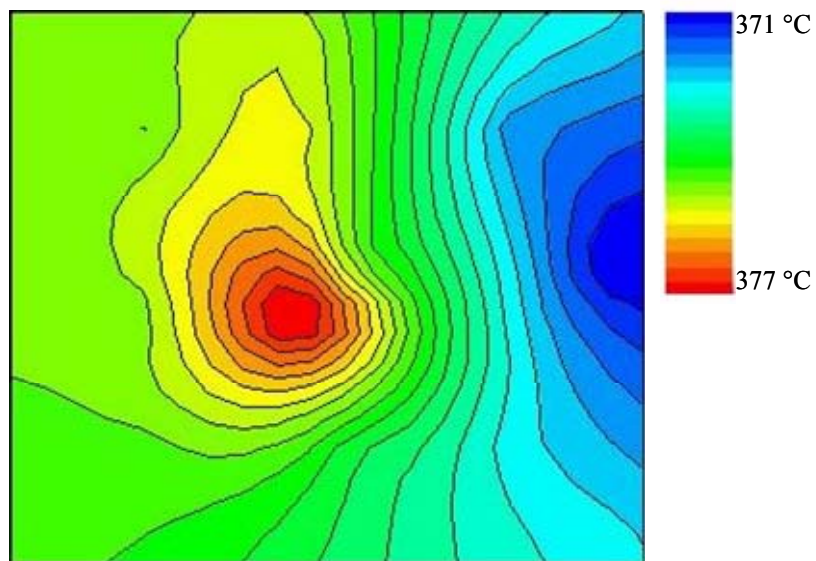


Figure 3.7 Reactor temperature profile measured on the slate plate surface at operating temperatures of 400 °C (a) and 450 °C (b)

3.2 Synthesis evaluation

The present study of soot oxidation includes the assessment of preparation methods of catalysts using combinatorial chemistry. The preparation method is an important aspect as it affects the final physical and chemical properties of catalysts needed for specific reactions. There are many preparation methods, for instance sol-gel [155], impregnation, precipitation, or the milling of solid matter [156]. Three preparation approaches were selected and their individual features are discussed with regard to combinatorial development of novel catalysts for soot oxidation, which is a subject little covered in the literature. Attention is given to preparation of supported, impregnated and unsupported catalysts. The second case is concerned with a paste synthesis that had to be developed, and to sol-gel synthesis using recipes which have been individually developed, optimized and introduced over many years by W. F. Maier's research group.

3.2.1 Paste synthesis

The paste synthesis method is well known in semiconductor technology [157] using the screen printing technique [158] whereas the rheological behavior plays a key role resulting in print quality [159]. However such synthesis has not been previously used for soot oxidation catalysts. The possibility of its combinatorial preparation and parallel analysis promise a considerable acceleration in novel materials discovery [160]. Paste is a mixture of solid matters, polymers and liquids forming a viscous mass. Some authors reported utilizing the combinatorial ceramic ink-jet printing method combined with high throughput screening [161] and their preparation using a combinatorial robot system [162]. The purpose is to use a new method that allows new findings and possibilities for using heterogeneous catalysis to reduce diesel particulate matter.

The starting elements, metal oxides of V, Mo and Ce for the combinatorial development of novel catalysts, were selected from elements known in the literature to have high activity in soot oxidation [163, 34, 78]. The suppliers and the purity of the metal oxides used are listed in Appendix in Table 7.3 and the polymers used are also depicted in the Appendix in Table 7.2. To develop novel catalyst materials the prepared metal oxide

pastes should be combined by a robotic system to maximize the number of new compositions, increasing the possibility of discovering novel katalysts for soot oxidation. The pastes need to have suitable rheological properties. On the one hand the viscosity gives a surface tension so it can be dispensed by the system, and on the other hand the paste has to be handled to generate a constant filling level in all library plate wells. The aim was to prepare pastes with viscous behavior dominating over elastic behavior. Once the viscosity was determined it should be the same for each paste to avoid inhomogeneity between single phases or segregation that can occur after mixing also reported in the literature to be a problem characteristic of thick film libraries [164]. Polymers of similar character, viscosity and composition should be used in each paste to avoid precipitation and other interactions. Also the number of polymers used should be kept as low as possible for rapid and simple preparation, and in order to convert the paste into solid catalyst matter in only a few heat treatment steps. The catalysts should exhibit a high specific surface area in order to obtain a narrow contact with soot particles. Therefore the single phase metal oxide powder was first milled using a planetary ball mill to a mean particle size diameter of as near to 200 nm as possible.

The pastes were prepared as described in Chapter 4.3.3 and dispensed using an automated robotic system named TR-300 / RC-500 (MTA automation AG, Switzerland). Its schematic is depicted in Figure 3.8. The system is highly suitable for viscous materials consisting of five material containers connected by tubes to the dosing system and mixing unit. The three dimensional dosing system can move along x, y and z axes including a mixing mode using propeller blades. The dosing system dispenser is programmed to move to the correct position in order to dispense a given amount of the paste mixture directly into the library wells. The libraries are placed on a table, on which a waste container is also situated, which is used when the mixture chamber is cleaned. Cartridges of a volume of 200 ml were filled with the prepared pastes and then inserted into the material containers which are set under pressure, therefore the pastes are pressed into the mixture chamber. The pastes are mixed by propeller blades and directly dispensed into library wells afterwards. The fill velocity, mixing time, revolutions per minute and the dosage volume can be adjusted, as required.

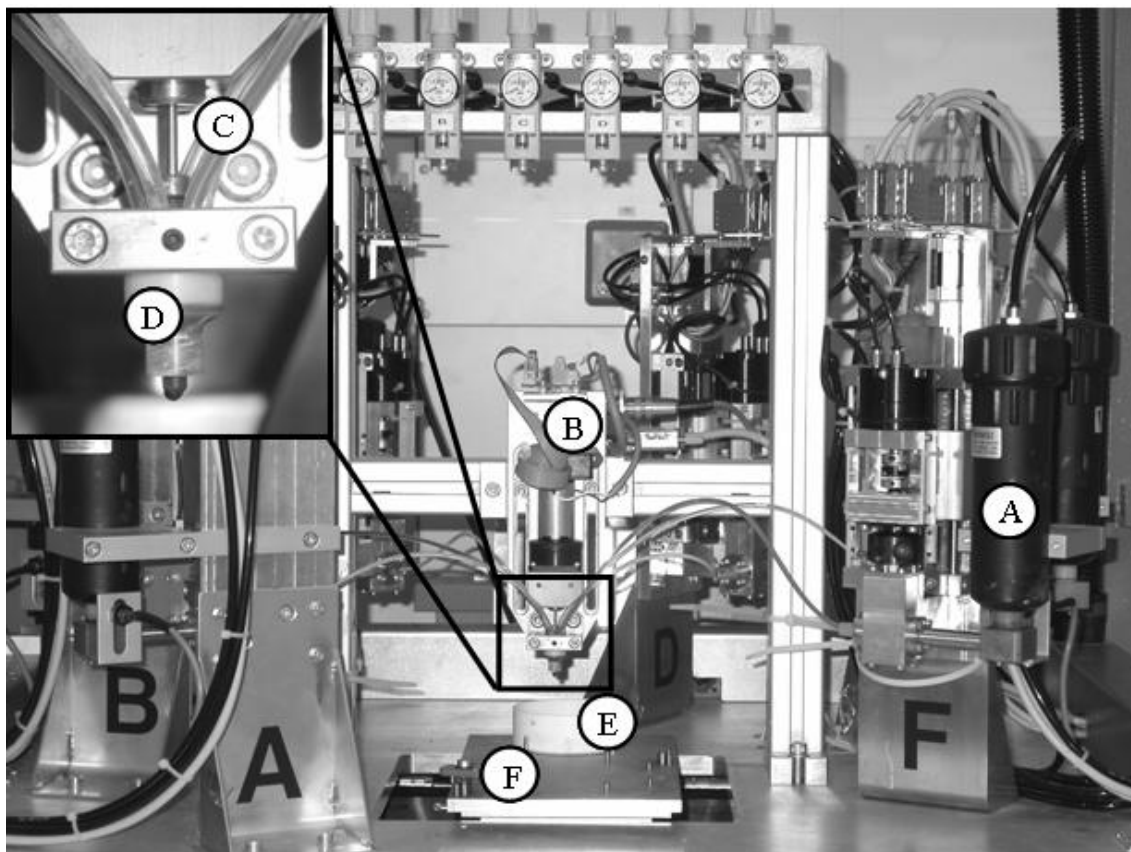


Figure 3.8 Automated paste robotic system; material container (A), dosing unit (B), tubes (C), mixing unit (D), waste container (E) and table on which the libraries were placed

In order to prepare binary composition the following explanation of the procedure used is described. The maximum volume of the mixture chamber is 32 μl therefore for example 10 μl of CeO_2 and 22 μl of MoO_3 , were simultaneously pressed into the mixing chamber with a fill velocity of 30 $\mu\text{l s}^{-1}$ and mixed by propeller blades. Subsequently 15 μl of the composition was dispensed into the well. After the dispensing was finished the cleaning program was activated and the whole procedure cycle started again however with other volume ratio.

The robotic system includes five material containers, which limits the combinations available. The cleaning of the combined dispensing and mixing chamber took place by pressing from any single cartridge until non-contaminated single paste comes out. The remaining paste mixture is unusable, and only inexpensive metal oxide powders should be used for this purpose.

Before using the robot the rheological behavior of the pastes was tested, which can vary depending on their powder size distribution and loading, morphology, polymer rheology and on the processing route. However, the paste preparation is more complicated for mixed metal oxide particles at the nanoscale and the process is time-consuming.

3.2.2 Impregnation

Impregnation is a common technique used for the preparation of catalyst materials and is also established for the preparation of soot oxidation catalysts [165-167]. It is an approach based on dissolved aqueous precursors deposited onto a support followed by drying and calcination into a catalytically active form. The catalysts may consist of one or more components introduced into the solution in a single step. It is important to achieve an homogenous dispersion of the catalyst's active components and to stabilize them against sintering. A higher specific surface area, associated with higher reaction rate, can be achieved with a smaller particle size distribution of the active catalytic material. The requirements of the support are high specific surface area and no reaction with the catalyst. Any interactions which do take place should, however, be controlled, and used to stabilize the active components or as synergy which could enhance the catalytic activity.

A pipetting robot is well suited for the preparation of single precursor solutions as well as for any combination of various different single solutions, and also for the automation of the deposition onto the supports. The dispensing velocity and the distance between the needle and support materials affect spreading and wetting. Therefore these parameters have to be defined.

3.2.3 Sol-gel synthesis

Sol-gel synthesis is a common method for the preparation of porous materials widely used in catalysis [155, 168]. It is based on hydrolysis and condensation, involving nucleophilic reactions. A sol is a colloidal dispersion, whereas a gel consists of a solid phase of three dimensional network, formed of colloid particles containing liquid in

their pores. The gel is dried and calcinated in its required porous shape. The detailed description of sol-gel process is given in Chapter 1.6.

The sol-gel synthesis is an attractive procedure, as several components can be introduced into one solution, and it is applicable for the preparation of binary or multicomponent catalysts composition. Several dopants can be present even in small amounts giving variable qualitative and quantitative compositions for preparation of different oxide materials. An advantage of this approach is that a narrow particle size distribution at the nanoscale is achieved, resulting in a high surface area. Also, mixing of the components is performed at ambient temperature and at normal pressure, therefore the synthesis preparation can be automated easily using a pipetting robot.

3.2.4 Discussion

Three different basic synthesis methods were studied and compared; paste synthesis, impregnation and sol-gel synthesis. Their characteristics and their suitability for preparing catalysts for high throughput screening of soot oxidation were assessed. The important features for the combinatorial process that play an essential role in the method development are depicted in the Table 3.1.

Table 3.1 Comparison of features of different synthesis procedures

Synthesis type	Procedure characteristic			
	Preparation	Quantity	Doping	Wastage
Paste	manually	large	not possible	high
Impregnation	automatically	small	possible	non
Sol-gel	automatically	small	possible	non

Comparison of the three synthesis methods revealed the following findings:

The paste preparation is very time-consuming as each paste has to be synthesized separately, and several batches must be prepared to obtain the mass needed to fill the cartridge. This makes the whole process unattractive. To synthesize pastes with consistent rheological properties from metal oxides with different characteristics and particle size distributions at the nanoscale is difficult, especially when using different

polymers which may affect each other or the viscosity and composition. Also, the high throughput design given by the catalyst compositions available is limited by the robotic system, which uses only five material containers. Small doping concentrations are not practicable. High wastage of pastes also occurred due to the high mass of paste required for cleaning the system, which is an unacceptable expense. In contrast impregnation and sol-gel synthesis are very rapid methods. Both are prepared in a single step and several components or dopants of any amount can be added. The prepared catalysts have narrow particle size distribution at the nanoscale and a high surface area. Also, wastage is minimal as only the required quantity of each component is used.

Based on these findings it was decided to use impregnation and sol-gel procedures. The characteristics and behavior with regards to catalytic soot oxidation were determined, and the HTT application by means of an ecIRT setup was studied, see the next Chapter 3.3.

3.3 High throughput technology

In the following chapter aspects of the individual measurement methods will be analyzed and described. The essential conditions for the detection of the relative activity by ecIRT were determined and discussed. We evaluated both automated soot deposition as well as manual mixing of soot and catalyst by spatula. In both techniques a loose contact mode was used in order to be as close as possible to practical conditions. To estimate the approaches of soot deposition the Pt/K/Ce catalysts were prepared as reported in literature to be highly active [73, 169]. The advantages and the disadvantages of both methods are discussed in relation to HTT using ecIRT.

3.3.1 Automated soot deposition

The soot was deposited onto slate plates by an automated spray coating system, see Chapter 4.1.3. Two different syntheses were attempted. On the one hand support material was impregnated on the other hand the catalysts were prepared via a sol-gel process.

In the first case the 72 library plate wells were each filled with 524 mg of Saffil CG alumina fibers, which were pressed using a rubber. The fibers were subsequently carefully extracted from each well using tweezers in order to find the average amount contained in the wells. Each one contained 7.3 ± 0.7 mg carriers impregnated with binary and ternary catalyst compositions. The high throughput synthesis of $\text{Pt}_y\text{K}_z\text{Ce}_{100-y-z}\text{O}_x$ catalysts was carried out using an automated pipetting robot. A detailed description of the impregnation is given in Chapter 4.3.2.

A soot layer was applied to the slate plates by preparing an optimized standard soot suspension, which is described in detail in Chapter 4.1.3. The samples covered with the soot layer were tested for their relative activities by ecIRT at temperatures up to 450 °C by placing them within the reactor chamber. The test execution procedure of ecIRT is described in Chapter 4.1.2.

The conditions of the automated soot deposition tool were kept constant. 150 ml of a fresh soot dispersion was prepared each time in a 250 ml bottle and used immediately. To avoid the agglomeration or sedimentation of soot particles in the bottle a maximum of 8 libraries were coated with a freshly prepared soot dispersion. In this way an homogenous soot layer was achieved, which, by calculation, has a mean soot thickness of about 1 ± 0.1 mm. Using this method it was not possible to obtain unambiguous measurements of the soot oxidation reaction by ecIRT. The reason for this was thought to be that weak contact was being made between soot and catalyst, and therefore soot ignition could not occur. This was investigated further, see Chapter 3.4.

In the case of catalyst preparation using sol-gel synthesis the catalysts were manually filled into the library plate wells and subsequently soot suspension was sprayed as described in previously paragraphs. While the soot was sprayed the samples were thereby expelled.

Although the automated soot coating approach is very fast, and an homogenous layer is obtained, this deposition method is unfortunately not applicable for the high throughput screening of soot oxidation. On the one hand by ecIRT using the impregnation method no heat increase was detected, on the other hand when the sol-gel process was used the

samples could not be soot sprayed since they were expelled by the blast of soot dispersion.

3.3.2 Soot and catalyst mixture by spatula

The other system used to detect the soot oxidation by ecIRT was the manual mixing of the soot and catalyst by spatula. The catalysts were synthesized by the sol-gel approach which is described in detail in Chapter 4.3.1. The high throughput synthesis of $\text{Pt}_y\text{K}_z\text{Ce}_{100-y-z}\text{O}_x$ metal oxide catalysts was performed using the automated pipetting robot. The single catalyst composition and its identification is specified in Appendix in Table 7.7. The soot and catalyst were mixed by spatula and these mixtures were manually filled into the wells of the libraries, see Figure 3.9, and the library plates were subsequently placed within the reactor to obtain the relative activities of individual metal oxide samples by esIRT. This measurement was performed as described in Chapter 4.1.2.

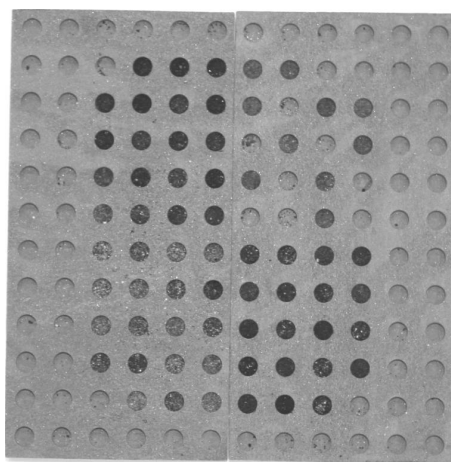


Figure 3.9 Schematic of library slate plates filled with the mixtures of soot and catalysts

An intensity change of soot oxidation was detected by ecIRT at an operating temperature of 400 °C, which is depicted and described in Figure 3.10. The maximum temperature alteration of 3.4 °C was detected for $\text{K}_{20}\text{Ce}_{80}\text{O}_x$ catalyst. Each sample was inserted into the library plate in duplicate and their positions randomized.

This eliminated any systematic error in the relative activity that may be linked with different positions in the reactor, which could, for example, mean that samples closer to the gas inlet may react with greater change in intensity or shadow effects caused by very active catalysts in the neighborhood and produces lower heat response.

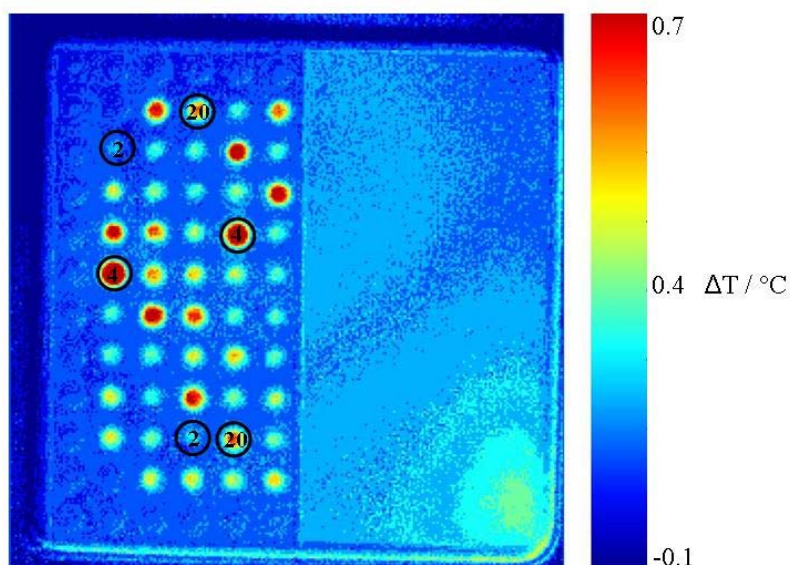


Figure 3.10 ecIRT image of $\text{Pt}_y\text{K}_z\text{Ce}_{100-y-z}\text{O}_x$ catalysts at 400 °C temperature in synthetic air 100 ml min^{-1} . The identical two catalysts in different positions are marked. Although the location of catalysts No. 2 ($\text{K}_5\text{Ce}_{95}\text{O}_x$), No. 4 ($\text{K}_{20}\text{Ce}_{80}\text{O}_x$), or No. 20 ($\text{Pt}_{15}\text{K}_{20}\text{Ce}_{65}\text{O}_x$) are different the measured heat increase ΔT is nearly equal.

As can be seen in the Figure 3.10 the same catalysts at different locations showed practically equal heat increase ΔT , independent of their position and the distance from the gas inlet. The relative activity of $\text{Pt}_y\text{K}_z\text{Ce}_{100-y-z}\text{O}_x$ is depicted depending on composition in Figure 3.11. The relative activity increased with a rise in K doped Ce.

The heat increase ΔT of all samples and their standard deviation is depicted in Figure 3.12. The samples No. 4 $\text{K}_{20}\text{Ce}_{80}\text{O}_x$, No. 3 $\text{K}_{15}\text{Ce}_{80}\text{O}_x$, and No. 9 $\text{Pt}_5\text{K}_{20}\text{Ce}_{75}\text{O}_x$ proved to be the most active for soot oxidation exhibiting relative heat increase to be above 1.5 °C while most catalysts showed heat increase lower than 1.5 °C .

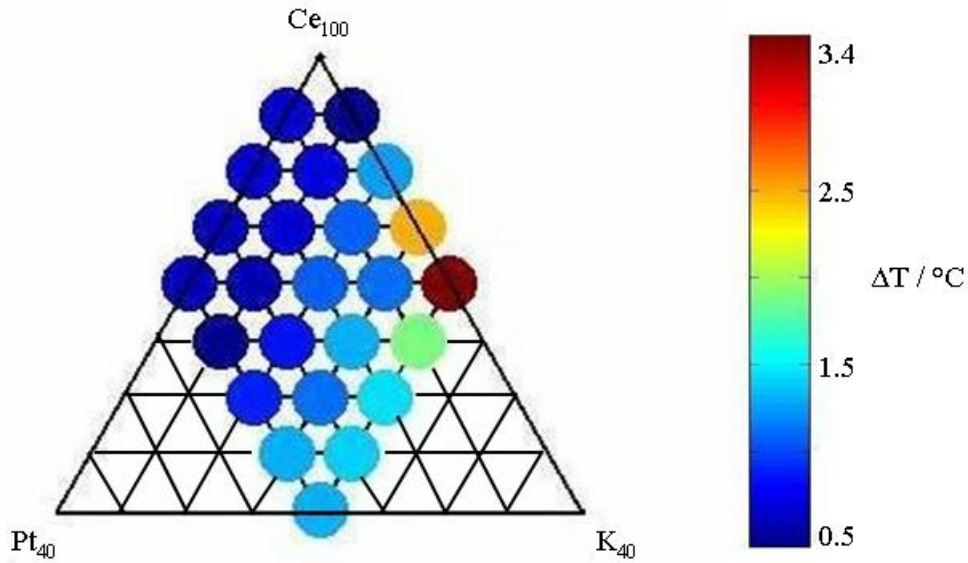


Figure 3.11 Schematic of composition spread of $\text{Pt}_y\text{K}_z\text{Ce}_{100-y-z}\text{O}_x$ catalysts and their heat increase ΔT from Figure 3.10

The relative activity of $\text{Pt}_y\text{K}_z\text{Ce}_{100-y-z}\text{O}_x$ samples has to be confirmed by TG-DTA to investigate the reliability of the high throughput screening method and the reliability of the mixing of catalyst and soot by spatula, see the following paragraph, for evaluation of HTT.

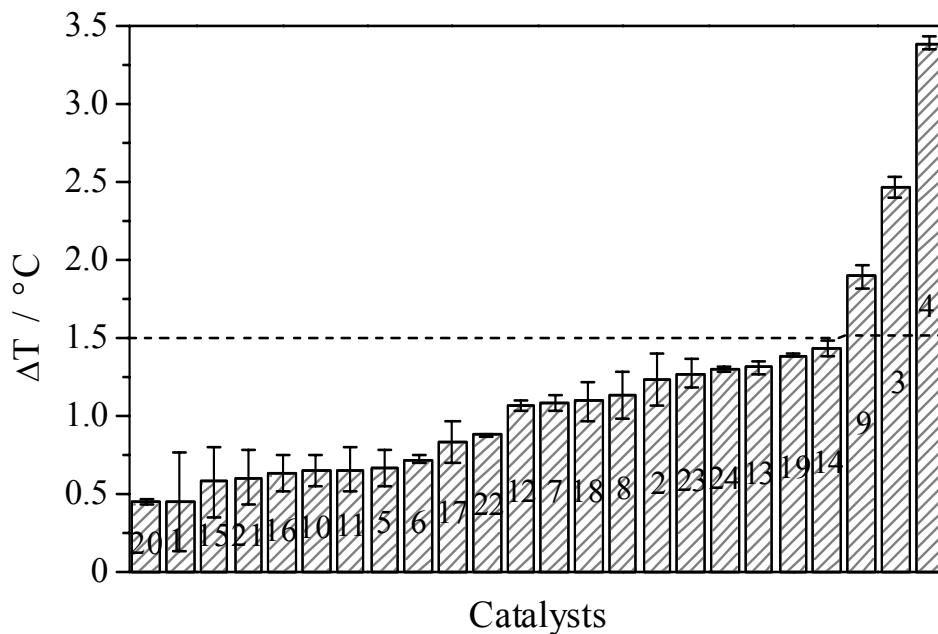


Figure 3.12 Heat increase ΔT of $\text{Pt}_y\text{K}_z\text{Ce}_{100-y-z}\text{O}_x$ catalysts, for details see Table 7.7, measured by ecIRT

3.3.3 Evaluation of high throughput technology

In order to test the reliability of the results of $\text{Pt}_y\text{K}_z\text{Ce}_{100-y-z}\text{O}_x$ catalysts, measured by ecIRT, the samples were validated conventionally by TG-DTA. This analysis method allowed qualitative measurements of soot weight loss dependent from temperature and time to give information about oxidation rates and also allows a comparison of temperature T_{50} between single catalysts.

Five PrintexU model soot samples of about 2 mg were oxidized to determine the reproducibility using TG-DTA. The conversion curves are presented in Figure 3.13 and their standard deviation of temperature T_{50} was found to be ± 2 °C. Also the reproducibility of homogeneity of the model soot to catalyst mixtures was measured each time five times for three different catalyst compositions. The soot and catalysts, at a weight ratio of 1:4, were mixed by spatula and measured by TG-DTA at temperatures of up to 700 °C.

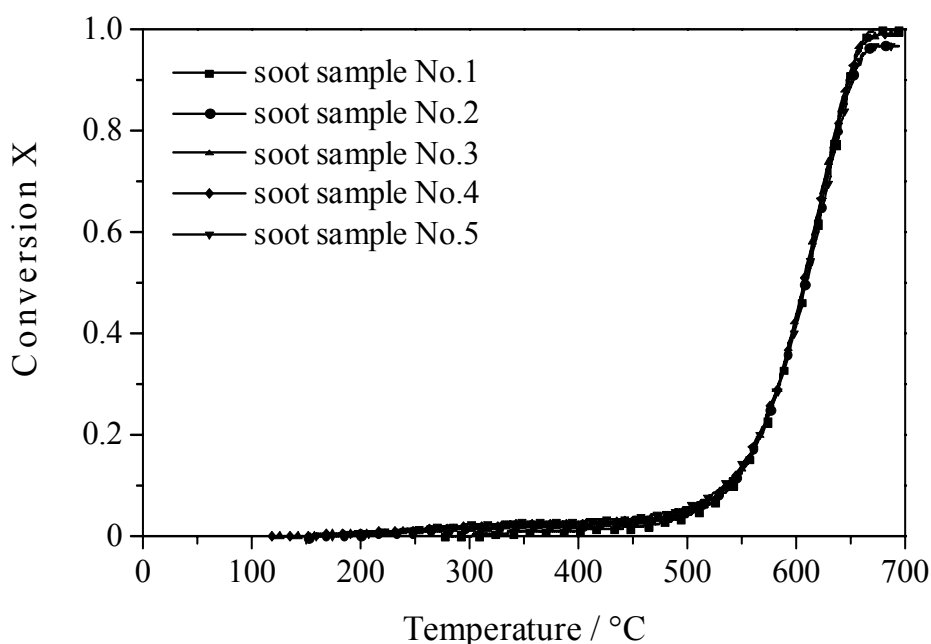


Figure 3.13 Reproducibility of the model soot oxidation measured by TG-DTA; measurement conditions: temperature ramp of 10 °C min⁻¹, volume rate of 100 ml min⁻¹ and 20% O₂ in N₂

The standard deviation of T_{50} -value at the temperature of 50% soot removal for the catalysts from the same batch was ± 2 °C, and ± 4 °C when the catalysts were newly produced each time. Based on these results the reproducibility is excellent.

The most active catalysts of the Pt/K/Ce composition identified by ecIRT at temperature of 400 °C were subsequently verified using TG-DTA, and the order of their activities was compared between the different measurement approaches. General provisions are for ecIRT measurement the higher the heat increase ΔT the higher is the activity of the catalyst and for TG-DTA the lower the temperature T_{50} the higher is the catalytic activity. The results are summarized in Table 3.2 and show that the order of the best catalysts measured by TG-DTA is very close to the order of the most active catalysts measured by ecIRT. Hence it can be concluded that the catalysts showing high catalytic activity determined by high throughput screening are the most active catalysts measured by TG-DTA. However, the conventional analysis is required to find the exact combustion temperature T_{50} of the potential catalysts investigated by HTT.

Table 3.2 Comparison of activity order of catalysts, for details see Table 7.7, on the basis of heat increase ΔT measured by ecIRT and on the basis of temperature T_{50} measured by TG-DTA

Sample No.	ecIRT ΔT (°C)	Order of activity	TG-DTA T_{50} (°C)	Order of activity
4	3.39	1	436	1
3	2.47	2	456	3
9	1.90	3	449	2
14	1.43	4	462	5
19	1.39	5	475	7
13	1.31	6	471	6
24	1.30	7	458	4

3.3.4 Discussion

Two preparation methods of automated soot deposition, and a mixture of soot and catalyst by spatula, were studied to determine their suitability for the detection of relative activity by ecIRT. In both methods the loose contact mode was used to simulate practical conditions. The following findings were made.

The automated soot deposition method was found:

- to be very quick
- the soot was not dispersed over the carrier inserted in a well, but formed a soot layer on the surface
- the soot layer was homogenous
- no intensity change was detected by ecIRT when using the impregnation method
- the samples prepared by sol-gel process were expelled by the blast of soot dispersion

Manual mixing of the soot and catalyst by spatula is:

- time-consuming, though
- a direct contact between soot and catalyst is present
- the intensity change is reliably measured by ecIRT
- the order of activity measured by parallel screening is confirmed by TG-DTA
- homogenous mixtures are achieved
- the measurement is reproducible

The relative temperature change measured in the mixtures of soot and catalyst at different positions within the reactor chamber was found to be similar, showing that the activity was independent of the position within the sample plate. The difference between the relative activities measured by ecIRT compared to that measured by TG-DTA was assessed. The slots were totally filled with the soot and the catalyst mixtures so that a variation in weight can appear which may explain such differences. Nevertheless the most active catalysts measured by TG-DTA also belonged to one of

the most active catalysts measured by ecIRT. This approach of mixing model soot and catalyst by spatula was reproducible, and given that it was the first high throughput screening of soot oxidation catalysts it is highly suitable for the purpose of this study. Based on these findings the mixture of soot and catalyst was used in this study, since no relative activity by automated soot deposition was measured using ecIRT.

3.4 Characterization of alumina support

Alumina is the most common support used for automotive catalysts. Its main function is to provide the high surface area needed for their dispersion. In this study Saffil catalytic grade (CG) alumina fibers (SAFFIL Ltd, UK) were impregnated with catalysts. Ceramic fibers coated with catalytic layer were applied in DPF elsewhere [170] in order to increase volume assimilation of soot [171], to afford thermal insulation from the high temperatures [172, 173], to reduce pressure drop [174] and to provide mechanical stress [175].

The structure of Saffil CG was characterized in order to analyze the behavior of the low activity detected using ecIRT. Other Saffil HX grade ceramic fibers (SAFFIL Ltd, UK) with properties different from Saffil CG were selected and also characterized, for the purpose of comparing changes in the catalytic activities between the different types of fibers. The pore size distribution of the carrier materials was determined by the Barrett-Joyner-Halenda (BJH) method and their specific surface area was obtained by the Brunauer-Emmet-Teller (BET) method. The crystalline phases were identified using X-ray diffractometer (XRD), and the catalysts distribution on alumina and the structure of fibers were investigated by scanning electron microscopy (SEM). Elemental analysis of the catalysts was carried out by means of inductively coupled plasma optical emission spectrometry (ICP-OES) and the catalytic effect of the coated fibers and catalysts was analyzed by thermogravimetric analysis (TGA). The purpose of this analysis was to determine the influence of different concentrations on the catalytic activity.

3.4.1 Pore structure and surface area

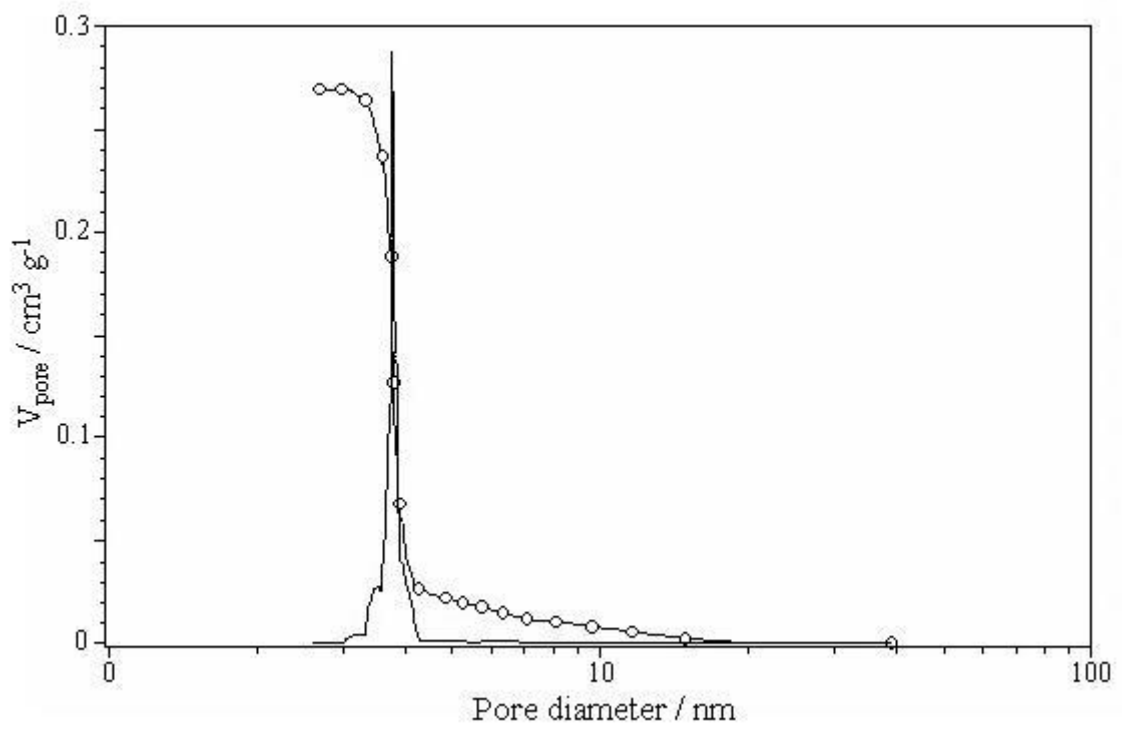
The BET surface area of Saffil CG and Saffil HX ceramic fibers, and their pore size distributions, the cumulative pore volume, and median and maximum at pore width were determined and the data are summarized in Table 3.3.

Table 3.3 BET surface area and pore size distribution of alumina supports

Support material	BET ($\text{m}^2 \text{g}^{-1}$)	Median at pore width (nm)	Maximum at pore width (nm)	Cumulative pore volume ($\text{cm}^3 \text{g}^{-1}$)
Saffil CG	148.7	3.78	3.77	0.27
Saffil HX	< 5	7.28	5.43	0.02

The results show that Saffil CG has BET surface area of $145 \text{ m}^2 \text{g}^{-1}$ whilst Saffil HX is a non-porous material. It is clear that Saffil CG has a pore volume of about $0.3 \text{ cm}^3 \text{g}^{-1}$ in contrast to the nearly non-porous Saffil HX with a pore volume of only $0.02 \text{ cm}^3 \text{g}^{-1}$. The pore size distribution of support materials is depicted in Figure 3.14 and presents that Saffil CG has a narrow pore size distribution characterized by a close monomodal pore size distribution with median and maximal pore widths around 4 nm. The Saffil HX also exhibits a narrow pore size distribution ranging from 3 to 12 nm with a multimodal structure with a maximum peak width at 5 nm and a median at a pore size of 7 nm. Both kinds of alumina fibers are classified as mesoporous.

(a)



(b)

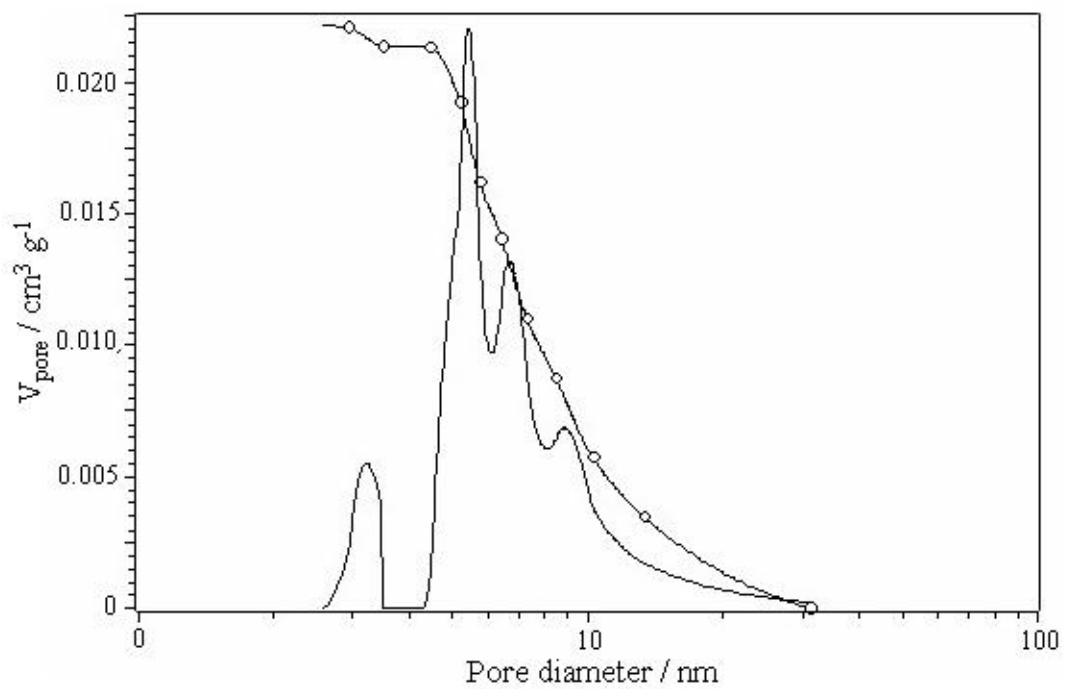


Figure 3.14 BJH pore size distribution of Saffil CG (a) and Saffil HX (b) ceramic fibers

3.4.2 X-ray diffraction analysis

The Saffil CG and Saffil HX fibers were analyzed using Bruker-AXS D8 diffractometer to determine their phase compositions. The XRD pattern of Saffil CG is presented in Figure 3.15. The Saffil CG XRD pattern shows a few very broad reflections that are clearly visible at a 2θ angle of 36.7, 40.0, 45.9 and 66.9. Saffil CG fibers contain two alumina phases with reflections at a 2θ angle of 39.5, 45.9 and 66.9 indicating to γ - Al_2O_3 and reflections at a 2θ angle of 31.5, 36.7, 40.0, 44.8 and 67.3 representing θ - Al_2O_3 . In the 2θ reflection range between 30 and 80 angles θ - Al_2O_3 was determined without forming obvious peaks.

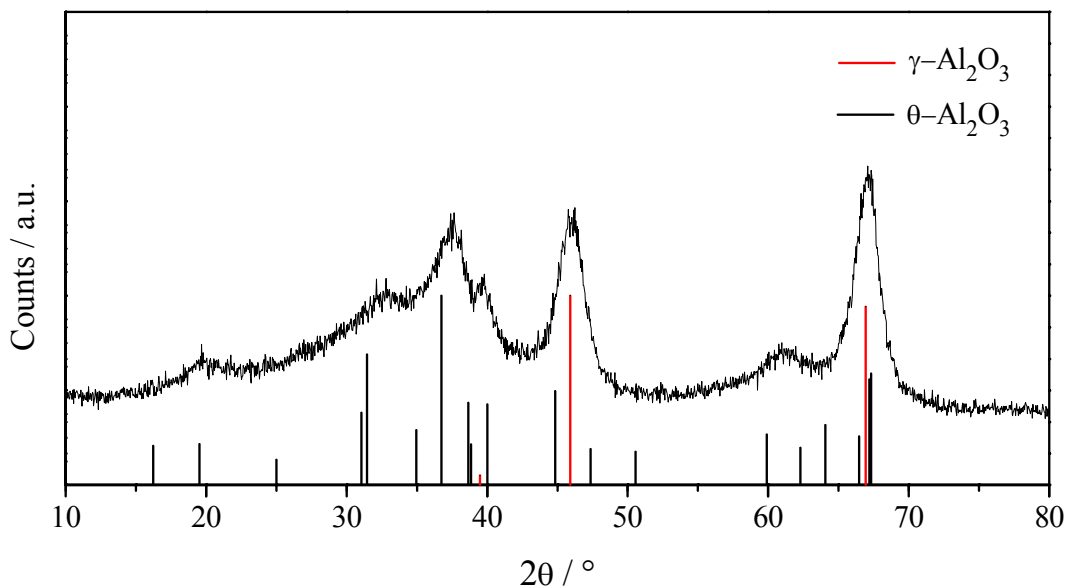


Figure 3.15 XRD patterns of Saffil CG ceramic fibres

Saffil CG consists of highly amorphous phases confirmed by the broader peaks, with a maximum amorphous peak observed at a 2θ angle of approx. 38. It is difficult to differentiate between γ - Al_2O_3 and θ - Al_2O_3 alumina as they have a less crystalline carrier with broad peaks.

In Figure 3.16 a pattern is depicted corresponding to Saffil HX. In this case a series of narrow reflections of different phases are observed, relative to the Saffil CG pattern.

The reflection represents α - Al_2O_3 , for instance, at a 2θ angle of 25.6, 35.1, 43.4, 52.6, 57.5, 68.2 and 76.9. θ - Al_2O_3 is indicated at a 2θ angle of 31.64, 32.88, 36.72 and 67.64, and also $3\text{Al}_2\text{O}_3 \cdot 2\text{SiO}_2$ (mullite) at a 2θ angle of 16.4, 26.0, 26.3, 35.3 and 40.9. The reflection at a 2θ angle of 19 shows the maximum amorphous peak, and Saffil HX indicated fewer amorphous phases.

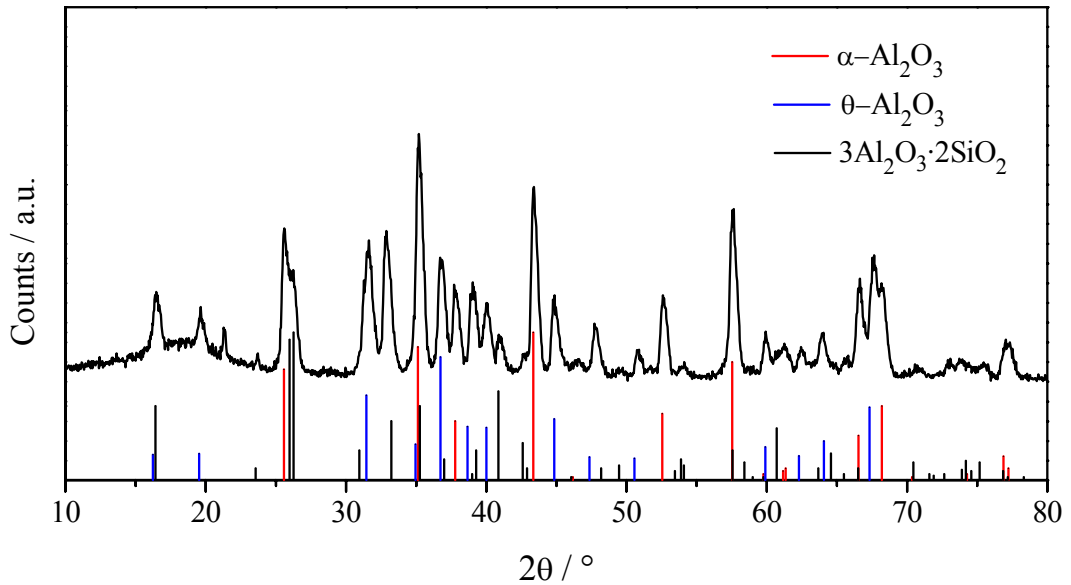


Figure 3.16 XRD patterns of Saffil HX ceramic fibers

3.4.3 Structure characteristics

The structural features of the Saffil CG and Saffil HX alumina fibers and the catalyst dispersion onto these materials were determined by scanning electron microscopy (SEM). The SEM images of Saffil CG and of Saffil HX are presented in Figure 3.17 and show that both appear to be very uniform in diameter, with a smooth surface and round cross-section. The calculated median diameters from the SEM images are $3.3 \pm 0.4 \mu\text{m}$ for Saffil CG and $3.9 \pm 0.6 \mu\text{m}$ for Saffil HX respectively, with abundant pores observed on the surface of Saffil CG fibers. Both types of fibers were impregnated with a $\text{Pt}_5\text{K}_{10}\text{Ce}_{85}\text{O}_x$ catalyst dispersion (Figure 3.17 c and f). This cannot be observed on the Saffil CG fibers, but on Saffil HX fibers agglomerates of various sizes and irregular shape were formed which are clearly shown in Figure 3.17 f.

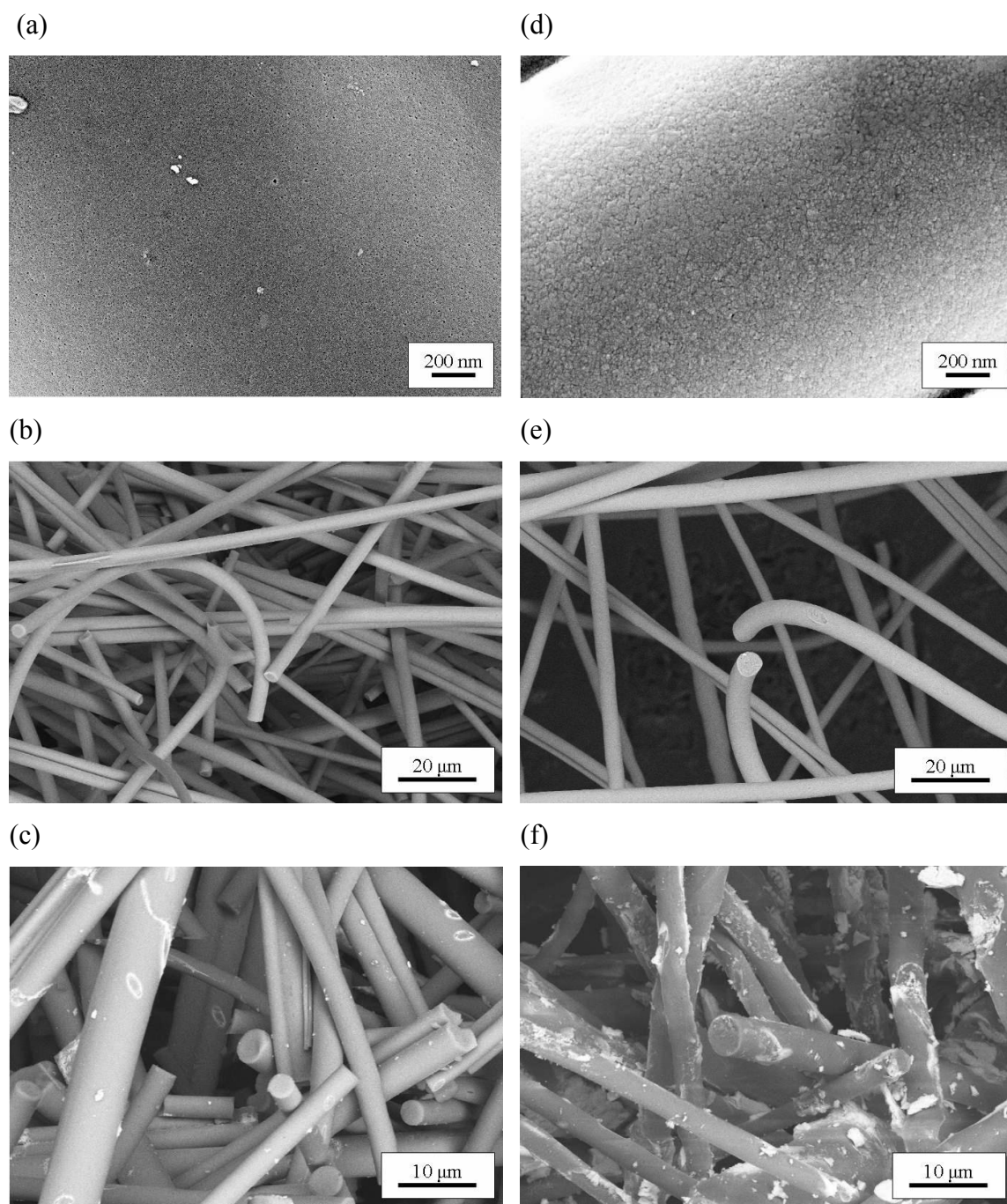


Figure 3.17 SEM micrographs of uncoated Saffil CG (a-b) and Saffil HX (d-e) alumina supports. $\text{Pt}_5\text{K}_{10}\text{Ce}_{85}\text{O}_x$ catalyst coated onto Saffil CG (c) and Saffil HX (f) fibers at a concentration rate of 0.55 mol l^{-1} .

3.4.4 Concentration influence on combustion temperature

The temperature T_{50} of alumina Saffil CG and Saffil HX impregnated with $\text{Pt}_5\text{K}_{10}\text{Ce}_{85}\text{O}_x$ catalyst solutions at a range of concentrations was investigated and compared with the temperature T_{50} of the unsupported catalysts to determine the concentration influence. The amount of the unsupported catalysts corresponded to the amount of catalysts coated onto the fibres.

The temperature T_{50} of the mixtures as a function of concentration was studied by TGA. The temperature was increased from ambient to 110 °C and was held for 30 minutes to evaporate the fibers moisture content, as Saffil CG contain approx. 6 wt% of moisture at ambient temperature in contrast Saffil HX only 0.5 wt%, at a heating rate of 10 °C min⁻¹ and at a flow rate of 100 ml min⁻¹ of synthetic air (20% O₂, balance N₂) and afterwards raised to a final temperature up to 700 °C in identical conditions.

Firstly the T_{50} -values of ceramic fibers were determined in order to eliminate their catalytic activities. Thus fibres and soot at a weight ratio of 14:1 were mixed by spatula and analyzed five times by TGA. The model soot samples of 1 mg were oxidized using the same condition to determine the T_{50} -value and reproducibility. The results of T_{50} -values and standard deviation σ_{T50} of fibres compared to pure model soot PrintexU are depicted in Table 3.4. The reproducibility of the temperature T_{50} of soot oxidation was found to be ± 1 °C and is therefore excellent. The Saffil CG and Saffil HX feature to be non catalytically active regarding soot combustion, since the T_{50} -values are equal to the one of pure soot and the results were clearly reproducible with standard deviation σ_{T50} of ± 2 °C.

Table 3.4 Temperature T_{50} and standard deviation σ_{T50} of model soot and alumina fibers

	T_{50} (°C)	σ_{T50} (°C)
Model soot	606	1
Saffil SG	603	2
Saffil HX	605	2

Figure 3.18 shows the influence of a concentration range from 0.05 to 0.55 mol l⁻¹ of Pt₅K₁₀Ce₈₅O_x on the temperature T₅₀ without support, in comparison with Pt₅K₁₀Ce₈₅O_x coated onto Saffil CG and Saffil HX alumina fibers. From this figure it is evident that the temperature T₅₀ is strongly affected by support characteristics. Whereas the T₅₀-value at a concentration of 0.05 mol l⁻¹ is identical, 590 °C, for all three cases, the T₅₀-value rose significantly with increasing concentration for the unsupported catalysts, and for Saffil HX coated with the catalyst at 110 and 90 °C respectively. In the last two cases the activity is proportional to the catalyst concentration. It can be concluded that the temperatures T₅₀ of Pt₅K₁₀Ce₈₅O_x and of Pt₅K₁₀Ce₈₅O_x coated onto alumina Saffil HX are nearly equal. On the other hand the T₅₀-values of the Pt₅K₁₀Ce₈₅O_x coated onto Saffil CG remain almost unaffected by concentrations, with a difference of only about 10 °C observed between minimum and maximum concentration. Since the catalysts with no carrier are in intimate contact with the model soot it was expected that the catalytic activity would increase with rising concentration, as shown by the Saffil HX

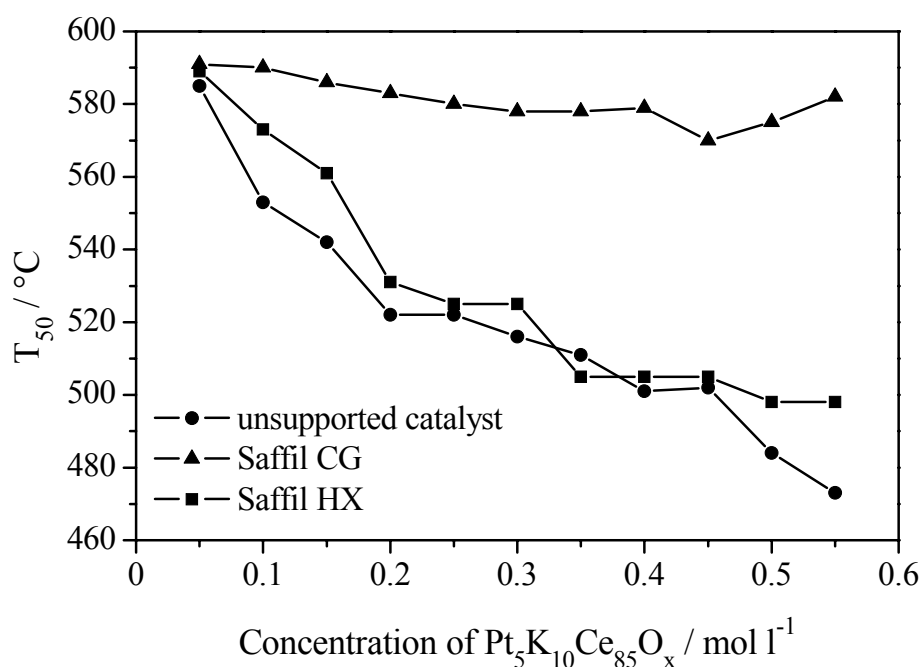


Figure 3.18 Concentration influence on the T₅₀-value. A plot of temperature T₅₀ as a function of concentration of unsupported Pt₅K₁₀Ce₈₅O_x (●) and Pt₅K₁₀Ce₈₅O_x coated onto Saffil CG(▲) and Saffil HX (■) alumina fibers. Measurement conditions: ambient temperature up to 700 °C at a heating rate of 10 °C min⁻¹ (100 ml min⁻¹) in synthetic air (20% O₂, balance N₂).

coated with the catalyst. This is because of the low BET ($<5 \text{ m}^2 \text{ g}^{-1}$), and the low cumulative pore volume ($0.02 \text{ cm}^3 \text{ g}^{-1}$) of the Saffil HX which result in catalyst agglomeration (Figure 3.17 f) on the support surface, providing direct contact with the model soot. The oxidation rate is dependent on the surface area size of the catalyst, therefore the activity is nearly linear. Saffil CG exhibits, in contrast, high surface area ($145 \text{ m}^2 \text{ g}^{-1}$) and high cumulative pore volume ($0.3 \text{ cm}^3 \text{ g}^{-1}$), and it was assumed that the catalysts penetrated into the pores instead of remaining on the surface. The elemental composition of the catalyst was analyzed further, as described in the next paragraph.

3.4.5 Elemental composition of catalyst

The objective of this study was to determine the elemental composition of a $\text{Pt}_5\text{K}_{10}\text{Ce}_{85}\text{O}_x$ catalyst coated onto Saffil CG and Saffil HX alumina fibers, and to interpret the catalytic activity behavior of the supported catalyst, the catalyst preparation is described in Chapter 4.3.2. The concentrations of the Pt, K and Ce stock solutions were determined separately for verification, and the catalyst composition was analyzed by inductively coupled plasma optical emission spectrometry (ICP-OES), see Chapter 4.4.2.

Table 3.5 Elemental analysis of 0.2 molar stock solutions

Nominal element concentration (mg ml^{-1})	Measured element concentration (mg ml^{-1})		
	Pt	K	Ce
Pt 67.57	66.26	n.d.*	n.d.*
K 7.82	0.82	7.56	0.31
Ce 28.02	n.d.*	n.d.*	27.89

* not detected

The elemental composition of 0.2 molar stock solutions is summarized in Table 3.5. The measured Pt, K and Ce concentrations were within 97 and 100% of the nominal values. K was detected in the Pt and Ce precursors at 0.8 and 0.3 mg ml^{-1} , respectively, although no K should be contained and contributed to its higher final concentration in $\text{Pt}_5\text{K}_{10}\text{Ce}_{85}\text{O}_x$ catalyst.

The target and current elemental values of the metals in the coated Saffil CG and Saffil HX are presented in Table 3.6. From the table it is obvious that the measured concentrations of Pt, K and Ce on the Saffil CG fibers were higher than on the Saffil HX fibers. The amount of K on Saffil CG was found to be approx. 20% higher than the nominal amount, which could be explained by the presence of K, previously measured in the Pt and Ce precursors. The Pt concentration of 9.1 mg ml⁻¹ agrees with the nominal concentration of 9.2 mg ml⁻¹. The Ce is the main component in the ternary composition, its measured concentration was 80% of this. The investigated concentrations of all three components coated onto Saffil HX were less than expected. K and Ce were found at only about 70% of the nominal concentration, and Pt content at 80% with the target concentration of 7.6 mg ml⁻¹.

Table 3.6 Elemental analysis of 0.55 molar Pt₅K₁₀Ce₈₅O_x catalyst composition coated onto alumina fibers

Carrier material	Pt (mg ml ⁻¹)	K (mg ml ⁻¹)	Ce (mg ml ⁻¹)
Target	9.23	2.15	65.5
Saffil CG	9.1	2.6	57.7
Saffil HX	7.6	1.4	44.2

A correlation was observed between the specific surface area and cumulative pore volume, and the detected elemental analysis. While Saffil CG shows high BET surface area and high porosity of 150 m² g⁻¹ and 0.3 cm³ g⁻¹ respectively, Saffil HX exhibits low BET surface area of only <5 m² g⁻¹ and is non-porous. The experiment using Saffil CG showed that the catalyst has penetrated predominantly into the pores and is not present on the surface. This is shown by the analysis results, where the measured concentrations of the various elements agree well with the nominal values. The amount of Pt, K and Ce found on the Saffil HX fibers was lower in comparison to Saffil CG fibers. Since the Saffil HX carrier exhibits a low BET surface area and is non-porous, the catalyst is forced to accumulate on its surface forming weakly adhesive surface agglomerates. During the transfer of the loaded fibers it is most likely that some catalyst agglomerates remained in the wells, so concentrations of only 65 to 80% of the nominal single component were detected.

3.4.6 Discussion

Two types of ceramic fibers, Saffil CG and Saffil HX, with different properties were impregnated with catalysts and characterized in order to study the low relative activity measured by ecIRT. The elemental compositions of the catalyst stock solutions and the catalysts coated onto the carriers were analyzed.

The investigation showed that the stock solutions of Pt and of Ce contained additional 15% more K than expected and the detected concentrations of the three metals in their respective stock solutions were in agreement with the nominal values. The amount of catalyst elements supported on the Saffil CG fibers was found to be close to the expected amount, except for K, which was about 20% higher, due to its elevated concentration in the Pt and Ce stock solutions.

The structure characterization of Saffil CG showed high BET surface area of $145 \text{ m}^2 \text{ g}^{-1}$ and high cumulative pore volume of $0.3 \text{ cm}^3 \text{ g}^{-1}$, and its predominant crystalline form is $\theta\text{-Al}_2\text{O}_3$ (boehmit). In order to obtain a loose contact mode the Saffil CG fibers loaded with catalysts were mixed by spatula. The increased catalyst concentration did not affect the temperature T_{50} which remained nearly constant, with a drop of only $10 \text{ }^\circ\text{C}$ observed. The temperature T_{50} at a concentration of 0.05 mol l^{-1} was $591 \text{ }^\circ\text{C}$ but only $582 \text{ }^\circ\text{C}$ was measured at a concentration of 0.55 mol l^{-1} although the total catalyst concentration was detected. This relates to the catalysts penetration and deposition respectively into the pores resulting in poor contact between soot and catalyst. The soot oxidation rate is dependant on the catalyst surface area associated with the active sites which are in contact with soot particles. The contact between soot and catalyst was poor. These observations are in agreement with the results of investigation of ceramic fibers impregnated with catalysts in the literature [176, 177]. It was found that contact between soot and catalyst is of critical importance for the ignition and oxidation of soot, as discussed by several authors [177].

In contrast to Saffil CG the measured concentrations of the single elements loaded onto the Saffil HX fibers was between 20 and 35% lower than the expected catalyst concentration. Saffil HX is non-porous and the crystalline structure is $\alpha\text{-Al}_2\text{O}_3$ (corundum) which has a characteristic low specific surface area ($< 5 \text{ m}^2 \text{ g}^{-1}$). The study

showed that the temperature T_{50} correlates with the catalyst concentration, thus generally it can be concluded that the activity rose with increased concentration. The T_{50} -values were nearly equal to these of the unsupported catalysts. Because of the low BET surface area and non-porosity of Saffil HX, the catalysts agglomerates on the fibers surface, as confirmed by the high catalytic activity at concentration of 0.55 mol l^{-1} , which increased by $90 \text{ }^\circ\text{C}$ for loaded Saffil HX fibers, and by $110 \text{ }^\circ\text{C}$ for the unsupported catalyst. The difference of these $20 \text{ }^\circ\text{C}$ is associated with lower measured concentration of the elements coated onto the carrier caused by losses during the transportation of the loaded carrier from the slot where the catalysts remained.

3.5 Soot characterization

A commercially available model soot, PrintexU (Degussa AG, Frankfurt), was used in this study and was characterized by structure and composition. The soot structure was investigated by transmission electron microscopy (TEM), measuring primary particle size, and its specific surface area was obtained using the Brunauer-Emmet-Teller (BET) method. The soot composition was determined by elemental analysis of C, H, N, O and S.

An image of soot particles is shown in Figure 3.19. The model soot consists mainly of spherical particles, which coagulate into chain-like agglomerations. The soot's mean primary particle diameter of 30 nm was calculated from TEM micrographs and the BET surface area of about $99 \text{ m}^2 \text{ g}^{-1}$ was determined. These results are summarized in Table 3.7.

Table 3.7 BET surface area and primary particle diameter of model soot PrintexU

	BET ($\text{m}^2 \text{ g}^{-1}$)	Particle diameter (nm)
Model soot	99	30
Standard deviation	0.7	3

The results of the elemental analysis of the model soot are given in Table 3.8. The major element of the soot is carbon at $96 \text{ wt}\%$, with lower concentrations of O at 2.4% , H and N at 0.7 and $0.5 \text{ wt}\%$ respectively and S was present at about 3000 ppm .

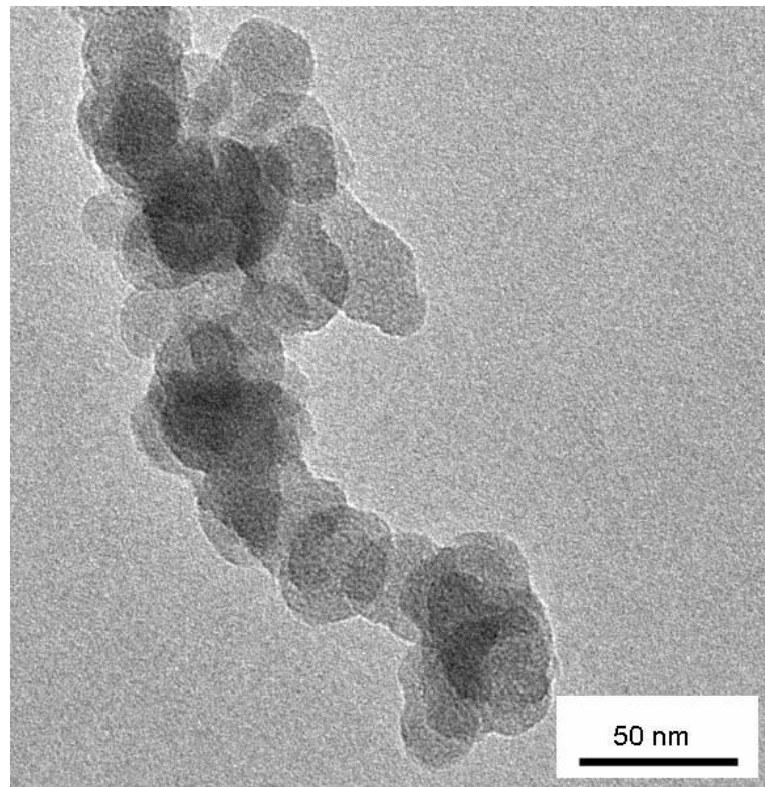


Figure 3.19 TEM micrograph of used model soot PrintexU

When the model soot PrintexU is compared to diesel engine soot [178, 179], it featured on the one hand higher content of C and on the other hand exhibited lower H, O and S amount. The composition of elemental analysis of model soot and diesel soot is depicted in Table 3.8. Neef [47] reported that the model soot has properties very similar to that of diesel engine soot, hence the PrintexU is highly suitable for the execution of experiments in this study.

Table 3.8 Elemental analysis of model soot PrintexU and of diesel engine soot

	Element (wt%)				
	C	H	N	O	S
Model soot	96	0.7	0.5	2.4	0.3
Diesel soot [178]	92.6	2.6	0.4	3.3	0.6
Diesel soot [179]	90.4	4.4	0.2	2.8	0.8

3.6 High throughput design of experiments

3.6.1 Synthesis design

Doped Pt catalysts were studied to find the most efficient and catalytically active and compare them with Pt free catalysts. The pure elements were not included in this thesis since they were widely studied as reported in the literature [180, 47] and moreover the main focus was on catalysts preparation using combinatorial chemistry and their screening by HTT. Moreover the discovery of new catalyst compositions was of greater interest than the refinement of single metal oxides.

Firstly, the starting elements for the oxidation catalysts were selected and the number and type decided. The selection of elements is important in combinatorial strategy and in high throughput synthesis design in order to efficiently plan the experiments to be performed, thus maximizing the amount of experimental combinations. Finally the method of synthesis was taken into account for the combinatorial catalysts development and process development.

There are two strategies which may be used to select elements for use in combinatorial developments [181]. On the one hand elements known in the literature to be catalytically active may be used, on the other hand elements may be selected based on random screens of the periodic table of elements in any combination. Using known elements from the literature decreases the probability of developing novel active materials, whereas the discovery of novel compounds is limited. The second method does not require any previous knowledge of particular components, and novel compounds may be detected. The elements selected for the combinatorial development of oxidation catalysts were based on the previous experimental experiences of N. Olong [182] working in W. F. Maier's research group. Therefore in this work the first strategy based on known elements was used to select the starting elements.

The metal oxides shown to be catalytically active were separated into Ce, Co and Mn based catalyst groups, and were combined with a second element which resulted from

[182]. To develop new active catalysts the base metal oxide should be combined with the selected element, see Table 3.9, at a specific concentration ratio. The objective of the combination was to vary the concentration of one component, resulting in a concentration change of the other, so-called binary composition spread. The concentration interval was chosen to produce a high number of new compounds to raise the chances of developing new active catalysts for soot oxidation. The highly active binary catalysts were subsequently Pt doped, in a certain concentration range, a so-called ternary composition spread, in order to analyze the influence on catalytic activity and combustion temperature.

The sol-gel approach was selected to synthesize the solid matter (Chapter 3.2 Synthesis evaluation) and was carried out by an automated pipette robot. After the elements were selected and the concentration intervals were determined the preparation steps for the pipette robot were planned at the beginning of the HTE. The catalytic activity of solid matter is dependent on the specific properties of the final powder, for instance; the surface area, pore size, pore volume, particle size and phase formed. These properties are affected by the process parameters, such as drying and calcination. However it is not only these parameters which affect the final activities of the catalysts, but among other factors' also the chemical composition and choice of precursors play an important role. In this thesis the composition spread for the catalyst preparation was established. In order to keep the possible parameter combinations low and hence to obtain a good comparison between the samples it was decided to use a constant calcination rate, temperature, duration, constant synthesis recipes and precursors while the chemical composition was chosen to be the key parameter for the evaluation of HTT.

3.6.2 Screening design

The screening process is depicted schematically in Figure 3.20. It consisted of primary screening, conventional investigation, followed by secondary screening and finally conventional investigation. In the first screening the first generation of catalysts was analyzed and in the second screening the second generation. In the first step, libraries containing several catalyst compositions were prepared and tested. The catalytic activities of the best catalysts from the first generation were confirmed conventionally

by TG-DTA. In the second phase the noble metal effect on the most promising catalysts from the first screening was studied and the best catalysts were subsequently verified by conventional method. The HTE based on Ce, Mn and Co for the development of catalysts for soot oxidation were investigated (Chapter 3.7 Catalysts development), whereas Pt was used as a dopant in the second generation.

In the first screening several catalysts of binary composition spreads were prepared to allow investigation of the composition range. The initial and final concentrations of one component were defined together with a range of concentrations in between. These catalysts were mixed with soot by spatula and were inserted into library wells and placed into the reactor to determine their relative activity by ecIRT (1). The most active catalysts shown from the IR thermography data as so-called “hot spots” were identified, selected (2) and further analyzed by TG-DTA (3) where the conversion rate was determined. The catalysts were compared to each other with respect to their catalytic activity. The binary catalysts identified by TG-DTA as the most active were selected (4), reserved for further work (4a), and used in the preparation of catalysts for a second screening.

Binary solid matter compositions with high catalytic activity detected during the first high throughput screening (4) were doped with noble metal to optimise and to raise its catalytic activity (5). The initial and final concentrations of the dopant were determined and the dopant level varied. The concentration of the lower components of the binary compositions was kept constant, while the concentration of the other components varied with the dopant concentration. For instance in $\text{La}_5\text{Co}_{95}\text{O}_x$ catalyst, the Co concentration varied with Pt level resulting in $\text{Pt}_y\text{La}_5\text{Co}_{95-y}\text{O}_x$ composition. The ternary catalysts doped with Pt were mixed with soot and these were subsequently analyzed by TG-DTA (6). The most active binary (4a) and ternary (4b) catalysts were selected and compared to each other in terms of their catalytic activity for soot oxidation, in order to prove the Pt effect (7). From these results the most active catalysts (8) were characterized (9).

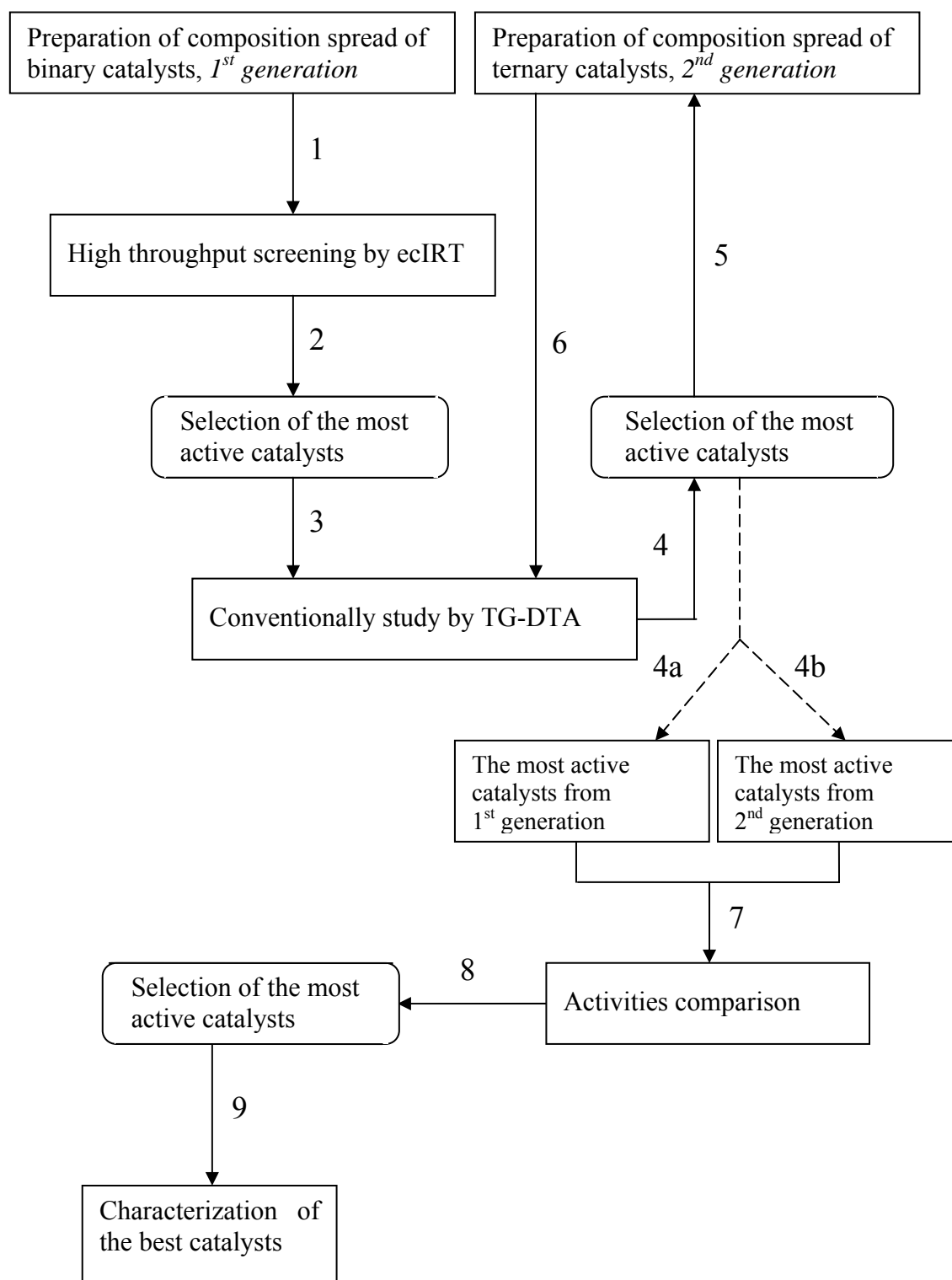


Figure 3.20 Schematic diagram of screening process

Since ecIRT does not provide information on selectivity or stability, additional studies were required. Therefore after the combinatorial procedure was completed the best materials were tested for their stability followed by tests for their activity. In order to determine the stability of catalysts deactivation was performed involving thermal and hydrothermal degradation and catalysts poisoning, for more detail see Chapter 3.8.1. The treated catalysts were characterised according to their physical and chemical properties, and the conversion rate was determined.

3.7 Catalysts development

3.7.1 Ce, Mn and Co based catalysts

A range of compositions of binary catalysts were prepared first for high throughput screening. Each catalyst contained a base element E (Ce, Mn and Co), which was combined with a different secondary element Z, in combinations shown in Table 3.9.

Table 3.9 Combination of base element with selected secondary element

Base element E	Secondary element Z						
Ce	La	Fe	Hf	Sr	Mo	Ag	Zn
Mn	La	Ca	Ce				
Co	La						

The mole ratio range was between 5 and 95 mol% of increments of 5 mol%, which covered the whole composition range. The single precursors, solvents and the concentrations used in these syntheses are summarized in Appendix in Table 7.1. All binary catalysts were first tested by ecIRT at temperatures of 400 and 450 °C. From these results the most active binary compositions were subsequently analyzed by TG-DTA. The results of activities measured by ecIRT expressed as heat increase ΔT and by TG-DTA expressed as temperature T_{50} are introduced and depicted in the following paragraphs.

Co based catalysts

Co oxide catalysts have been reported to be active in soot oxidation [183, 167]. The interaction of CO with Co_3O_4 was described and conversion to CO_2 was observed at temperatures ≥ 50 °C [184]. Although oxygen interacts on the surface of Co_3O_4 at temperatures ≥ 50 °C, it does not significantly promote the CO_2 formation [184]. The activities of Co and La oxide mixtures were tested by ecIRT and are depicted in Figure 3.21. From the ecIRT image it is clear that a heat increase related to an exothermic reaction of soot oxidation with composition of Co and La was measured. Therefore the temperature T_{50} as a function of Co concentration in La was further conventionally studied by TG-DTA.

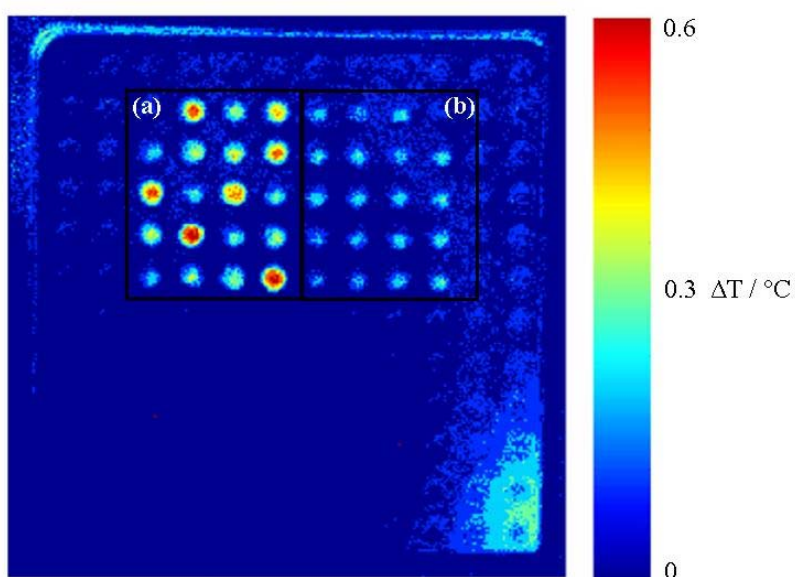


Figure 3.21 ecIRT image of soot oxidation of Co/La (a) and Ce/La (b) composition spreads; measurement conditions: temperature of 450 °C and a volume rate of 100 ml min^{-1} synthetic air

A linear regression of temperature T_{50} as a function of Co/La composition spread measured by TG-DTA is depicted in Figure 3.22. The conventional measurement was determined for Co concentration ranges between 5 and 100 mol% and as can be seen from the graph the combustion temperature T_{50} decreased with increased Co concentration. This indicates that the Co oxide is the active site. A difference of 100 °C of temperature T_{50} was observed between $\text{Co}_5\text{La}_{95}\text{O}_x$ and $\text{Co}_{95}\text{La}_5\text{O}_x$ catalysts. While the T_{50} -value of $\text{Co}_5\text{La}_{95}\text{O}_x$ exhibited only 500 °C, the T_{50} -value of $\text{Co}_{95}\text{La}_5\text{O}_x$ was about 400 °C. Therefore the $\text{Co}_{95}\text{La}_5\text{O}_x$ was Pt doped and studied by TG-DTA. As

can be seen from Figure 3.22 the tendency is shown that the more Co the lower T_{50} and the addition of La leads to Co deactivation.

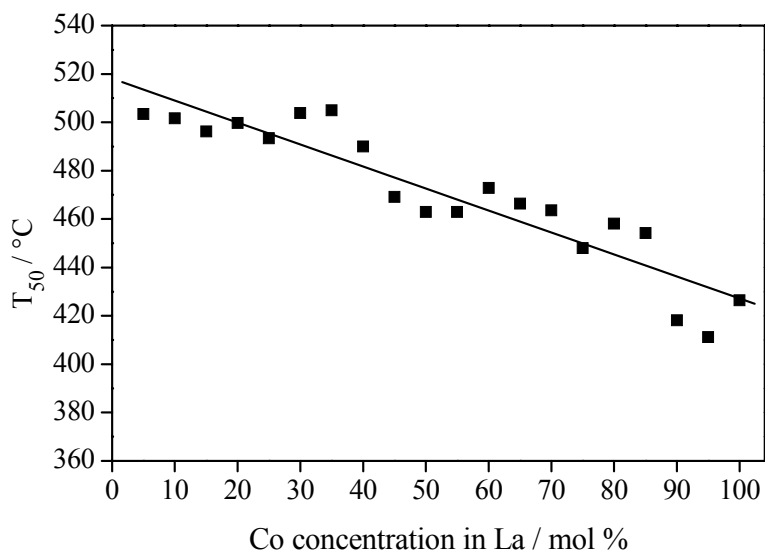


Figure 3.22 Temperature T_{50} as a function of concentration of Co/La composition spread

Catalyst to soot ratio

The influence of $\text{La}_5\text{Co}_9\text{O}_x$ catalyst to soot ratio on catalytic activity was determined by TG-DTA. It is known that the reactions in heterogeneous catalysis occur on the surface of the catalysts itself referred to as active centers. In reaction rate controlled reactions, the activity of catalysts correlates with the number of active centers and hence the purpose is to increase the catalyst surface area in order to maximize the number of active sites by dispersion of catalytic components at the nanoscale. The temperatures T_{50} at different catalyst to soot ratio are summarized in Table 3.10.

Table 3.10 Temperature T_{50} at different catalyst to soot ratios

Temperature	$\text{La}_5\text{Co}_9\text{O}_x$ to soot ratio (wt/wt)								
	0	1	2	3	4	5	6	7	8
T_{50} (°C)	606	438	450	430	411	405	400	400	400

The results of T_{50} -values are plotted as a function of catalyst to soot ratio in Figure 3.23 whereas the catalyst to soot ratio varied between 1:1 and 8:1. The diagram shows the linear effect between catalyst to soot ratio 1:1 and 1:3 while the activity becomes independent resulting in nearly constant temperatures T_{50} from ratio 4:1 and decreases when this ratio decreases. The lowest concentration of optimal activity was found at a ratio of 3.7. To conclude, since the catalyst particle size is defined and thus the active centers through the catalyst mass rise the specific surface area increased, and consequently, the number of active centers resulting in linear catalytic effect. The higher the catalyst to soot ratio the catalytic activity levels.

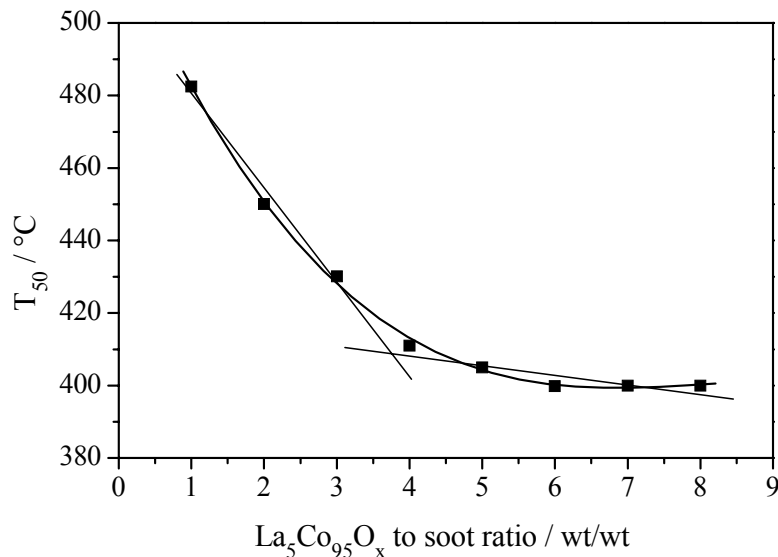


Figure 3.23 Temperature T_{50} as a function of $\text{La}_5\text{Co}_{95}\text{O}_x$ to soot ratio

Mn based catalysts

The activities of Mn oxide catalysts combined with La, Ca and Ce oxides measured by ecIRT at a temperature of 450 °C are shown in Figure 3.24. The composition spread of Mn/La and Mn/Ce oxides exhibit nearly no heat increase ΔT in contrast to Mn/Ca mixtures where higher heat increase was observed. Based on these results at a temperature of 450 °C the catalytic activity was studied conventionally by TG-DTA depending on Ca concentration.

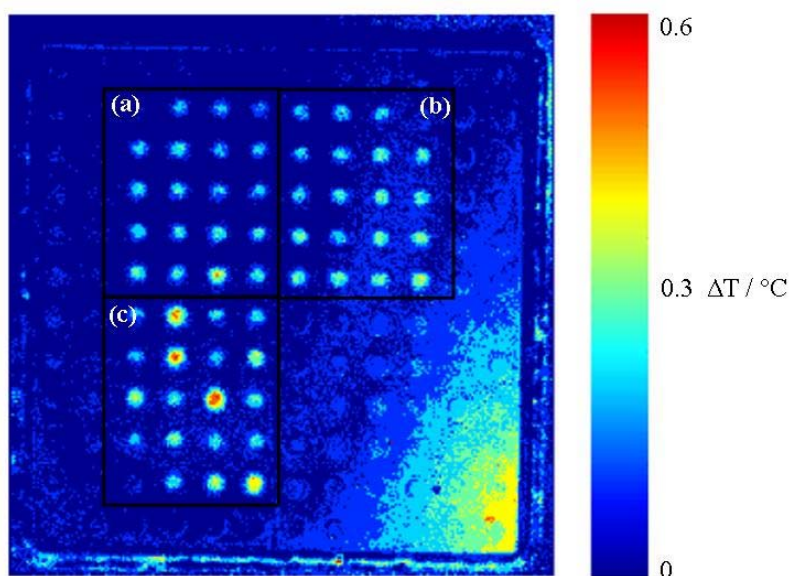


Figure 3.24 ecIRT image of soot oxidation of Mn/Ce (a), Mn/La (b), and Mn/Ca (c) composition spreads; measurement conditions: temperature of 450 °C and at a volume rate of 100 ml min⁻¹ synthetic air

The temperature T_{50} , measured by TG-DTA, is plotted as a function of Mn concentration in Ca and is depicted in Figure 3.25. In order to compare the T_{50} -values all binary and ternary catalysts were prepared under identical conditions, but the preparation of $Ce_yMn_{100-y}O_x$ binary compositions was difficult to prepare in the required form, the catalysts adhered to the vials, therefore the temperature T_{50} was measured for Mn only at a concentration range between 60 and 100 mol%. The T_{50} -value declined with rising Mn concentration as seen in Figure 3.25, indicating that Mn oxide is the active site and that the addition of Ca to Mn results in catalyst deactivation. The T_{50} -values between $Mn_{60}Ca_{40}O_x$ and $Mn_{95}Ca_5O_x$ catalysts differ by 70 °C. The temperature T_{50} of the $Mn_{60}Ca_{40}O_x$ catalyst was approx. 500 °C, whereas of the $Mn_{95}Ca_5O_x$ catalyst it was approx. 430 °C. From these results the influence of Pt on $Mn_{95}Ca_5O_x$ catalyst was studied by TG-DTA.

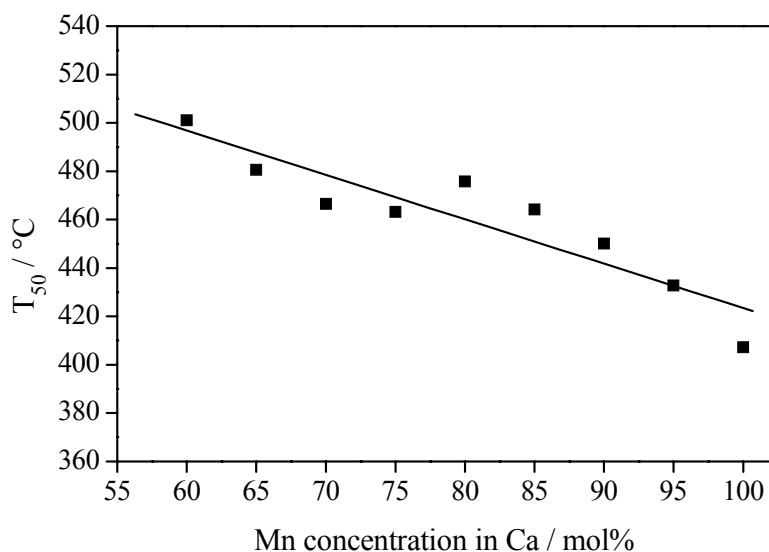


Figure 3.25 Temperature T_{50} as a function of concentration of Mn/Ca composition spread

Ce based catalysts

The activities of soot oxidation of composition spreads of Ce/Fe, Ce/Ag and Ce/Zn oxides were first tested by ecIRT. All catalysts exhibited nearly no activity with the exception of Ce/Ag oxide mixtures. An ecIRT image of soot oxidation of Ce/Fe, Ce/Ag and Ce/Zn catalysts is shown in Figure 3.26. From this image it is obvious that the Ce/Fe and Ce/Zn composition spreads do not exhibit any heat increase ΔT at temperature of 400 °C whereas heat increase ΔT of Ce/Ag oxide mixtures catalysts was determined and therefore studied by TG-DTA.

The temperature T_{50} was measured for Ce at a concentration range of between 5 and 95 mol% by TG-DTA and is plotted as a function of Ce concentration in Ag. The polynomial regression is depicted in Figure 3.27.

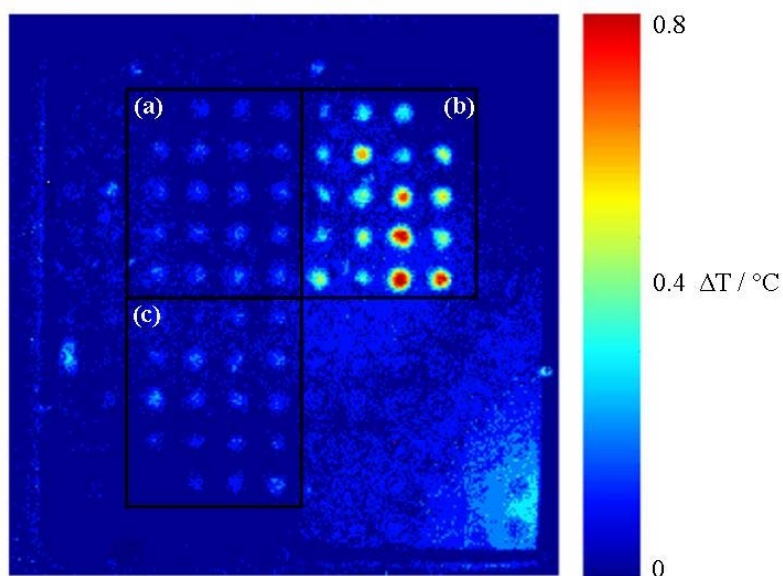


Figure 3.26 ecIRT image of soot oxidation of Ce/Fe (a), Ce/Ag (b), and Ce/Zn (c) composition spreads; measurement conditions: temperature of 400 °C and at a volume rate of 100 ml min⁻¹ synthetic air

The optimum of Ce in Ag for soot oxidation was found to be between 45 and 55 mol%. The temperature T_{50} of $Ce_{50}Ag_{50}O_x$ measured by TG-DTA exhibits about 420 °C, in contrast temperature T_{50} for instance of $Ce_5Ag_{95}O_x$ features about 480 °C and of $Ce_{95}Ag_5O_x$ shows only 490 °C. Due to time limitations, an additional Pt doping could not be tested.

3.7.2 Pt doped binary catalysts

To study the effect of Pt on the binary catalysts, which showed high catalytic activity, a range of ternary composition spreads was prepared. The previous study revealed the most active catalysts were $La_5Co_{95}O_x$ and $Ca_5Mn_{95}O_x$. The ternary composition tested was of $Pt_yLa_5Co_{95-y}O_x$ and $Pt_yCa_5Mn_{95-y}O_x$ respectively, with Pt ranging $y = 0.2-2$ mol% and increment of 0.2 mol%.

Each composition was analyzed conventionally by TG-DTA. The temperature T_{50} is plotted as a function of the dopant concentration and depicted in Figure 3.28. As may be seen from the figure there is a linear relationship between the temperature T_{50} and the Pt

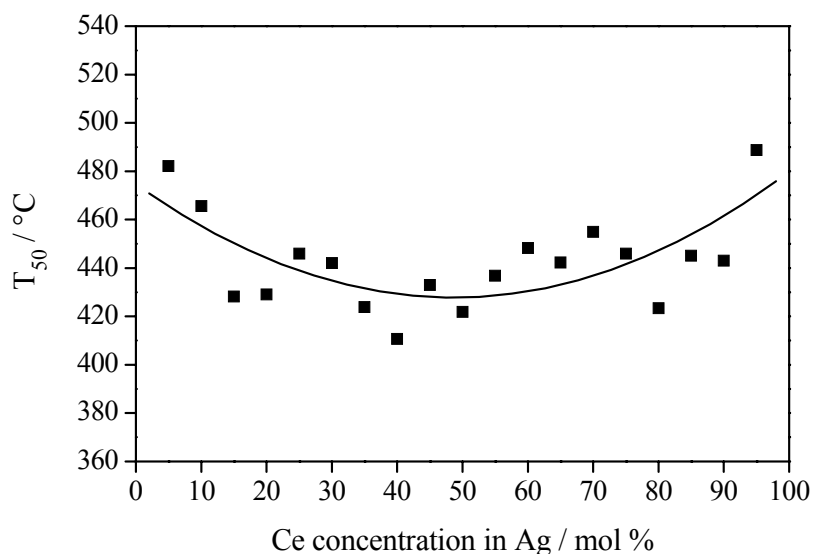
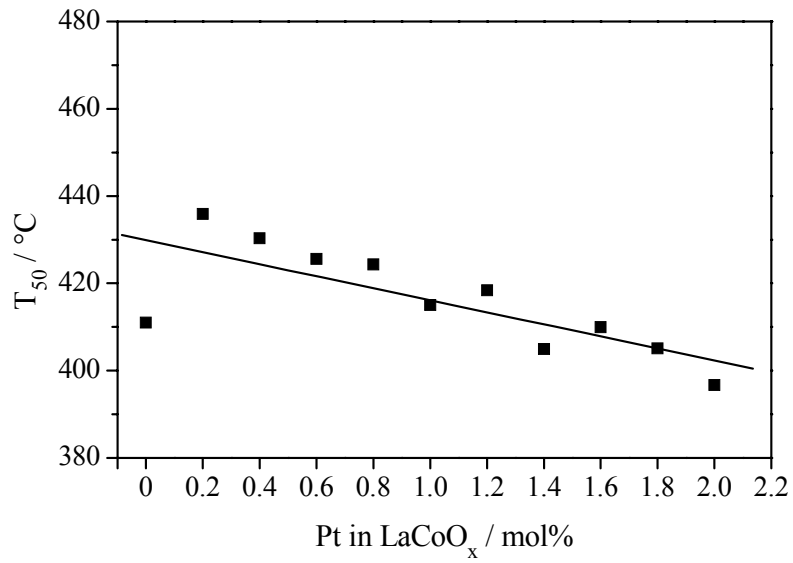


Figure 3.27 Temperature T_{50} as a function of concentration of Ce/Ag composition spread

concentration for both catalyst compositions. Different effects of the Pt were observed with the two mixed oxides, on the one hand for the $\text{La}_5\text{Co}_{95}\text{O}_x$ composition there was a linear increase with higher Pt concentrations, while on the other hand for the $\text{Ca}_5\text{Mn}_{95}\text{O}_x$ composition the opposite effect was observed. A comparison of the catalysts showed the higher Pt concentration in $\text{La}_5\text{Co}_{95}\text{O}_x$, the higher catalytic activity while the higher Pt concentration in $\text{Ca}_5\text{Mn}_{95}\text{O}_x$ deactivated. The T_{50} -values difference between Pt 0.2 and 2 mol% was nearly the same at $\text{La}_5\text{Co}_{95}\text{O}_x$ and at $\text{Ca}_5\text{Mn}_{95}\text{O}_x$ about 40 °C and 30 °C respectively. The effect of Pt compared to Pt undoped $\text{La}_5\text{Co}_{95}\text{O}_x$ and $\text{Ca}_5\text{Mn}_{95}\text{O}_x$ catalysts is shown in Figure 3.28. The temperature T_{50} of $\text{La}_5\text{Co}_{95}\text{O}_x$ features 411 °C and is in the same range as Pt doped, such as $\text{La}_3\text{Co}_{95}\text{Pt}_2\text{O}_x$ exhibits approx. 400°C. However it is assumed the measurement of the $\text{La}_5\text{Co}_{95}\text{O}_x$ catalyst is an anomalous data point, and the same assumption applies to the measurement of $\text{Ca}_5\text{Mn}_{95}\text{O}_x$ catalyst showing the temperature T_{50} of 432°C.

(a)



(b)

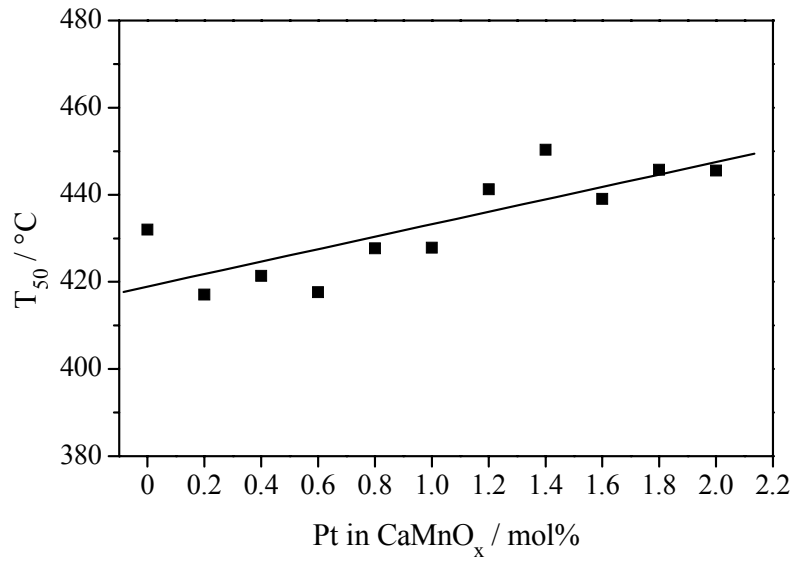


Figure 3.28 Temperature T_{50} of $\text{Pt}_y\text{Co}_{95-y}\text{La}_5\text{O}_x$ (a) and of $\text{Pt}_y\text{Mn}_{95-y}\text{Ca}_5\text{O}_x$ (b) as a function of Pt concentration

3.7.3 Discussion

The different binary compositions based on Ce, Mn and Co were first investigated by ecIRT. The combinatorial analyses showed that $\text{La}_y\text{Co}_{100-y}\text{O}_x$, $\text{Ca}_y\text{Mn}_{100-y}\text{O}_x$ and $\text{Ag}_y\text{Ce}_{100-y}\text{O}_x$ catalysts are the most active soot oxidation catalysts. Maier and Saalfrank [185] reported that oxide mixtures of Co and Mn are highly active materials for CO oxidation at low temperatures and a number of studies reported Co and Mn oxides are active in soot combustion [34]. The $\text{La}_y\text{Co}_{100-y}\text{O}_x$, $\text{Ca}_y\text{Mn}_{100-y}\text{O}_x$ and $\text{Ag}_y\text{Ce}_{100-y}\text{O}_x$ catalysts were studied conventionally by TG-DTA afterwards. The results showed that the temperature T_{50} is not always of a linear increase with rising concentration of the tested element. While linear regression of catalytic activity for $\text{Ca}_y\text{Mn}_{100-y}\text{O}_x$ and $\text{La}_y\text{Co}_{100-y}\text{O}_x$ was determined, polynomial regression for $\text{Ag}_y\text{Ce}_{100-y}\text{O}_x$ was observed. Some studies showed that the reactivity of soot or graphite is proportional to the catalyst concentration [186] whereas other authors reported that concentration has less influence [50]. It is clear, that the catalyst concentration determines the activity levels of individual catalysts, however this is dependant on the characteristics of the catalyst itself. The highly active binary compositions of $\text{La}_5\text{Co}_{95}\text{O}_x$ and $\text{Ca}_5\text{Mn}_{95}\text{O}_x$ were Pt doped subsequently and tested for their catalytic activity using TG-DTA. From the studies clear effects were observed. Whereas the catalytic activity rose with increased Pt concentration doped $\text{La}_5\text{Co}_{95}\text{O}_x$, high catalytic activity was found for $\text{Ca}_5\text{Mn}_{95}\text{O}_x$ with decreased a Pt amount. However, the increase of catalytic activity of $\text{La}_5\text{Co}_{95}\text{O}_x$ is less promoted than of $\text{Ca}_5\text{Mn}_{95}\text{O}_x$ when Pt is added. It was also assumed that the measurement of $\text{La}_5\text{Co}_{95}\text{O}_x$ and $\text{Ca}_5\text{Mn}_{95}\text{O}_x$ catalysts were anomalous data points. $\text{La}_5\text{Co}_{95}\text{O}_x$ exhibited a temperature T_{50} nearly equal to $\text{Pt}_2\text{La}_5\text{Co}_{93}\text{O}_x$. Also the temperature T_{50} of $\text{Ca}_5\text{Mn}_{95}\text{O}_x$ and of $\text{Pt}_2\text{Ca}_5\text{Mn}_{93}\text{O}_x$ showed a difference of only 10 °C. From these results the following binary and ternary $\text{La}_5\text{Co}_{95}\text{O}_x$, $\text{Pt}_2\text{La}_5\text{Co}_{93}\text{O}_x$, $\text{Ca}_5\text{Mn}_{95}\text{O}_x$ and $\text{Pt}_{0.2}\text{Mn}_{94.8}\text{Ca}_5\text{O}_x$ catalysts were studied for their stability. Also their BET surface area, their particle size, structure and crystalline phases were examined further, see the next Chapter 3.8.

3.8 Catalysts characterization

The study showed that mixed oxide catalysts based on Co and Mn exhibit the highest catalytic activity for soot oxidation compared to other investigated binary systems. Therefore catalysts of $\text{La}_5\text{Co}_{95}\text{O}_x$, $\text{Pt}_2\text{La}_5\text{Co}_{93}\text{O}_x$, $\text{Ca}_5\text{Mn}_{95}\text{O}_x$ and $\text{Pt}_{0.2}\text{Ca}_5\text{Mn}_{94.8}\text{O}_x$ compositions were analyzed for their stability and structure and their thermal and hydrothermal stabilities were determined. The influence of SO_2 and of stem on the catalyst stability and activity was investigated. The BET surface area, the crystalline phases, the catalyst structure and particle size were determined. The temperature T_{50} was tested by means of a TG-DTA instrument. The chemical and physical characterization methods mentioned above were applied to freshly prepared and treated catalysts in order to compare their individual properties and behavior.

3.8.1 Catalysts deactivation

The deactivation behavior is important in heterogeneous catalysis, especially in practical applications. The catalytic activity is dependent on the number of active sites which are related to the surface area, and hence to the particle size of the catalyst, therefore the effect of catalyst deactivation on soot oxidation based on the catalyst structure was characterized.

Two modes were used in this study to determine the catalyst stability; thermal degradation and catalyst poisoning. The thermal stability of the catalyst is important to study due to the heat generated during soot combustion and the temperature increase in the trap. For example, local temperature peaks, so-called “hot spots”, up to 1200°C were measured in the literature [187]. These are the kinds of extreme temperatures that the catalyst must be able to withstand in practical conditions.

The SO_2 present is of particular importance since S is contained in both diesel fuel and lube oil. Therefore the activity of catalysts before and after thermal and hydrothermal treatment and exposure to SO_2 as poisoning agent were studied. The degree of deactivation was estimated comparing the temperatures T_{50} of the fresh ones to those

catalysts treated. Thermal aging (dry) was performed under synthetic air conditions, and hydrothermal ageing (wet) was carried out by adding 10% steam to 10% O₂, balance N₂. Catalyst poisoning took place under an atmosphere of synthetic air containing 20 ppm SO₂, 500 ppm NO₂, 10% steam and 10% O₂ in N₂. The samples were placed in an oven, heated to 700 °C and held 70 h. This kind of treatment was used for all the procedures described above.

Specific surface area

The BET surface areas of La₅Co₉₅O_x, Pt₂La₅Co₉₃O_x, Ca₅Mn₉₅O_x and Pt_{0.2}Ca₅Mn_{94.8}O_x catalysts, all freshly prepared and treated with the described deactivation procedure are summarized in Table 3.11. The addition of Pt to La₅Co₉₅O_x when freshly prepared resulted in BET surface area increase of about 40% with the same trend being observed in a Ca₅Mn₉₅O_x sample where the surface area rose considerably, by about 170%. Due to sintering a significant loss of specific surface area, of between 50 and 60% for Pt₂La₅Co₉₃O_x and Mn_{94.8}Ca₅Pt_{0.2}O_x, respectively, was found.

Table 3.11 BET surface area (m² g⁻¹) of freshly prepared and treated catalysts

Catalyst	Fresh	700 °C, 70 h dry	700 °C, 70 h wet	700 °C, 70 h wet, SO ₂ /NO ₂
La ₅ Co ₉₅ O _x	25	11	7	8
Pt ₂ La ₅ Co ₉₃ O _x	35	17	12	13
Ca ₅ Mn ₉₅ O _x	20	8	5	4
Pt _{0.2} Ca ₅ Mn _{94.8} O _x	54	20	7	6

The presence of steam also led to a loss of specific surface area of the catalysts. Pt_{0.2}Ca₅Mn_{94.8}O_x lost the largest BET surface area of 87% between the fresh and hydrothermal aged states, whereas the lowest BET surface area decline of 66% was observed in Pt₂La₅Co₉₃O_x. The BET surface area of the catalysts dropped by an average of about 20% between the dry and wet treatments, with the BET surface area of the Pt₂La₅Co₉₃O_x sample being the most affected by the aging treatment procedure. From Table 3.11 it is evident that the presence of SO₂/NO₂ did not affect the specific surface area modification.

Determination of temperature T_{50}

The temperatures T_{50} of fresh catalysts were measured and compared to that of aged catalysts under different air conditions at 700 °C for 70 h. The summarized data are presented in Table 3.12. All catalysts exhibit a slight loss of temperature T_{50} , approx. 20 °C, after the thermal treatment, except for $\text{Ca}_5\text{Mn}_9\text{O}_x$ showing a difference of 40 °C. In contrast the results show a drop of the T_{50} -value for all samples after hydrothermal treatment, which corresponds to sintering resulting in significant BET surface area decrease. As already presented in the previous paragraph the $\text{Pt}_{0.2}\text{Ca}_5\text{Mn}_{94.8}\text{O}_x$ catalyst lost the largest BET surface area resulting in a decrease of T_{50} -value of just over 70 °C. This was also measured for $\text{Ca}_5\text{Mn}_9\text{O}_x$ whereas the other catalysts had an average drop of 50 °C.

Table 3.12 Temperature T_{50} (°C) of freshly prepared and treated catalysts

Catalyst	Fresh	700 °C, 70 h dry	700 °C, 70 h wet	700 °C, 70 h wet, SO_2/NO_2
$\text{La}_5\text{Co}_9\text{O}_x$	411	434	467	508
$\text{Pt}_2\text{La}_5\text{Co}_9\text{O}_x$	397	427	445	500
$\text{Ca}_5\text{Mn}_9\text{O}_x$	433	477	510	505
$\text{Pt}_{0.2}\text{Ca}_5\text{Mn}_{94.8}\text{O}_x$	417	434	488	487

The Mn based catalysts were not deactivated by SO_2/NO_2 , since the same temperature T_{50} was determined after hydrothermal treatment. Conversely the T_{50} -value of Co based catalysts increased after SO_2/NO_2 treatment. The T_{50} -value rose for both Co containing catalysts by almost 100 °C when exposed to S. However on the contrary only a 70 °C increase of the T_{50} -value of the $\text{Ca}_5\text{Mn}_9\text{O}_x$ catalyst was detected.

The temperature T_{50} is plotted as a function of the specific surface area and depicted in Figure 3.29. In the figure the results are presented of freshly prepared, thermal and hydrothermal treated $\text{La}_5\text{Co}_9\text{O}_x$, $\text{Pt}_2\text{La}_5\text{Co}_9\text{O}_x$, $\text{Ca}_5\text{Mn}_9\text{O}_x$ and $\text{Pt}_{0.2}\text{Ca}_5\text{Mn}_{94.8}\text{O}_x$ samples. From the figure it is obvious there is a correlation between the temperature T_{50} and BET specific surface area of single catalysts; the higher BET specific surface area the higher catalytic activity and vice versa. But comparing two different catalysts with

the same BET surface area the T_{50} -vaules differs and the composition is in this case determining.

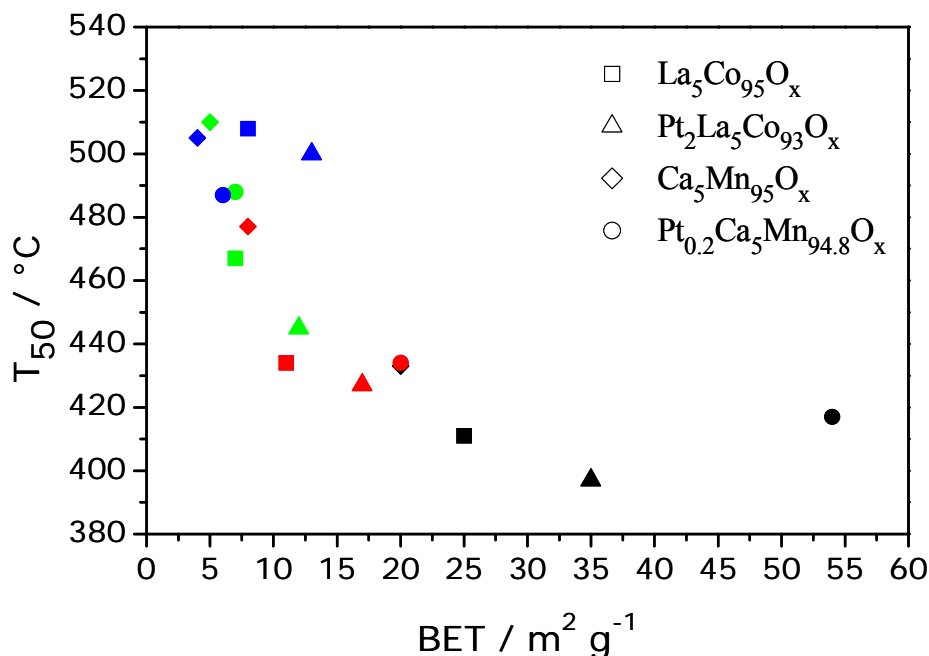


Figure 3.29 Temperature T_{50} as a function of BET surface area; — freshly prepared, — thermal, — hydrothermal, — hydrothermal & SO_2/NO_2 treated samples

3.8.2 X-ray diffraction analysis and structure characteristics

Analysis of the crystalline phase of the $\text{La}_5\text{Co}_{95}\text{O}_x$, $\text{Pt}_2\text{La}_5\text{Co}_{93}\text{O}_x$, $\text{Ca}_5\text{Mn}_{95}\text{O}_x$ and $\text{Pt}_{0.2}\text{Ca}_5\text{Mn}_{94.8}\text{O}_x$ catalysts were carried out by X-ray diffraction (XRD), and their structural features and particle size were determined by scanning electron microscopy (SEM). The freshly prepared, hydrothermal & SO_2/NO_2 treated catalysts were studied using XRD. In contrast the freshly prepared, thermal, hydrothermal, hydrothermal & SO_2/NO_2 treated catalysts were analyzed for their morphology and particle size.

Co based catalysts

The XRD pattern of freshly prepared and hydrothermal & SO_2/NO_2 treated $\text{La}_5\text{Co}_{95}\text{O}_x$ and $\text{Pt}_2\text{La}_5\text{Co}_{93}\text{O}_x$ catalysts, respectively, are shown and compared in Figure 3.30. The reflections of fresh and hydrothermal & SO_2/NO_2 treated $\text{La}_5\text{Co}_{95}\text{O}_x$ are identical at a

2θ angle of 31.27, 36.85, 44.80, 59.35, 65.23 and 94.0, whereas the poisoned sample shows additional reflections at a 2θ angle of 19.00, 28.76 and 29.82. In the XRD pattern only one phase was identified with a position and intensity indicating Co_3O_4 . Both samples consist of crystalline phases and the additional peaks in the treated catalyst indicate that new crystalline phases were formed. The reflections of hydrothermal & SO_2/NO_2 treated $\text{La}_5\text{Co}_9\text{O}_x$ became narrow, which is explained by thermal treatment resulting in crystallite growth. A La_2O_3 phase could not be determined in any of the analyzed catalysts, probably due to a concentration below the detection limit of the XRD.

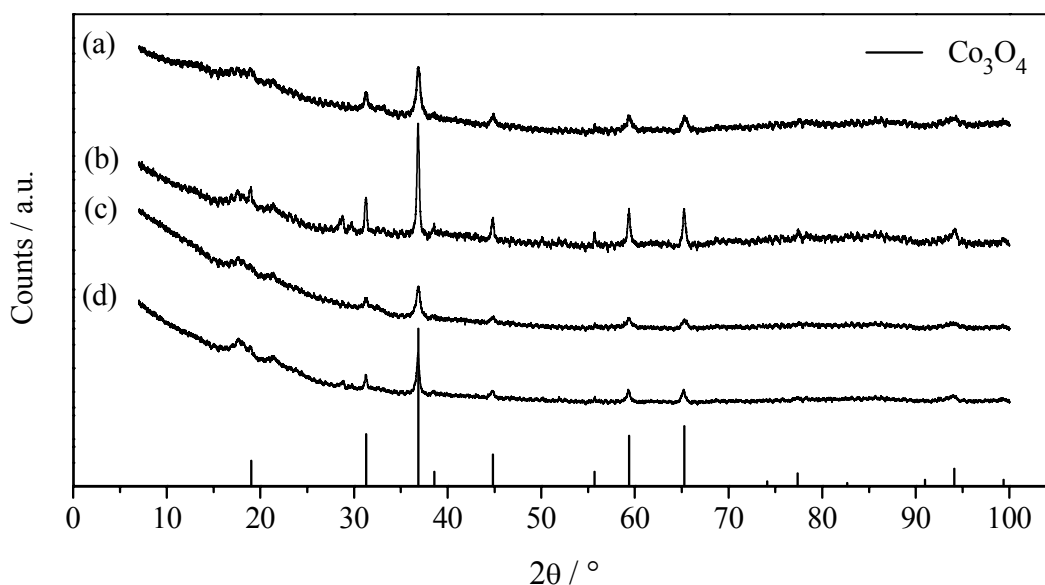


Figure 3.30 XRD patterns of $\text{La}_5\text{Co}_9\text{O}_x$ freshly prepared (a) hydrothermal & SO_2/NO_2 treated (b) and $\text{Pt}_2\text{La}_5\text{Co}_9\text{O}_x$ freshly prepared (c) hydrothermal & SO_2/NO_2 treated (d)

The XRD pattern of the $\text{Pt}_2\text{La}_5\text{Co}_9\text{O}_x$ catalyst showed some peaks were absent when compared to $\text{La}_5\text{Co}_9\text{O}_x$, revealing that no new crystalline phases were formed. The reflections detected at a 2θ angle of 31.27, 36.85, 59.35 and 65.23 indicated Co_3O_4 as already mentioned above. The results show that no modification between the XRD pattern of fresh and hydrothermal & SO_2/NO_2 treated $\text{Pt}_2\text{La}_5\text{Co}_9\text{O}_x$ catalyst could be observed. Neither La_2O_3 nor Pt could be detected due to their concentrations which were also probably below the detection limit of the XRD.

Particular SEM images of $\text{La}_5\text{Co}_9\text{O}_x$ are shown in Figure 3.31 and the overviews are shown in Appendix 7.4. From the images it can be seen that the freshly prepared catalyst exhibits an homogenous particle dispersion forming a foam shape with a mean particle size of between 20 and 40 nm. The bigger particles are angular, while the smaller ones are, in contrast, round. Particle sizes of 25 and 40 nm respectively could be measured in the thermally treated sample. Sintering processes caused clusters to be increasingly formed in the hydrothermally treated sample, but the primary particles could be still recognized. Crystallites were also formed in the poisoned samples, which is in agreement with the XRD analysis.

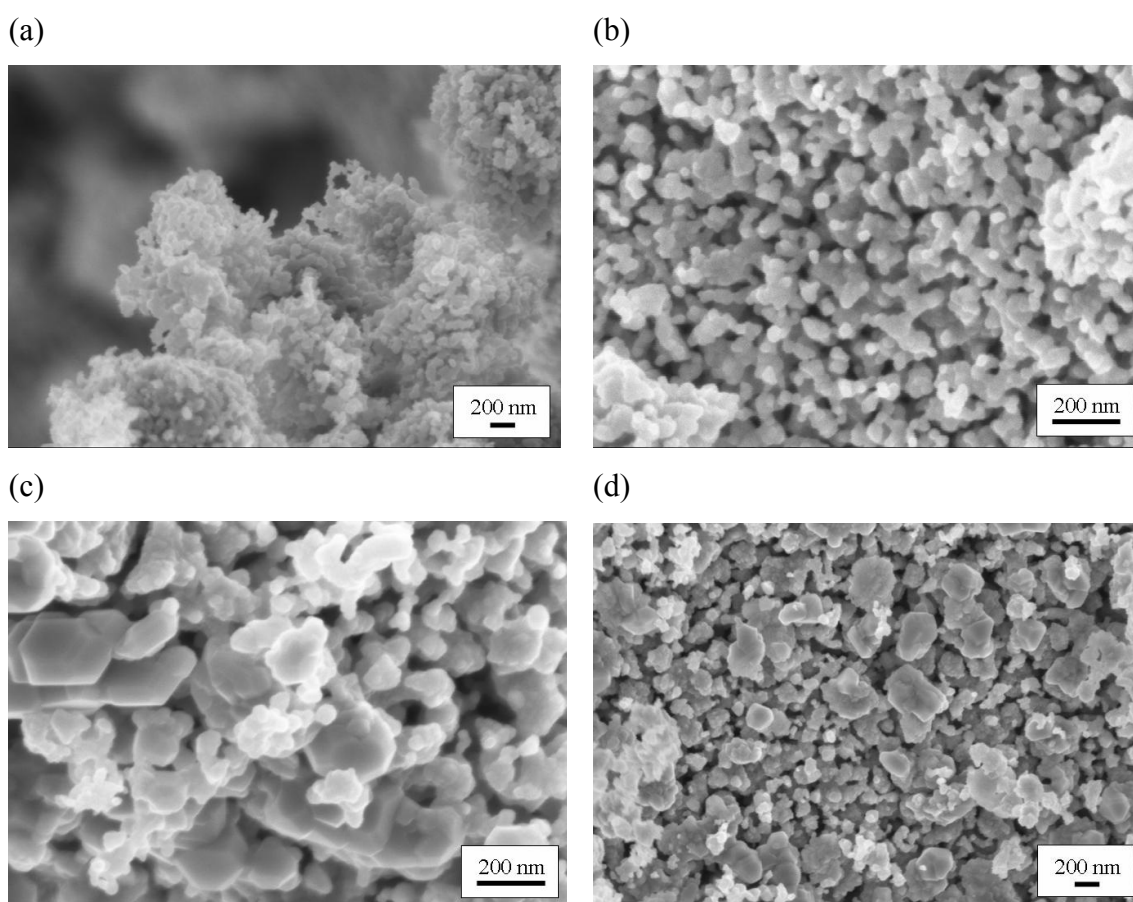


Figure 3.31 SEM micrographs of $\text{La}_5\text{Co}_9\text{O}_x$; freshly prepared (a), thermal (b), hydrothermal (c), hydrothermal & SO_2/NO_2 treated (d). The samples b-d were treated at temperature of 700 °C for 70 h.

The mean particle size of freshly prepared $\text{Pt}_2\text{La}_5\text{Co}_9\text{O}_3$ was measured as 20 to 40 nm. The particles formed irregular shapes similar to foam. Clusters of particles with smooth surfaces were also observed, with the particles showing an homogenous dispersion. The

treated samples exhibit more clusters, which could be explained by sintering, and which were partly porous. The particles in the hydrothermal sample were strongly sintered together in various clusters exhibiting a number of crystallites. These were also found in samples treated in the presence of SO_2/NO_2 . The cluster surface appeared to be smooth containing smooth small plate like particles, and fine particles can also be seen. The SEM images are shown in Figure 3.32 while the overviews are depicted in Appendix 7.4.

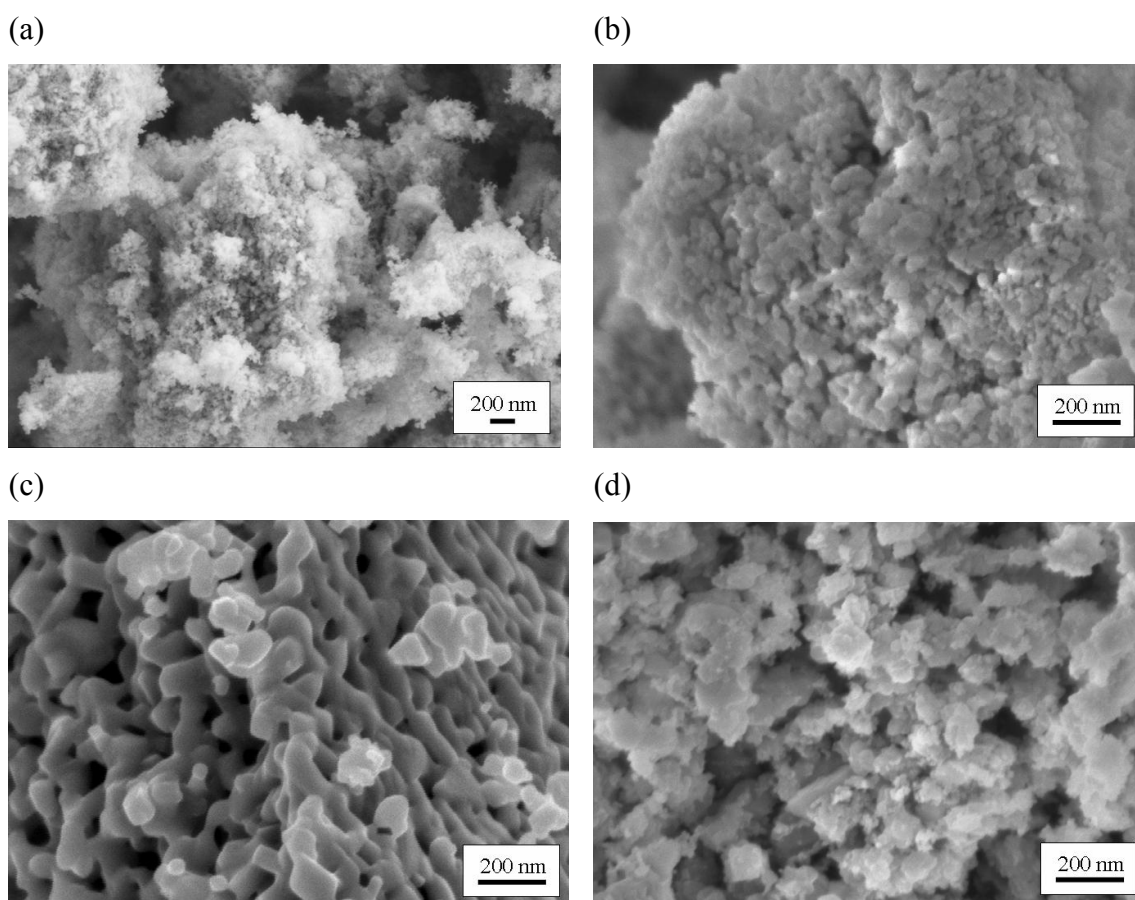


Figure 3.32 SEM micrographs of $\text{Pt}_2\text{La}_5\text{Co}_{93}\text{O}_x$; freshly prepared (a), thermal (b), hydrothermal (c), hydrothermal & SO_2/NO_2 treated (d). The samples b-d were treated at temperature of $700\text{ }^\circ\text{C}$ for 70 h.

Mn based catalysts

Figure 3.33 shows the results of XRD patterns of $\text{Ca}_5\text{Mn}_9\text{O}_x$ and $\text{Pt}_{0.2}\text{Ca}_5\text{Mn}_{94.8}\text{O}_x$ catalysts. These patterns correspond to those of freshly prepared and treated by SO_2/NO_2 samples and show that all the catalysts exhibit crystallinity. The reflections of $\text{Ca}_5\text{Mn}_9\text{O}_x$ are identical at a 2θ angle of 23.12, 32.92, 38.20, 45.14, 49.32, 55.14, 64.05,

65.72 and 67.40 for freshly prepared as well as treated samples, which indicates one phase. These reflections reveal the presence of Mn_2O_3 . Due to the low concentration of Ca in the $\text{Ca}_5\text{Mn}_9\text{O}_x$ catalyst the CaO phase could not be detected as it was probably below the XRD detection limit.

The XRD patterns of $\text{Pt}_{0.2}\text{Ca}_5\text{Mn}_{94.8}\text{O}_x$ (Figure 3.33 c-d) compared to those of $\text{Ca}_5\text{Mn}_9\text{O}_x$ (Figure 3.33 a-b) exhibit reflections at identical angles for both freshly prepared and hydrothermal & SO_2/NO_2 treated catalysts. It may be noted that the mean crystallite size of $\text{Ca}_5\text{Mn}_9\text{O}_x$ was slightly lower than of $\text{Pt}_{0.2}\text{Ca}_5\text{Mn}_{94.8}\text{O}_x$. As already noted above also the Pt could not be found due to its low concentration added to the catalyst composition and probably because of the detection limit of XRD.

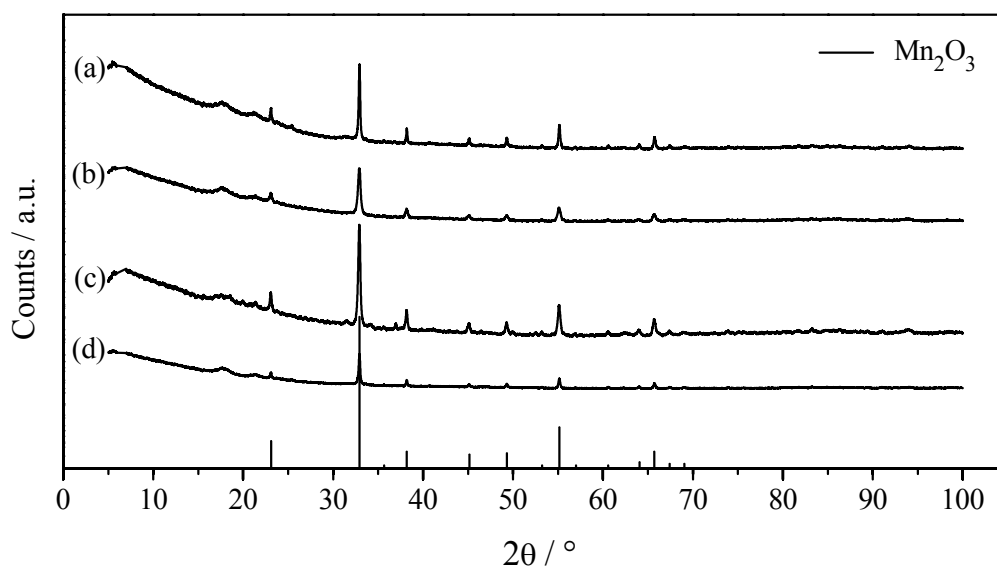


Figure 3.33 XRD patterns of $\text{Ca}_5\text{Mn}_9\text{O}_x$ freshly prepared (a) hydrothermal & SO_2/NO_2 treated (b) and $\text{Pt}_{0.2}\text{La}_5\text{Co}_{94.8}\text{O}_x$ freshly prepared (c) hydrothermal & SO_2/NO_2 treated (d)

Figure 3.34 depicts the particular SEM images of $\text{Ca}_5\text{Mn}_9\text{O}_x$ catalyst and their overviews are presented in Appendix 7.4. The freshly prepared sample formed various clusters in the solid structure. The image Figure 3.34 a shows particles with a mean size of 50 nm forming clusters. The smaller particles are round while the larger ones tend to have an angular shape. The thermally treated sample contains more clusters due to a longer sintering time. Various crystalline structures are formed and the solid matter has

a porous structure. Fewer single particles can be recognized of 60 nm mean size. Due to the presence of the steam the clusters have a crystalline structure and are less porous than those formed in the thermally treated sample, thus single particles could no longer be detected. The deactivated sample consists of strongly sintered particles forming a less porous structure.

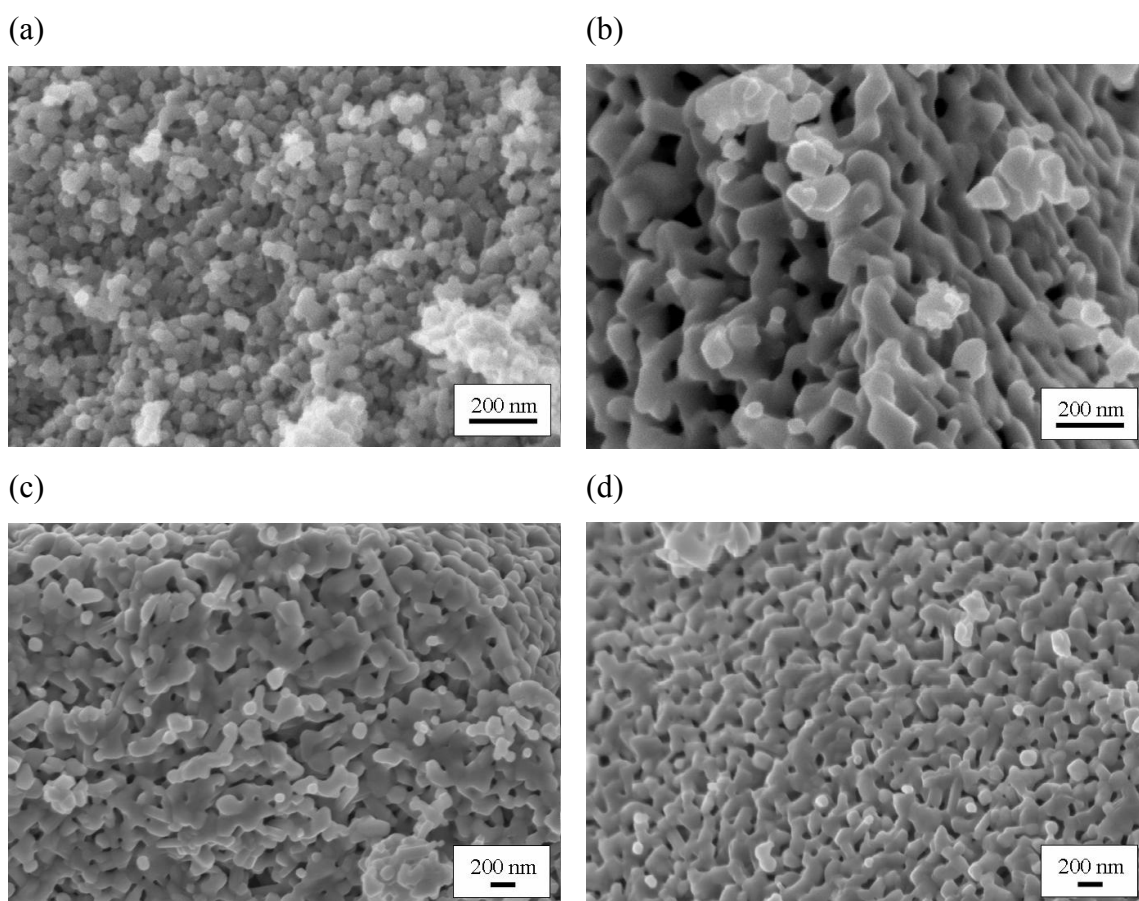


Figure 3.34 SEM micrographs of $\text{Ca}_5\text{Mn}_{95}\text{O}_x$; freshly prepared (a), thermal (b), hydrothermal (c), hydrothermal & SO_2/NO_2 treated (d). The samples b-d were treated at temperature of 700 °C for 70 h.

The $\text{Pt}_{0.2}\text{Ca}_5\text{Mn}_{94.8}\text{O}_x$ catalyst in a fresh condition consists only of clusters of various sizes with a crystalline structure. The images seem to indicate a second phase was formed, and fewer primary particles of 60 nm size can be recognized (Figure 3.35 a). The thermally treated sample consists of clusters that are strongly sintered on the surface in contrast to the porous layer inside. Some particles from 5 up to 10 nm can be found on the surface as well as inside the clusters. The hydrothermal treated clusters exhibit fissures, formed by faster evaporation of the liquid on the surface than from the

interior, producing shrinkage gradients. A crystalline structure is formed containing rod shaped particles, amongst others. The image of the sample treated by SO_2/NO_2 also indicates the formation of a second phase, and strong sintering of the particles into a crystallite structure. The SEM images are depicted in Figure 3.35 and their overviews are shown in Appendix 7.4.

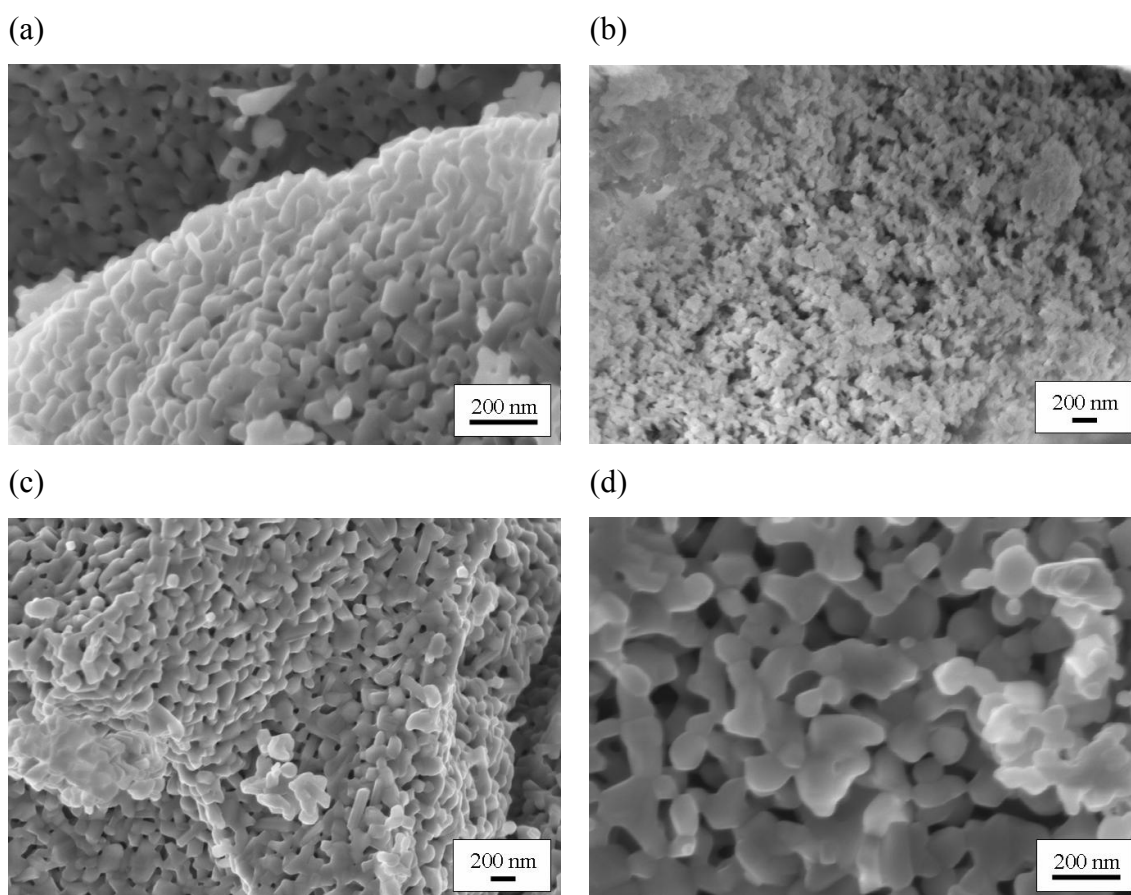


Figure 3.35 SEM micrographs of $\text{Pt}_{0.2}\text{Ca}_5\text{Mn}_{94.8}\text{O}_x$; freshly prepared (a), thermal (b), hydrothermal (c), hydrothermal & SO_2/NO_2 treated (d). The samples b-d were treated at temperature of $700\text{ }^\circ\text{C}$ for 70 h.

3.8.3 Discussion

Deactivation of catalysts based on Co ($\text{La}_5\text{Co}_9\text{O}_x$, $\text{Pt}_2\text{La}_5\text{Co}_9\text{O}_x$) and Mn ($\text{Ca}_5\text{Mn}_9\text{O}_x$, $\text{Pt}_{0.2}\text{Ca}_5\text{Mn}_{94.8}\text{O}_x$) were studied. After hydrothermal treatment at temperature $700\text{ }^\circ\text{C}$ for 70 h the BET surface area significantly dropped approx. 70 % except for $\text{Pt}_{0.2}\text{Ca}_5\text{Mn}_{94.8}\text{O}_x$ where BET surface area loss of 87 % was determined resulting in activity loss. The temperature T_{50} of Co based catalysts decreased by $50\text{ }^\circ\text{C}$ while of Mn

based catalysts approx. by 70 °C. In contrast all catalysts feature thermal stability, only a slight drop of T_{50} -values after thermal aging was determined, except for $\text{Ca}_5\text{Mn}_{95}\text{O}_x$ where drop of 70 °C was measured. It was observed that the loss of specific surface area correlates with the loss of catalytic activity. Mn based catalysts in combination with Ca are resistant to S and N exposure. Indeed the temperature T_{50} of Co based catalysts poisoned by SO_2/NO_2 was reduced by 100 °C.

Chapter 4

4. Experimental setup

4.1 High throughput screening of catalysts

4.1.1 IR thermography setup

The relative catalytic activity of up to 144 different materials placed on each slate library was detected in parallel by emissivity corrected infrared thermography (ecIRT) [188]. This is a primary screening method, which supplies information only about catalysts' activity, however not about selectivity or stability, therefore in order to investigate these characteristics additional tests had to be performed. The principal parts of the IR thermography setup are the IR camera head, the reactor, gas supply, gas flow controller and temperature controller, the schematics for which are depicted in Figure 4.1. The detailed description of the setup design and the individual parts is given below.

IR camera

An IR camera head (Thermosensorik GmbH, Erlangen) with a high performance platinum silica (PtSi) focal plane array (FPA) detector was utilized. An advantageous feature of the detector was its long-term stability of up to 24 h, which was essential for the 6 point calibration. The camera head was equipped with an 8 mm lens of middle wavelength IR (MWIR) in a spectral range of 1-5 μm . The full frame rate for 256 x 256 pixels was 50 Hz and the detector operated with 14 bit resolution. The camera was controlled and operated by the MPS 5 program (multi purpose software) and attached to a tripod over the reactor and adjusted to full library view. Its integration time was adjustable in steps between 0.156 to 20 ms, and when any integration time was set the MPS 5 software [189] selected a time as close as possible to the time entered. The integration time was selected so that the mean intensity value of pixels within the region of interest (ROI) did not exceed 6000 at the temperature of experiment. If the detector

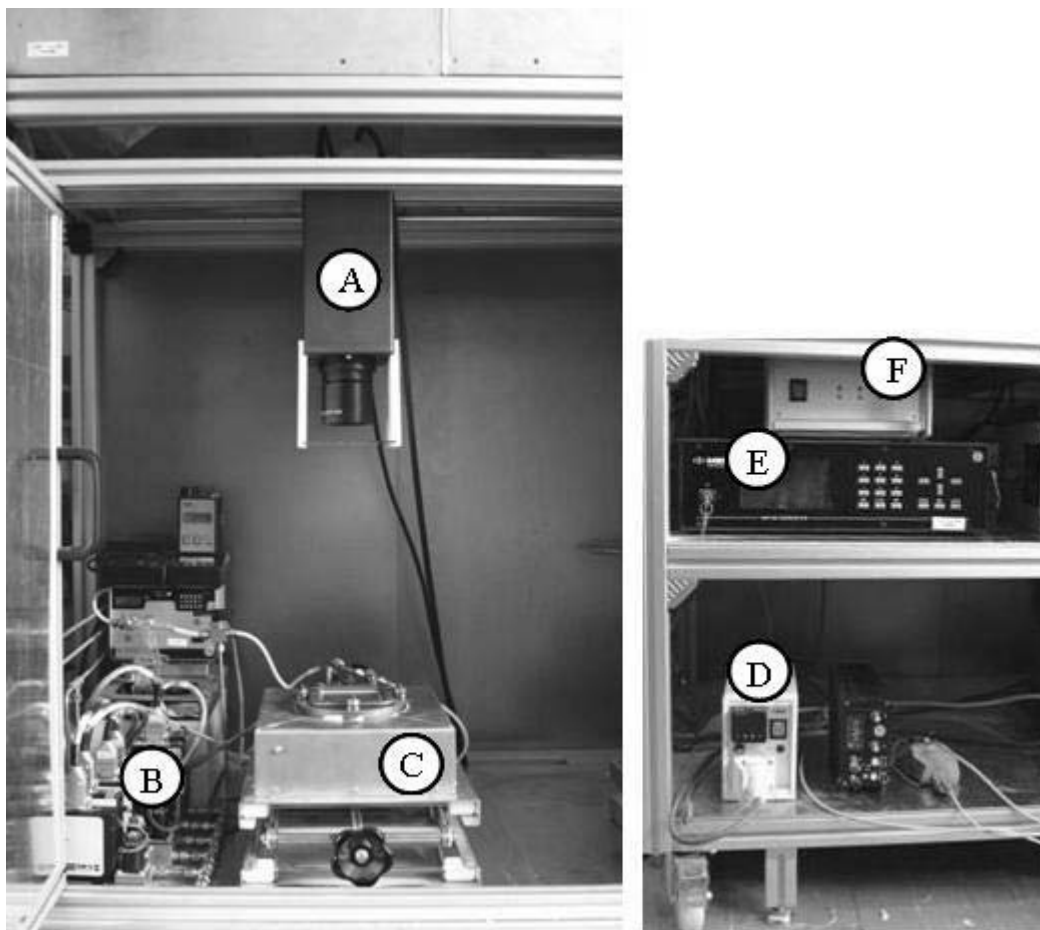


Figure 4.1 Setup of IR thermography; IR camera head (A), gas supply (B), reactor (C), temperature controller (D), gas flow controller (E) and main supply of IR camera head

reaches saturation the data are lost, and this occurred at temperatures above 400 °C, even when the lowest integration time of 0.156 ms was set. Therefore an attenuating borosilicate glass plate 2 mm thick was attached in front of the lens to absorb part of the IR radiation. Consequently, saturation of the detector was prevented while the experiments were performed at higher temperature and the minimal integration time was chosen.

The data were transmitted digitally to the measurement computer by the RS 422 interface. The A/D converter was integrated within the detector head. The exposure and also the display of live images, single images or image sequences were controlled by the MPS 5 program, which also worked at up to 50 frames per second (FPS). It was possible to vary the FPS value continuously using a configuration option to take up to 1000 images in approx. 20 s, and also to calculate an average value. In this way the

noise was reduced. External control of the detector head was performed by another program, and the experiments were automatically controlled. The resulting differential temperature was calculated by the “IRTestRig” program developed by J. Scheidtmann [190] based on modified Stefan-Boltzmann-law (Equation 4.1),

$$M = \varepsilon\sigma T^4 \quad (4.1)$$

where T is the absolute temperature, ε is the emissivity dependent on temperature and σ is the Stefan-Boltzmann-constant. Since different materials exhibit different radiated intensity of surface at the same temperature, these intensities were converted in temperatures, which are derived from the Equation 4.1. The intensity change depends on the temperature change, therefore a correlation $I(T)$ using 6 point calibration at different temperatures was determined. Such ecIRT enables to measure very low temperature differences. This correction essentially subtracts the images from before the reaction, so only temperature differences are recorded.

Reactor

The reactor body was constructed from austenitic X15-steel with a size of 154 x 154 mm and a height of 48 mm. Four high performance cartridge heaters, type HLP, 160 mm long with a diameter of 10 mm and with spacing of 20 mm were placed within the reactor. Each heater produced a power of 400 W and was controlled simultaneously by a dTRON 16.1 (Jumo, Fulda) temperature controller. A NiCr-Ni (type K) thermocouple was positioned in a lateral bore diameter of 1.5 mm situated approximately in the middle of the reactor at 5 mm under the samples in order to control the temperature. This temperature controller is compatible with a type K thermocouple. The computer was equipped with an RS 232 serial interface and the temperature controller with an RS 485 interface, so a signal converter was needed. In order to reduce heat radiation the reactor was laterally cased with endplates made from 1.4301 steel. The space between the reactor and the endplates was filled with alumina fleece. The reactor was also screwed to a stand, on which a ceramic isolation plate, a so-called stenan, consisting predominantly of silica and alumina, was placed.

A gas line of an outside diameter of 4 mm was connected by a swagelok fitting. The sectional view of the reactor and its gas line is illustrated in Figure 4.2. The gas input

and output were linked to a gas distribution frame made from 1.4571 high-grade steel. To achieve homogenous gas distribution the gas inlet and outlet bores were drilled in the gas distribution frame to sizes varying from 0.9 to 1.2 mm. In total 40 holes were made on each side. Within the gas distribution frame there was a longitudinal slot in each side to distribute the gas flowing into the reaction space and the continuous gas flow leaving the reaction space. A pressure regulating valve set to approx. 1.2 bars was attached to the end of the gas outlet tube. In this way an homogenous gas distribution within the reactor was achieved.

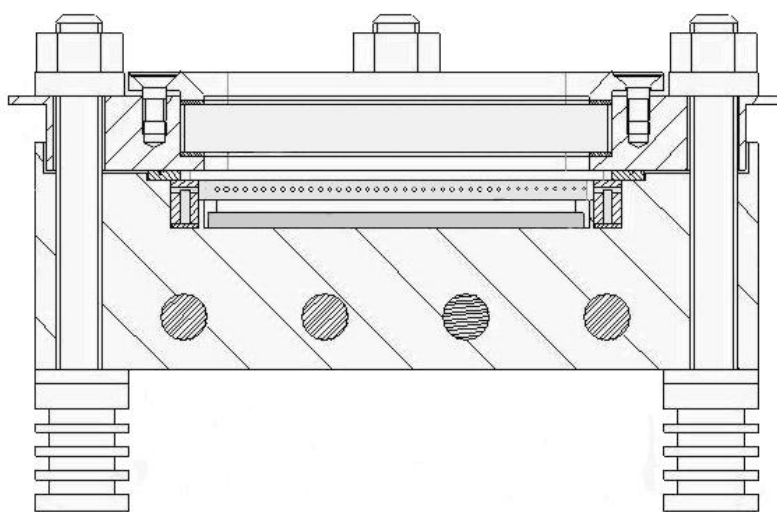


Figure 4.2 Sectional view of the reactor and its gas line. In evidence are bores in gas distribution frame.

The gas stream was controlled by an eight port gas flow controller MKS 647B (MKS Instruments, München) with an IEEE 488 interface. The controller was connected and controlled by a general purpose interface bus (GPIB). The mass flow controllers (MKS Instruments, München) were coupled to the mass flow controller by sixteen pin connectors. Each mass flow controller is calibrated using N_2 for the correct flow measurement under standard conditions (pressure 1013 mbar and zero °C temperature). A bubble counter for the calibration of the gas output was attached.

A sapphire glass sealed with Isoplan 1000 was integrated in the reactor lid. The advantages of sapphire glass for IR thermography compared to other materials are:

- high mechanical strength
- a high melting point
- constant transparency in near and mid IR and
- a low refraction index

A 1 mm deep layer on the reactor was milled to seal the reactor lid. A seal based on ceramic fibers, which could resist high temperatures of up to 1000 °C and pressures of up to 3 bars was positioned between the gas distribution frame, the reactor body and the reactor lid. The sapphire glass was attached onto the lid by a support frame with 12 counter-sunk screws M5. The frame was made from 1.4301 high-grade steel and the lid from 1.4828 high-grade steel and attached by a M3 hexagonal nut to a headless pin that was fitted within the reactor.

Inside the reactor body an area 82 x 82 mm and 10 mm high was milled out where two library plates made of slate were placed. The library plate is a slate plate cut to 40 x 80 mm and 6 mm deep using a water jet. In the surface of the milled library plate 72 slots of 3.5 mm diameter and of 2 mm depth were made. Slate is characterized by high absorption and low reflection of IR radiation, giving low background readings in IR thermography, making it very suitable for this purpose. The reaction chamber was sized to give the smallest possible dead volume above the libraries in order to reduce the influence of gas heat radiation on the measured intensity. Its volume was approx. 30 cm³.

Temperature profile of the reactor

The temperature profile of the reactor with the slate plates in place was measured, with the sapphire glass in the reactor lid opening exchanged for a steel plate of equal size. Five holes were bored in the steel block, in the positions shown in Figure 4.3, where the temperature could be measured by a type K thermocouple of 1 mm diameter. The block was turned three times by 90 ° to measure the temperature distribution in each area. Altogether 20 different temperature measurements were made while N₂ was flowing (100 ml min⁻¹) to emulate the catalyst measurement conditions.

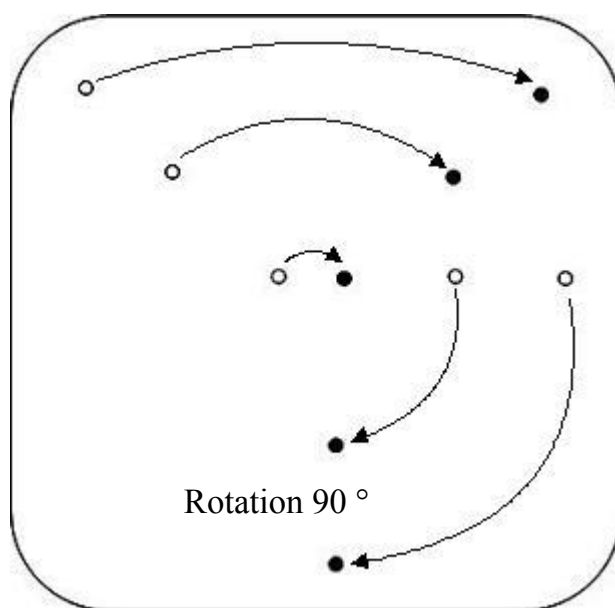


Figure 4.3 The starting position of holes (○) drilled into the steel block. After the rotation by 90 ° the bores assume a new position (●).

Flow profile of reactor

The flow profile within the reactor was confirmed by using two libraries in which every well was filled with zeolite beta H-Form. The plates were positioned in the reactor, and its seal was verified using a bubble counter connected to the gas output line. A stream of N_2 at ambient temperature was passed at a flow rate of 100 ml min^{-1} through a wash bottle containing concentrated (35%) aqueous ammonia. The ammonia adsorbs on the zeolite and the generated reaction heat is conveyed detectable by the IR camera [190].

4.1.2 Test procedure

The relative activities of synthesized metal oxides for the oxidation of soot were studied by means of ecIRT in a synthetic air atmosphere and at different temperatures. The model soot PrintexU and the catalyst were mixed by spatula at a weight ratio of 1:4 and put into the slots of the library slates by hand. The filled libraries were placed in the reactor and the reactor seal was confirmed each time by means of a bubble counter. The procedure was repeated with new libraries at each test temperature. In this way it was ensured that no soot oxidation took place before the experiment and all the catalysts had the identical initial conditions.

Before execution of the main experimental phase the N₂ was switched on (50 ml min⁻¹). The integration time of the IR camera was always set so that the mean intensity of pixels was about 6000 at the measurement temperature. This left sufficient capacity for the rise in temperature during the exothermic reaction. The reactor was first set up at an operating temperature of 400 °C. When this temperature was reached, it was held for 1 h to ensure the libraries were at an homogenous temperature. Then the 6 point calibration was started and the emissivities of the samples were measured at temperature intervals of 2 °C (396-406 °C). When the temperature in the reactor was stable for 15 min a calibration image was taken in which a median image of 1000 was produced. In this way different emissivities of the solids were determined. After the calibration at different temperatures was performed, the measurement temperature was set again. A background image was taken and the N₂ gas was switched on to active gas (100 ml min⁻¹) which consisted of 20 vol% O₂ in N₂. A range of IR images were taken within reaction times of between 30 s and 15 min.

The background image was subsequently subtracted from the test images and the relative catalytic activity was calculated for all the IR thermal images also referred to as heat increase ΔT . The IR camera, the temperature controller and the gas system were controlled automatically by the “IRTestRig” program. The calculation of the catalytic activity, heat increase respectively and the subtracted single images were also carried out using this program. The identical procedure was repeated at a temperature of 450 °C.

4.1.3 Soot coating system

The soot deposition on the library was performed by an automated spray coating system constructed by U. Hasenkox at Robert Bosch GmbH. The instrument (Figure 4.4) consisted of a material feed container, a spray gun affixed to a moveable slide, a nozzle, 2 manometers and a control unit. The system used N₂ as a propellant. The atomizing gas valve pressure could be adjusted by manometers in the range of 0.8 to 2 bar and the material pressure could be adjusted between 0.2 and 0.4 bar. The slide velocity and the distance were adjustable up to 300 mm s⁻¹ and 800 mm respectively. These adjustments were made using the “ESlight” program.

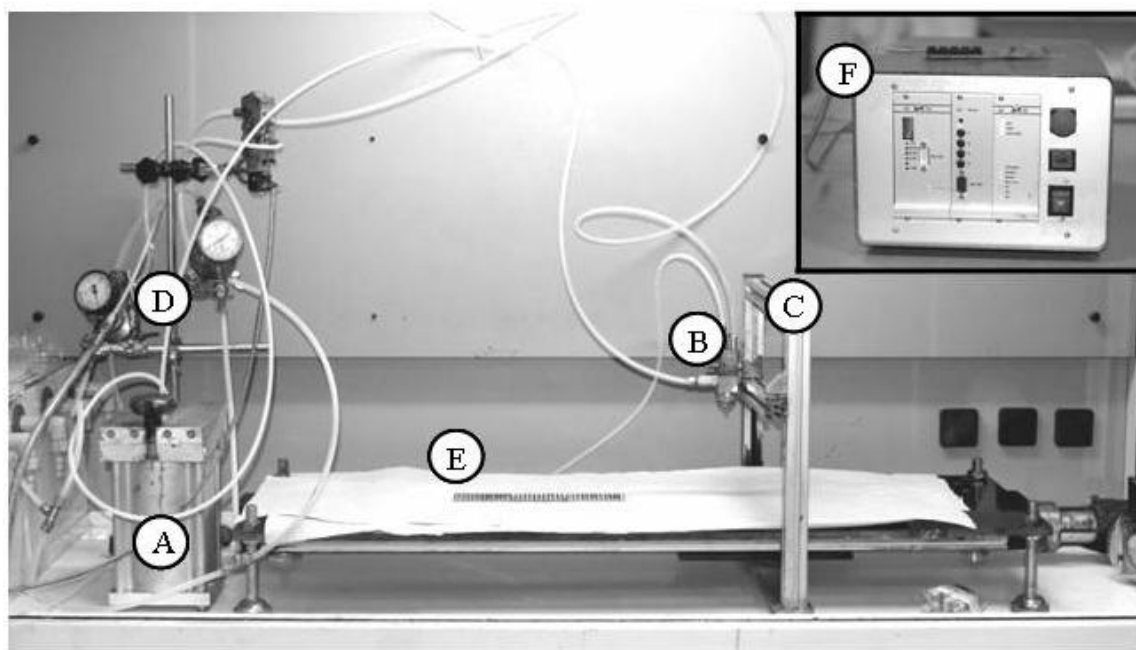


Figure 4.4 Setup of the automated soot coating system; material container (A), nozzle (B), moveable slide (C), manometer (D), libraries including samples (E) and control unit (F)

In order to achieve an homogenous soot layer on the slate library plate a slide velocity of 100 mm s^{-1} , an atomizing gas valve pressure of 0.2 bar, and a material pressure of 0.3 bar were selected and kept constant. The soot dispersion was sprayed from the spray gun above the samples. The libraries were subsequently placed on a heating plate at $120 \text{ }^\circ\text{C}$ for 1 h to evaporate moisture from the soot dispersion.

Soot dispersion

For soot deposition using the spray coating system 150 ml of optimized soot dispersion was prepared in a 250 ml bottle. The soot suspension consisted of approx. 8 wt% commercially available soot PrintexU (Degussa AG, Frankfurt), 37 wt% 2-propanol and 55 wt% de-ionized water. Into this solution a few drops of polyoxyethylenesorbitan monolaurate were added as a surfactant.

4.2 Thermogravimetric and differential thermal analysis

The catalytic activity was performed using thermogravimetric and differential thermal analysis (TG-DTA) on Setsys Evolution 12 Wetsys, commercially available from Setaram Instrumentation (Caluire, France), which was coupled with the water circulation cooling system Julabo FC 1200T. It has to be noted that a part of this study was executed by TGA and other one by TG-DTA, since TGA was later on upgraded to DTA.

The analyzer was equipped with an electronic beam balance which was articulated on a torsion strip. The measurement of mass variation was correlated with the proportionality ratio between the current intensity and the force of electromagnetic balancing. The balance worked in a range ± 200 mg with ± 0.3 μg resolution and was mechanically equilibrated to get a correct TG signal. The furnace temperature was controlled by a thermocouple which operated from ambient temperature up to 1000 $^{\circ}\text{C}$, with a scanning rate of 0.01 to 50 $^{\circ}\text{C min}^{-1}$. The carrier gas N_2 flowed through the measurement head at the furnace to the sample.

$$X = (m_{S,0} - m_S) / m_{S,0} \quad (4.2)$$

The efficiency of the catalysts to oxidize soot is measured by conversion X , which is depicted in Figure 4.5 and is easily calculated by Equation 4.2. Where $m_{S,0}$ is the initial soot mass and m_S is the current soot mass. The conversion curve is given when plotting the conversion as a function of the temperature. The catalytic activity is defined as the temperature at which conversion of the initial soot mass reaches 50% referred to as T_{50} (Figure 4.5). By comparing the temperature T_{50} of two or more different catalysts, the catalyst, which shows lower T_{50} -value features higher catalytic activity. As a rule the lower temperature T_{50} the higher is catalytic activity. Characteristic TGA curve of the soot oxidation is presented in Figure 4.5.

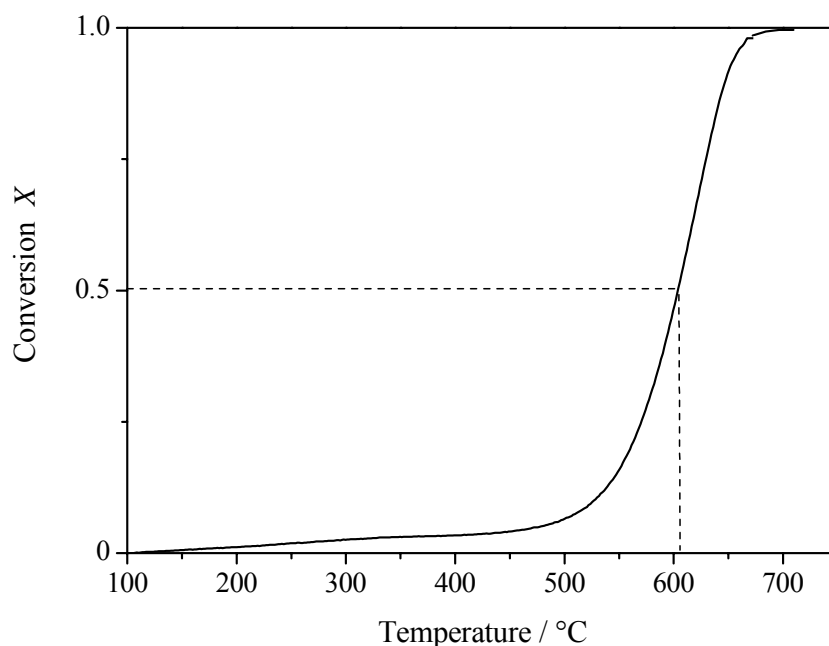


Figure 4.5 Plot of soot conversion X as a function of temperature

In the TGA version the analyzed sample was placed in a 350 μl silica crucible which was suspended at the end of a Pt beam connected to the balance. A thermocouple was placed in the furnace chamber 2 cm under the crucible and active gas O_2 flowed from the bottom of the furnace up to the sample. The analysis was carried out in the range between ambient temperature and 700 °C (10 °C min^{-1}) and 50 ml min^{-1} gas flow (20 vol% O_2 in N_2). The model soot and catalyst were mixed at a weight ratio of 1:4 via spatula achieving loose contact mode.

The TG-DTA unit allowed simultaneous measurement of the TGA and the DTA profile. The operation principle is depicted in Figure 4.6. A 100 μl alumina crucible was used for the measurement which was placed on an alumina bead, part of triple DTA rod in which three platinum thermocouples were positioned. Three thermocouples gave improved detection sensitivity of weak transitions. The alumina pan was, however, not in direct contact with the thermocouple junction. The temperature was controlled by the thermocouple situated 5 mm under the sample, the temperature correction was used and the feed gas streamed down the furnace to the sample.

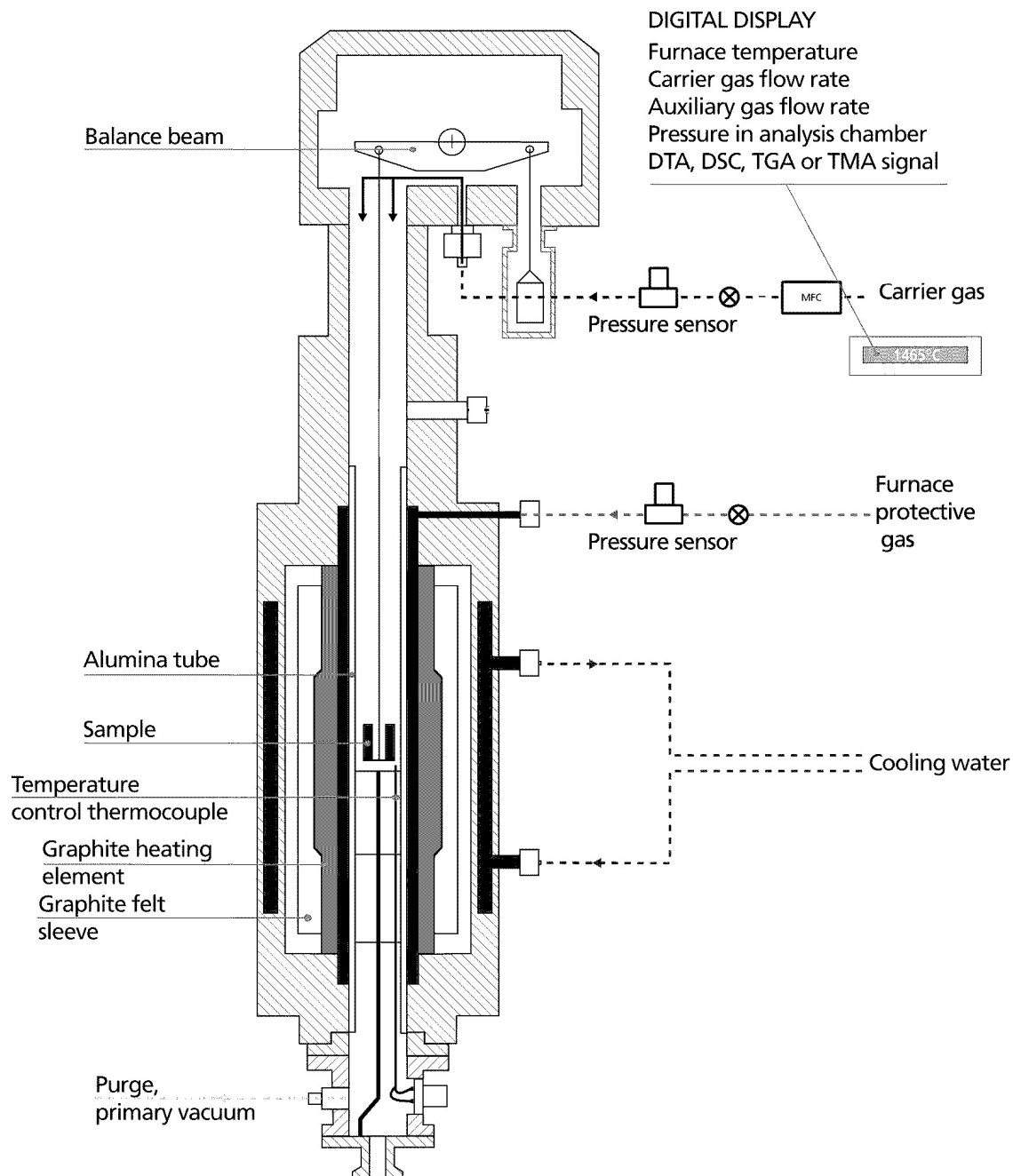


Figure 4.6 TG-DTA schematic from SETARAM brochure [191]

The tests were performed at a temperature range up to 700 °C (10 °C min^{-1}) and 100 ml min^{-1} gas flow (20 vol% O_2 , balance N_2). Soot and catalyst were mixed at the weight ratio of 1:4 by a spatula as described above.

All catalysts were first preheated in the oven up to 700 °C at a heating rate of 10 °C min^{-1} and a flow rate of 1 l min^{-1} of synthetic air before the TG-DTA

measurement was executed in order to combust the organic compound from the preparation procedures.

4.3 Preparation methods of catalysts

4.3.1 Sol-gel synthesis

Metal oxide catalysts were synthesized according to the modified sol-gel recipes of Schmidt [192]. The automated high throughput synthesis of the catalysts was performed using a commercially available pipetting robot, Freedom evo 150 (Tecan Deutschland GmbH), see Figure 4.7. Binary and ternary metal oxide compositions were prepared based on Ce, Co and Mn, using metal oxide nitrates as a precursor for the syntheses and molybdenum (V) isopropoxide, respectively. The concentration of all oxide nitrates used was 1M, with the exception of molybdenum (V) isopropoxide and of platinum (II) nitrate used as a dopant, which were both prepared at 0.1M.

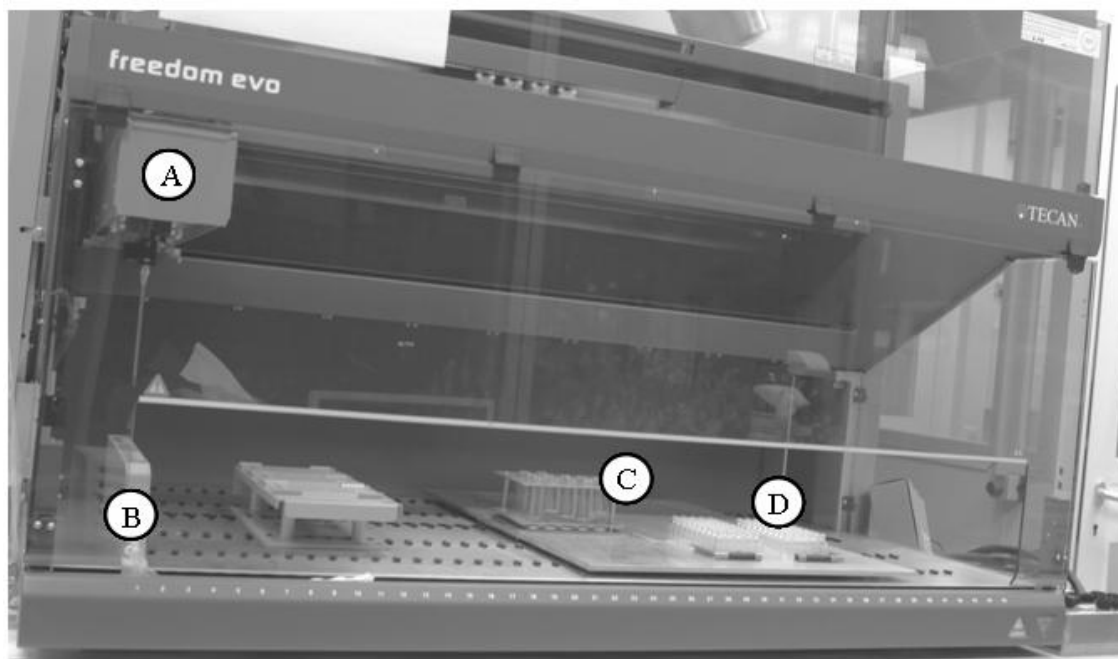


Figure 4.7 Tecan pipetting robot used for high throughput synthesis; robot head including four needles (A), their washing station (B), rack holder for precursor solutions (C) and rack holder for synthesis vials (D)

The following recipe was used for synthesis of the binary composition:

$$A \cdot [E \cdot (1-x) + x \cdot Z + 3 \cdot CA + 0.02 \cdot PA] \quad (4.3)$$

$$x = i \cdot 0.05$$

$$1 \leq i \leq 19$$

The optimum yield was found at X_E and at X_Z with $X_E = 1 - X_Z$. The minority element was doped with Pt. The following synthesis was later used for ternary catalyst composition:

if $X_E > X_Z$

$$A \cdot [E \cdot (1 - X_Z - y) + X_Z \cdot Z + y \cdot D_{Pt} + 3 \cdot CA + 0.02 \cdot PA] \quad (4.4)$$

if $X_E < X_Z$

$$A \cdot [X_E \cdot E + Z \cdot (1 - X_E - y) + y \cdot D_{Pt} + 3 \cdot CA + 0.02 \cdot PA] \quad (4.5)$$

$$y = i \cdot 0.002$$

$$1 \leq i \leq 10$$

A = substance amount 400 μ mol

E = basis element (cerium (III) nitrate hexahydrate, cobalt (II) nitrate hexahydrate and manganese (II) nitrate tetrahydrate)

Z = any element

D_{Pt} = dopant (platinum (II) nitrate)

CA = complexing agent (4-hydroxy-4-methyl-2-pentanone)

PA = propionic acid

The following explanation of the procedure used is based on the example of $Pt_2La_5Co_{93}O_x$, which represents a composition of 93 mol% Co, 5 mol% La and 2 mol% Pt as the precursor. 1M solutions of cobalt (II) nitrate hexahydrate and lanthanum nitrate hexahydrate and a 0.1M solution of platinum (II) nitrate were prepared in methanol in separate 15 ml vials. The dopant was always prepared at 0.1M. The sol

amount prepared was always 400 μmol in 1.5 ml vials. The test vials were placed in a 50 vial rack. The sol solution was prepared by pipetting single compound solutions with 372 μl cobalt (II) nitrate hexahydrate (372 μmol), 20 μl lanthanum nitrate hexahydrate (20 μmol) and 80 μl platinum (II) nitrate (8 μmol). Subsequently 149 μl 4-hydroxy-4-methyl-2-pentanone (1.2 mmol) and 0.6 μl propionic acid (8 μmol) were added.

After the synthesis was completed the rack with the samples was placed onto a horizontal shaker (HS 250 basic, IKA Labortechnik) at 270 rpm for 30 minutes. The rack with the open samples vials was then placed into a drying cupboard at 40 $^{\circ}\text{C}$ for 5 days. Calcination was performed afterwards at a temperature of 450 $^{\circ}\text{C}$ by placing the samples on alumina plates and putting them in an oven with a gas flow rate of 1 l min^{-1} (20 vol% O_2 , balance N_2). The oven was heated to 450 $^{\circ}\text{C}$ at a heating rate of 0.5 $^{\circ}\text{C min}^{-1}$, held for 5 h and cooled down at 2 $^{\circ}\text{C min}^{-1}$ to ambient temperature. The conditions of shaking, drying and calcination process were kept identical for all samples. The calcined solid was manually milled in the vials with a glass stirrer. The catalysts obtained were mixed with soot by spatula in 1.5 ml vials, at a weight ratio of catalyst to soot of 4:1, and manually transferred into the individual wells of the slate library plate.

Ce/K/Pt catalysts

The recipe for all binary compositions and Pt doped materials were constant as described above, with the exception of Ce/K/Pt catalysts. The composition was prepared using the Equation 4.6.

$$A \cdot [Ce \cdot (1 - x - y) + x \cdot K + y \cdot Pt] \quad (4.6)$$

$$x + y \geq 0.5$$

$$x = i \cdot 0.05 \quad 0 \leq i \leq 4$$

$$y = i \cdot 0.05 \quad 0 \leq i \leq 4$$

A = substance amount 300 μmol

Ce = cerium (III) nitrate hexahydrate

K = potassium nitrate

Pt = platinum (II) nitrate

Metal oxide nitrates were used as a precursor. The substance amount A was 300 μmol . 1M Cerium (III) nitrate hexahydrate was solved in methanol, and 1M potassium nitrate and 0.1M platinum (II) nitrate dissolved in water. The steps of the synthesis are as described in the previous paragraph

4.3.2 Impregnation

The alumina fibers were impregnated with catalyst. The high throughput syntheses were performed by using a commercially available automated pipetting system, Freedom evo 150 (Tecan Deutschland GmbH), to dispense the metal oxide composition solutions onto the carrier material. Nitrates were used as a precursor for the ternary system.

The metal oxide synthesis consisted of the following:

$$Ce \cdot (1 - x - y) + x \cdot K + y \cdot Pt \quad (4.7)$$

$$x + y \geq 0.5$$

$$x = i \cdot 0.05 \quad 0 \leq i \leq 4$$

$$y = i \cdot 0.05 \quad 0 \leq i \leq 4$$

Ce = cerium (III) nitrate hexahydrate

K = potassium nitrate

Pt = platinum (II) nitrate

For the impregnation 1M solutions of cerium (III) nitrate hexahydrate, potassium nitrate, and platinum (II) nitrate were prepared in de-ionised water in separate 15 ml vials where 100 μmol aliquots of the single parent solutions were pipetted into 2 ml wells of several 96 well microtitre plates. For instance, to prepare a $\text{Pt}_5\text{K}_{10}\text{Ce}_{85}\text{O}_x$ composition an automated synthesis was carried out with 5 μl platinum (II) nitrate solution (5 μmol), 10 μl potassium nitrate solution (10 μmol) and 85 μl cerium (III) nitrate hexahydrate solution (85 μmol). The numbers in the catalyst composition represent the mol ratio. The microtitre plate with the completed ternary catalysts was shaken on a microtiterplate shaker (Minishaker MS1, IKA Labortechnik) at 1800 rpm

for 5 minutes. 13 μl aliquots of each composition were then dispensed by an automated pipetting robot into the wells containing the alumina carrier of the slate library plates.

The library plates were placed into an oven at synthetic gas flow at a volume rate of 1 l min^{-1} and heated up to $110\text{ }^{\circ}\text{C}$, with a heating rate of $1\text{ }^{\circ}\text{C min}^{-1}$, and held for 2 h to evaporate the moisture content. The temperature was increased to $450\text{ }^{\circ}\text{C}$ with a heating rate of $1\text{ }^{\circ}\text{C min}^{-1}$ and held for 2 more h. After the calcination process in synthetic air was completed the oven was cooled down to ambient temperature.

The libraries were covered with a label mask in order to protect the surface area of the slate plates from the soot dispersion. Holes were stamped in the label to correspond with the wells on the library plate. Soot was subsequently deposited in the wells of the slate library plates using the automated spray tool system, as described in detail in Chapter 4.1.3. The label mask was removed and the libraries were situated on a heating plate at $120\text{ }^{\circ}\text{C}$ for 2 h to evaporate the moisture associated with the soot dispersion.

Carrier material

Commercially available alumina fibers were employed as a base material for the catalyst impregnation. The alumina materials used were Saffil Catalytic Grade (CG) fibers and Saffil HX grade fibers (SAFFIL Ltd, UK). The Saffil CG fibers were used as a catalyst carrier for the high throughput screening evaluation. The catalysts were also coated onto alumina Saffil HX and confirmed by TGA.

The Saffil CG fibers were inserted into the library plate wells by means of a rubber spatula. The plate with 72 wells was first covered with a label mask to ensure that the contamination on the surface area with the fibers is avoided. 524 mg of fibers was pressed into the wells, giving about 7 mg in each. The label mask was removed after the alumina fibers were evenly distributed.

Concentration range

To determine the concentration influence on temperature T_{50} 14 mg of alumina fibers were weighed and inserted into wells of a steel library, and impregnated with $26\text{ }\mu\text{l}$ of $\text{Pt}_5\text{K}_{10}\text{Ce}_{85}\text{O}_x$ catalyst at a concentration range from 0.05 to 0.55 mol l^{-1} of 0.05 mol l^{-1} increments. The impregnation was carried out by an automated pipetting robot using

metal nitrates dissolved in de-ionized water as a precursor. After the catalyst composition was coated onto the supports the steel plates were placed in an oven and heated up to 110 °C and held for 2 h in synthetic air to evaporate the moisture. The temperature was subsequently increased to 450 °C with a heating rate of 1 °C min⁻¹, to calcinate the catalysts to their final shape, and held there for 2 h before cooling to ambient temperature. The complete coated fibers were carefully taken out of each library well using tweezers. 1 mg (0.95 ± 0.1 mg) of model soot was added to each set of fibers and mixed by spatula.

For reference measurement the unsupported Pt₅K₁₀Ce₈₅O_x catalyst, of a concentration range from 0.05 to 0.55 mol l⁻¹ of 0.05 mol l⁻¹ increments, was prepared in which the nitrate solution of catalyst compositions were synthesized by dispensing these solutions directly into 1.5 ml vials and given the same treatment as explained in the previous paragraph to obtain its final form. The amount of each concentration used to coat the fibers was calculated, weighed and 1 mg of soot was added in an analogous manner and mixed by spatula.

In order to analyze the elemental composition of the unsupported catalysts and the catalysts supported on the alumina (see Chapter 4.4.3), their preparation took place as described in the paragraphs above.

4.3.3 Paste synthesis

Another method of catalyst preparation used in this study to test the activity of soot oxidation is the synthesis of metal oxide powder using an organic complex, in this work referred to as the paste synthesis method. The pastes were synthesized by following developed recipes, using single phase metal oxide powders of V₂O₅, MoO₃ and CeO₂, as starting materials, for their purity and supplier see Appendix 7.3.

A high particle size distribution of the starting metal oxide powders was required, so the materials were ground to particle size with a mean diameter as close to 200 nm as possible and measured using ultra fine particle analyzer (UPA) 3.150 (Grimm Aerosol Technik GmbH, Ainring). The milling was carried out in planetary ball mills PM 4000

(Retsch GmbH, Haan) including 4 milling stations, which are based on the rotation movement between the grinding jar and the sun wheel. 80 ml of ZrO₂ milling balls of 3 mm diameter were placed in a 125 ml ZrO₂ grinding jar which left sufficient space for the milling material and the solvent. 15 vol% of the total volume of starting material was diluted in 40 ml 2-propanol and added into the grinding jar. This left a headspace of approx. 20%, sufficient for the milling balls to move freely. The metal oxide powders were milled 14 to 24 h depending on the starting material with a sun wheel speed of 250 min⁻¹ reversal direction. The measurement of the particle size distribution was performed by an UPA, see Chapter 4.4.5. When the milling was completed the polymers were added and milled for another 5 min to homogenize. The remainder of the polymers which did not fit into the grinding jar was decanted into a 150 ml beaker, a magnetic stirrer bar was added, and the beaker placed on a heated magnetic stirrer. The milled suspension was sieved into the beaker in order to separate the milled product from the milling balls. In order to recover the maximum amount of solids the grinding jar and the balls were rinsed with 2-propanol afterwards. The material was continuously stirred at 80 °C under a stream of N₂ to evaporate the 2-propanol. When nearly all the 2-propanol had evaporated and the viscosity of the suspension was high enough, the suspension was transferred from the beaker to a three cylinder mill. The pastes were milled until all the 2-propanol had evaporated and until they were well dispersed. Agglomerate formation was avoided due to the shear force between the single cylinders.

The pastes consisted of 15 vol% of metal oxide powder and of 85 vol% of different developed polymer compositions. The composition of the polymers for each metal oxide is listed in Appendix in 7.3 Compound composition, the polymers and their supplier are listed also in Appendix in the 7.2 Chemical list.

4.4 Characterization methods

4.4.1 Catalysts deactivation

The metal oxide catalysts prepared by sol-gel synthesis were deactivated by thermal and hydrothermal aging and poisoning. Of these, thermal aging and catalyst poisoning were found to be the most effective deactivation methods. The catalysts were aged in an oven at 700 °C for 70 h in synthetic air in order to determine their thermal stability. For the hydrothermal aging (10% H₂O and 10% O₂, and balance N₂) and S poisoning (20 ppm SO₂, 500 ppm NO₂, 10% H₂O, 10% O₂, and balance N₂) the catalysts were placed in an oven also at 700 °C for 70 h.

The water dosage was performed using a liquid mass flow meter LIQUI-FLOW series L10/L20 (Bronkhorst High-Tech BV). A control valve is integrated onto the body of the liquid meter in order to achieve flow control. The evaporation was carried out by controlled evaporation and mixing (CEM) liquid delivery system consisting of the liquid flow controller, a mass flow controller for carrier gas and a temperature controlled mixing and evaporation tool. The water, drawn from a container and measured by liquid mass flow meter, was mixed with the carrier gas (N₂) and transported from the mixing valve into the heat exchanger resulting in completed evaporation.

4.4.2 Inductively coupled plasma optical emission spectrometry

The elemental composition was investigated by inductively coupled plasma optical emission spectrometry (ICP-OES) using a Perkin Elmer Optima 3300 DV with axial and radial plasma observation, and an integrated auto sampler and simultaneous detection by a CCD-chip. In this instrument the valence electrons are excited to unfilled electronic levels by means of ICP. The electrons fall back into their ground state emitting characteristic spectral lines, which are analyzed to measure the elemental concentration. The qualitative information is obtained from the wavelength, while the

intensity gives the elemental concentration. The detection limits of the spectrometer are in a range between $5 \mu\text{g l}^{-1}$ and 200 mg l^{-1} .

The alumina fibers coated with catalysts were weighed and placed into a 10 ml beaker. 4 ml of aqua regia (a mixture of HNO_3 and HCl at a ratio of 1:3) was added and boiled for about 1 h, after which the carrier material was separated by filtration. The solution was diluted in 10 ml de-ionized water and immediately measured against a suitable calibration. The precursors were diluted at a ratio of 1:1000 in de-ionized water in 15 ml vials and measured directly.

4.4.3 X-ray diffraction analysis

The phase composition of ceramic fibers was analyzed by an X-ray diffractometer (XRD). The instrument used was a Bruker AXS D8 Advance with a Cu X-ray tube and Bragg Brentano lens. A graphite secondary monochromator and Cu-K α radiation was employed with an angle range between 5 and 85° 2θ and generator settings of 40 kV and 50 mA. The diffraction data were collected with a step width of 0.04° and a counting time of 2.5 s per step. Sample preparation was done by tearing up the fibers and placing them onto silica glass.

4.4.4 Specific surface area determination

The specific surface area of the solid materials was measured by the Brunauer-Emmett-Teller (BET) method using an automated gas adsorption analyzer (TriStar 3000, Micromeritics). 0.5 g sample was pretreated in a sample tube at 350°C for 3 h in a FlowPrep 060 Degasser with N_2 streaming. The 5-point BET surface area was obtained with relative pressure in a range from 0.06 to 0.20.

4.4.5 Ultra fine particle analyzer

The particle size distribution was determined by means of an ultra fine particle analyzer (UPA) 3.150 (Grimm Aerosol Technik GmbH, Ainring) using a light scattering

technique, based on the Doppler effect and Brownian molecular motion. A beam of light from a laser source is scattered and diffracted less than 180° by particles in the liquid phase to the photo detector. The velocity distribution of dispersed particles is a function of particle size. The measurement is applicable for particle sizes ranging from 5 nm to 3 μm .

A 10 ml sample was inserted into the analyzer sample cell by pipette. The solid was dispersed in 2-propanol and was pre-treated in an ultrasonic bath for one minute. The measurement time (180 s), refractive index and the viscosity values of the dispersing fluid were taken into account when calculating the results.

4.4.6 Rheological properties determination

The rheological properties of the pastes were determined utilizing a cone plate rheometer (Physica Meßtechnik GmbH, Stuttgart) coupled to a thermostat Viscotherm VT2. The cone plate measurement system (CP-MS) worked with automatic gap setting and automatic gap control. The measurement was performed using a cone, type MK 20, with a 12.5 mm radius cone, an angle of 1° and cone truncation of 50 μm . Cone point decrease was required. On the one hand there is no material attrition on either the cone or the plate so the measuring geometry size is not changed during the operation time. On the other hand there is no friction between the cone and the plate so the cone and the plate torque are not added, which would affect the results. Only the sample torque is applied. In order to fill the measurement gap fully, a 0.7 cm^3 sample volume was employed. The shear conditions are homogenous, the air bubbles are pressed outward and small volumes of sample are needed.

Linear viscoelastic range determination

The stress sweep test was employed with constant frequency and shear stress τ between 1 and 2000 Pa to determine the linear viscoelastic (LVE) range. This LVE range described a range in which the paste structure is stable and the storage modulus G' and loss modulus G'' are at their constant plateau values. In the LVE range it was observed that the sample structure exhibited the followed correlations. The elastic dominated over the viscose behavior ($G' > G''$) and the sample was a little bit stiffer.

This is observed e.g. by pastes or solids which have a gel character. The linear elastic behavior obeyed Hooke's law (Equation 4.8) where the applied stress τ is proportional to the elastic deformation.

When the viscosity dominated over the elastic behavior ($G'' > G'$) the sample has a fluid characteristic so-called sol character. It is based on Newtonian behavior (Equation 4.9) for ideal viscous materials, where the shear viscosity η is independent from changing shear rates $\dot{\gamma}$.

$$\tau = G \cdot \gamma \quad [Pa] \quad (4.8)$$

$$\tau = \eta \cdot \dot{\gamma} \quad [Pa] \quad (4.9)$$

Polymers' behavior determination

The test was performed by the application of the frequency sweep which is an oscillation with constant shear stress τ and varied angular frequency ω with $\omega = 2\pi \cdot f$ with the unit s^{-1} , and requires the prior determination of the LVE range. The frequency sweep can be obtained subsequently. The stress sweep test is used to determine the median shear stress value. The angular frequency was set up between 100 and 0.1 Hz. Measurement result is the depicted dependency of $\log G'$ and $\log G''$ from $\log \omega$.

Viscosity determination

The viscosity was determined by a shear controlled rate (SCR₂) approach. In this method the shear rate is controlled and it is used to simulate the technical processes at certain flow rates e.g. particulate sedimentation, coating. The viscosity is defined as the ratio between shear stress τ and shear rate $\dot{\gamma}$ (Equation 4.9). The shear rate was kept constant at $30 s^{-1}$ with 30 measuring points in 5 min for the complete set of measurements. The viscosity result is not constant, but depends on the length of time the shear stress is applied.

Chapter 5

5. Summary and outlook

5.1 Summary

The aim of this work was the determination and evaluation of high throughput synthesis as well as of HTT to develop new low temperature noble metal free soot oxidation catalysts. The combinatorial chemistry and HTT provide fast methods for the discovery and evaluation of heterogeneous catalysts. The development process was optimized and confirmed by a conventional investigation analysis. The development of novel noble metal free catalysts and their improvement is still required due to impending stringent diesel emissions limits and the high costs of noble metal.

The first requirement was to design a measurement setup and reactor equipment which was constructed to facilitate parallel screening of 144 samples for the discovery and evaluation of catalysts for a DPF. The relative activities of soot oxidation catalysts were measured at temperatures of up to 450 °C by ecIRT with full automation in synthetic air conditions. The maximum temperature difference between the center and the periphery of the reactor was 4 and 6 °C at an operating temperature of 400 and 450 °C respectively. The difference between the set temperature and the temperature of the substrate surface was 70 °C at a temperature of 400 °C and 80 °C at a temperature of 450 °C. An homogeneous gas distribution was achieved within the reactor by using a gas distribution frame with a configuration of bore holes of 0.9 to 1.2 mm diameter on each side and also by using a pressure regulating valve connected to the gas outlet.

The samples were placed within wells in libraries made of slate plates. The investigation of this library material showed it to be most suitable, exhibiting very favorable IR properties in comparison to steel libraries sprayed with black high-temperature paint causing surface modification during the experimental process.

Three different syntheses were studied resulting in the sol-gel process using a commercially available pipetting robot that is most applicable for the catalysts' preparation and most suitable as regards HTT using ecIRT. The paste synthesis method was found to be inapplicable for high throughput preparation of soot oxidation catalysts because of the required rheological properties of the single paste, their manual preparation, the high preparation quantity and high material waste. In contrast impregnation and sol-gel are fast methods, where several components and dopants of any amount can be added in a single step and the wastage is minimal, which saves costs.

Within the scope of this thesis different soot deposition techniques have been studied, playing a key role for the detection of relative activities by ecIRT. Automated soot deposition and the manual mixing of model soot and catalyst by spatula were investigated using a loose contact mode in order to be as close as possible to practical conditions. The catalysts prepared by sol-gel synthesis were mixed with soot by spatula achieving an homogenous mixture and good contact between soot and catalyst was present hence any heat change was reliably measured by ecIRT. The reliability of the performance determined by ecIRT was confirmed by TG-DTA. Moreover it was demonstrated that the HTT using IR thermography is a fast method giving reproducible results and is suitable for the initial investigation of soot combustion catalysts. The sol-gel process was successfully used for the catalysts preparation in comparison to impregnation, where activities could be measured neither by ecIRT nor by TG-DTA. Moreover the process possesses additional advantages such as a narrow particle size distribution at the nanoscale and a high surface area of the final catalysts. Saffil CG alumina fibers with a high specific surface area of $145 \text{ m}^2 \text{ g}^{-1}$ were impregnated and the soot was subsequently deposited automatically onto the carrier surface by a spray coating system. This soot deposition method is fast and an homogenous layer is achieved. No relative activity could be detected by ecIRT when using this deposition technique. The catalyst penetrated into the pores of the Saffil CG fibres, resulting in poor contact between soot and catalyst.

Catalysts known to be highly active from the literature are based on oxides of Co, Mn and Ce, which were chosen as the starting points for the search for a new soot oxidation catalyst. From 250 catalysts tested by ecIRT the mixed oxides of Co/La, Ca/Mn and Ag/Ce were shown to be most active and subsequently studied conventionally by

TG-DTA. The compositions of $\text{La}_5\text{Co}_{95}\text{O}_x$, $\text{Ca}_5\text{Mn}_{95}\text{O}_x$ and $\text{Ce}_y\text{Ag}_{100-y}\text{O}_x$ ($y = 45, 50$ and 55) each reduced the combustion temperature by up to approx. $400\text{ }^\circ\text{C}$. The T_{50} -value showed a linear increase with Co and Mn concentrations, respectively, in contrast to the polynomial regression which was determined by Ag/Ce. The temperature T_{50} was investigated for $\text{La}_5\text{Co}_{95}\text{O}_x$ at different catalyst to soot ratios and its optimum was found to be 3.7.

The mixed oxides of $\text{La}_5\text{Co}_{95}\text{O}_x$ and $\text{Ca}_5\text{Mn}_{95}\text{O}_x$ were doped with Pt in order to find their effect on catalytic activity analyzed by TG-DTA. Whereas linear regression of catalytic activity of $\text{La}_5\text{Co}_{95}\text{O}_x$ was observed to increase proportionally with increased concentration of Pt doping a linear decrease of catalytic activity was measured with increased doping of Pt in $\text{Ca}_5\text{Mn}_{95}\text{O}_x$. The results of conventional analysis are reproducible, which confirms the applicability of the technique used in this work.

Catalyst composition of $\text{La}_5\text{Co}_{95}\text{O}_x$, $\text{Pt}_2\text{La}_5\text{Co}_{93}\text{O}_x$, $\text{Ca}_5\text{Mn}_{95}\text{O}_x$ and $\text{Pt}_{0.2}\text{Ca}_5\text{Mn}_{95}\text{O}_x$ were subjected to a thermal aging process of 70 h at $700\text{ }^\circ\text{C}$. This did not affect their catalytic activity, however the addition of 10% steam during the aging process increased their T_{50} -value by $50\text{ }^\circ\text{C}$ for Co based catalysts, and by $70\text{ }^\circ\text{C}$ for Mn based catalysts. A large reduction of the specific surface area of the catalysts was observed after hydrothermal aging, which revealed a sintering effect and agreed with the SEM micrographs showing particle size growth. The loss of catalytic activity correlates with loss of specific surface area. The catalysts were treated by the presence of 20 ppm SO_2 and 500 ppm NO_2 , which did not show any change in activity for $\text{Ca}_5\text{Mn}_{95}\text{O}_x$ and $\text{Pt}_{0.2}\text{Ca}_5\text{Mn}_{95}\text{O}_x$ catalysts, while on the other hand degradation of approx. $40\text{ }^\circ\text{C}$ and $55\text{ }^\circ\text{C}$ was measured for $\text{La}_5\text{Co}_{95}\text{O}_x$ and $\text{Pt}_2\text{La}_5\text{Co}_{93}\text{O}_x$, respectively.

It was demonstrated that the synthesis procedure, the selection of the support material and the soot deposition manner are very important parameters in the development of soot combustion catalysts using ecIRT. The investigation of different soot deposition techniques results in the conclusion that contact between soot and catalyst is crucial for the soot oxidation rate.

This study showed that the combination of combinatorial chemistry and HTT is very efficient to discover good catalyst candidates in a short time and presents new

feasibilities for the development and for the improvement of heterogeneous catalysis in diesel exhaust aftertreatment. Therefore catalyst compositions with a significant reduction in soot combustion temperature could be discovered rapidly and effectively. It has to be noted that the conventional measurement by TG-DTA is indispensable giving more precise information about the catalysts. The best catalysts found are good starting compositions for further optimization.

5.2 Outlook

The reduction of DPM will be a great challenge in the coming years especially regarding the stringent diesel emissions limits, which have already been established. Therefore the combination of different catalyst technologies is required in order to meet such limits. The application of catalyst coated DPF presents a very promising regeneration system. The commonly used Pt based catalysts have drawbacks, these are firstly that sulfate particulates are generated and secondly the high cost. The discovery of an alternative catalyst composition is the focus of current research.

Using combinatorial chemistry and HTT highly active oxidation catalysts are obtained rapidly and effectively, nevertheless the established HTT can be still optimized. Whereas the preparation of the catalysts is fully automated the weighing out of soot and also of the catalysts and their mixing occurs manually and is extremely time-consuming. A robotic system is recommended to automate and accelerate the execution of the tests, so that the evolutional development can be carried out.

Future studies should include the determination of catalysts selectivity. The ecIRT is an optimal tool to get the primary information of the catalysts' activity and from this data to take a selection of highly active oxidation catalysts can be chosen. This can be complemented by an additional measurement in a parallel reactor using automated mass spectrometry (MS). The samples are placed in libraries and sequentially automatically screened providing precise information of catalyst selectivity. Only the highly active catalysts should be analyzed using this HTT. This combination of ecIRT, TG-DTA and MS, each fully automated, could contribute to the effective discovery and optimizing of future oxidation catalysts.

To conclude, the catalysts discovered in this study showing high activity in soot combustion should be analyzed in future research work with regards to the interaction between the catalyst itself and a different carrier which has to be considered for the practical application. It should be kept in mind that particle size, the catalyst quantity and its dispersion are all parameters affecting the catalytic soot oxidation, therefore its

determination in combination with carrier material should be analyzed to obtain the optimum catalytic activity.

6. Bibliography

- [1] Schindler, K.P. *Advances in diesel engine technologies for european passenger vehicles*. Diesel engine emissions reduction (DEER) Conference. **2002**. San Diego, CA
- [2] DieselNet, Technology guide, <http://www.dieselnet.com/tg.html>, **2006**
- [3] Alander, T.J., A.P. Leskinen, T.M. Raunemaa, and L. Rantanen, *Characterisation of diesel particles; effect of fuel reformulation, exhaust aftertreatment, and engine operation on particle carbon composition and volatility*. Environ. Sci. Technol., **2004**. 38(9), 2707-2714
- [4] Johnson, J.H., S.T. Bagley, L.D. Gratz, and D.G. Leddy, *A review of diesel particulate control technology and emission effects*. Diesel exhaust aftertreatment, SAE 940233 SP-1020, **1994**, 1-35
- [5] Abdul-Khalek, I.S., D.B. Kittelson, B.R. Graskow, and Q. Wei, *Diesel exhaust particle size: measurement issue and trends*. In-cylinder diesel particulate and NO_x control, SAE 980525 SP-1326, **1998**, 133-145
- [6] Kittelson, D., W. Watts, and J. Johnson, *Diesel aerosol sampling methodology - CRC E-43, Final report*. University of Minesota, **2002**
- [7] Virtanen, A.K.K., J.M. Ristimäki, K.M.cVaaraslahti, and J. Keskinen, *Effect of engine load on diesel soot particles*. Environ. Sci. Technol., **2004**. 38(9), 2551-2556
- [8] Kim, W.S., S.H. Kim, D.W. Lee, S. Lee, C.S. Lim, and J.H. Ryu, *Size analysis of automobile soot particles using field-flow fractionation*. Environ. Sci. Technol., **2001**. 35(6), 1005-1012
- [9] Sturm, P.J., U. Baltensperger, M. Bacher, B. Lechner, S. Hausberger, B. Heiden, D. Imhof, E. Weingartner, A.S.H. Prevot, R. Kurtenbach, and P. Wisen, *Roadside measurements of particulate matter size distribution* Atmospheric Environment, **2003**. 37, 5273-5281
- [10] Mathis, U., M. Mohr, R. Kaegi, A. Bertola, and K. Boulouchos, *Influence of diesel engine combustion parameters on primary soot particle diameter*. Environ. Sci. Technol., **2005**. 39(6), 1887-1892
- [11] Collin, F., M.F. Gonnord, J.C. Momique, R. Monier, and C. Walther, *Particulate matter size distribution and associated polycyclic aromatic hydrocarbon content from indirect and direct injection diesel engines*. Int. J. Engine Research, **2001**. 2(1), 23-31

- [12] HEI, *Understanding the health effects of components of the particulate matter mix: progress and next steps*. HEI Perspectives, Health Effects Institute, Boston, **2002**
- [13] Nemmar, A., P.H.M. Hoet, B. Vanquickenborne, D. Dinsdale, M. Thomeer, M.F. Hoylaerts, H. Vanbilloen, L. Mortelmans, and B. Nemery, *Passage of inhaled particles into the blood circulation in humans*. *Circulation*, **2002**. 105, 411-414
- [14] Oberdörster, G., Z. Sharp, V. Atudorei, A. Elder, R. Gelein, W. Kreyling, and C. Cox, *Translocation of inhaled ultrafine particles to the brain*. *Inhalation Toxicol.*, **2004**. 16, 437-445
- [15] Oberdörster, G., J.N. Finkelstein, C. Johnston, R. Gelein, C. Cox, R. Baggs, and A.C.P. Elder, *Acute pulmonary effects of ultrafine particles in rats and mice*. Research report 96, Health Effects Institute, Boston MA, **2000**
- [16] NIOSH, *Carcinogenic effect of exposure to diesel exhaust*. National institute for occupational safety and health, Current intelligence bulletin No. 50, DHHS, **1988**. Pub. No. 88-116
- [17] Somers, C.M., B.E. McCarry, F. Malek, and J.S. Quinn, *Reduction of particulate air pollution lowers the risk of heritable mutations in mice*. *Science*, **2004**. 304, 1008-1010
- [18] Summers, J.C., J.E. Sawyer, and A.C. Frost, *The 1990 Clean Air Act and catalytic emission control technology for stationary sources*. ACS Symposium series 495, American chemical society, **1992**, 98-114
- [19] DieselNet, Emission standards, <http://www.dieselnet.com/standards.htm>, **2006**
- [20] Itoh, A., K. Shimato, T. Komori, H. Okazoe, T. Yamada, and K. Niimura, *Study of Sic application to diesel particulate filter (Part 1) Material development*. SAE 930360, **1993**
- [21] Sorenson, S.C., J.W. Høj, and P. Stoobe, *Flow characteristics of Sic diesel particulate filter materials*. SAE 940236, **1994**
- [22] Merkel, G.A., W.A. Culter, and C.J. Warren, *Thermal durability of wall-flow ceramic diesel particulate filters*. SAE 2001-01-0190, **2001**
- [23] Goldenberg, E., M. Prigent, and J. Caillod, *Depolluting exhaust gases from diesel engines by catalytic mufflers*. *Oil & Gas Sci. Techn. - Rev. IFP*, **1983**. 38(6), 793-805
- [24] Moulijn, J.A. and F. Kapteijn, *Towards a unified theory of reactions of carbon with oxygen-containing molecules*. *Carbon*, **1995**. 33(8)
- [25] Neeft, J.P.A., T.X. Nijhuis, E. Smakman, M. Makkee, and J.A. Moulijn, *Kinetics of the oxidation of diesel soot*. *Fuel*, **1997**. 76(12), 1129-1136

- [26] Long, F.J. and K.W. Sykes, *The catalysis of the oxidation of carbon*. J. Chim. Phys., **1950**. 47, 361-378
- [27] Neumann, B., C. Kröger, and E. Fingas, *Die Wasserdampfzersetzung an Kohlenstoff mit aktivierenden Zusätzen*. Zeitschr. Anorg. Allg. Chem., **1931**. 197(1), 321-338
- [28] McKee, D.W., *Carbon oxidation catalyzed by low melting point oxide phases*. Carbon, **1987**. 25(4), 587-588
- [29] Marsh, H. and K. Kuo, *Kinetics and catalysis of carbon gasification*. in Introduction to carbon science, ed. H. Marsh. **1989**: Butterworth-Heinemann. 107-151
- [30] Baker, R.T.K., *Factors controlling the mode by which a catalyst operates in the graphite-oxygen reaction* Carbon, **1986**. 24(6), 715-717
- [31] Goethel, P.J. and R.T. Yang, *Mechanism of catalyzed graphite oxidation by monolayer channeling and monolayer edge recession* J. Catal, **1989**. 119(1), 201-214
- [32] Setten, B.A.A.L.v., M. Makkee, and J.A. Moulijn, *Science and technology of catalytic diesel particulate filters*. Catalysis Reviews, **2001**. 43(489-564)
- [33] Ciambelli, P., M. D'Amore, V. Palma, and S. Vaccaro, *Catalytic oxidation of an amorphous carbon black*. Combust. Flame, **1994**. 99(2), 413-421
- [34] Neeft, J.P.A., M. Makkee, and J.A. Moulijn, *Catalysts for the oxidation of soot from diesel exhaust gases I. An exploratory study*. Appl. Catal. B, **1996**. 8, 57-78
- [35] Neeft, J.P.A., O.P.v. Pruisen, M. Makkee, and J.A. Moulijn, *Catalysts for the oxidation of soot from diesel exhaust gases II. Contact between soot and catalyst under practical conditions*. Appl. Catal. B, **1997**. 12, 21-31
- [36] Neeft, J.P.A., M. Makkee, and J.A. Moulijn, *Diesel particulate emission control*. Fuel Proc. Techn., **1996**. 47, 1-69
- [37] Sorenson, S.C., N. Ladegaard, and J. Schramm, *Fuel additive effects on particulate emissions from a diesel engine*. SAE 970181, **1997**
- [38] Bonnefoy, F., P. Gilot, B.R. Stanmore, and G. Prado, *A comparative study of carbon black and diesel soot reactivity in the temperature range 500-600°C - effect of additives*. Carbon, **1994**. 32(7), 1333-1340
- [39] Miyamoto, N., Z. Hou, and H. Ogawa, *Catalytic effects of metallic fuel additives on oxidation characteristics of trapped diesel soot*. SAE 881224, **1988**
- [40] Howard, J.B. and W.J. Kausch, *Soot control by fuel additives*. Prog. Energy Combust. Sci., **1980**. 6, 263-276

- [41] Jelles, S.J., M. Makkee, and J.A. Moulijn, *Diesel particulate control. Application of an activated particulate trap in combination with fuel additives at an ultra low dose rate.* Diesel exhaust aftertreatment, SAE 1999-01-0113, **1999**, 69-74
- [42] Baker, R.T.K., P.S. Harris, and R.B. Thomas, *Direct observation of particle mobility on a surface in a gaseous environment* Surf. Sci. , **1975**. 46(1), 311-316
- [43] Baker, R.T.K., *In-situ electron microscopy studies of catalyst particle behavior.* Catal. Rev., Sci. Eng. , **1979**. 19(2), 161-209
- [44] Baker, T., *Catalytic gasification of graphite.* Chem. Ind. (London), **1982**. 18, 698--702
- [45] Abthoff, J., H.D. Schuster, and J.H. Langer, *The regeneration trap oxidizer - an emission control technique for diesel engines.* Diesel particulate control, SAE 850015 P-158, **1985**, 75-85
- [46] Stommel, P., R. Backes, and H. Luders, *Applications for the regeneration of diesel particulate traps by combining different regeneration systems.* SAE 970470, **1997**
- [47] Neeft, J.P.A., *Catalytic oxidation of soot*, Ph.D. thesis, Delft University of Technology, **1995**
- [48] Setten, B.A.A.L.v., J.M. Schouten, M. Makkee, and J.A. Moulijn, *Realistic contact for soot with an oxidation catalyst for laboratory studies.* Appl. Catal. B, **2000**. 28, 253-257
- [49] McKee, D., *Metal oxides as catalysts for the oxidation of graphite.* Carbon, **1970**. 8, 623-635
- [50] McKee, D.W., *The copper-catalyzed oxidation of graphite.* Carbon, **1970**. 8(2), 131-136
- [51] Ahlström, A.F. and C.U.I. Odenbrand, *Catalytic combustion of soot deposits from diesel engines.* Appl. Cat., **1990**. 60(1), 143-156
- [52] Hoffmann, H.U. and T. Rieckmann, *Reduction of diesel particulate emissions by catalytic filtration.* Chem. Ing. Tech., **1994**. 17, 149-160
- [53] Doorn, J., J. Varloud, P. Mériaudeau, and V. Perrichon, *Effect of support material on the catalytic combustion of diesel soot particulates.* Appl. Cat. B, **1992**. 1, 117-127
- [54] McKee, D.W., *Mechanisms of the alkali metal catalysed gasification of carbon.* Fuel, **1983**. 62(2), 170-175

- [55] Ahlstroma, A.F. and C.U.I. Odenbrand, *Combustion of soot deposits from diesel engines on mixed oxides of vanadium pentoxide and cupric oxide*. App. Cat., **1990**. 60(1), 157-172
- [56] Leocadio, I.C.L., S. Braun, and M. Schmal, *Diesel soot combustion on Mo/Al₂O₃ and V/Al₂O₃ catalysts: investigation of the active catalytic species*. J. Catal., **2004**. 223, 114-121
- [57] Ciambelli, P., P. Corbo, M. Gambino, V. Palma, and S. Vaccaro, *Catalytic combustion of carbon particulate*. Catal. Today, **1996**. 27, 99-106
- [58] Ciambelli, P., P. Corbo, P. Parrella, M. Scialò, and S. Vaccaro, *Catalytic oxidation of soot from diesel exhaust gases. I. Screening of metal oxide catalysts by TG-DTG-DTA analysis*. Thermochem. acta, **1990**. 162, 83-89
- [59] Ciambelli, P., M. D' amore, V. Palma, and S. Vaccaro, *Catalytic combustion of carbon particulate at high values of the carbon/catalyst mass ratio*. Twenty sixth symposium on combustion, the combustion institute, **1996**, 1789-1796
- [60] Ciambelli, P., V. Palma, and S. Vaccaro. *Carbon-oxygen reaction on Cu/V/K catalyst for soot oxidation*. New frontiers in catalysis Conference. **1992**. Budapest
- [61] Ciambelli, P., V. Palma, and S. Vaccaro, *Low temperature carbon particulate oxidation on a supported Cu/V/K catalyst*. Catal. Today, **1993**. 17(1-2), 71-78
- [62] Badini, C., G. Saracco, and V. Serra, *Combustion of carbonaceous materials by Cu-K-V based catalysts. I. Role of copper and potassium vanadates*. Appl. Catal. B, **1997**. 11, 307-328
- [63] Serra, V., G. Saracco, C. Badini, and V. Specchia, *Combustion of carbonaceous materials by Cu-K-V based catalysts II. Reaction mechanism*. Appl. Catal. B, **1997**. 11, 329-346
- [64] Mul, G., J.P.A. Neeft, F. Kapteijn, M. Makkee, and J.A. Moulijn, *Soot oxidation catalyzed by a Cu/K/Mo/Cl catalyst: evaluation of the chemistry and performance of the catalyst* App. Catal. B, **1995**. 6(4), 339-352
- [65] Neeft, J.P.A., W. Schipper, G. Mul, M. Makkee, and J.A. Moulijn, *Feasibility study towards a Cu/K/Mo/(Cl) soot oxidation catalyst for application in diesel exhaust gases*. App. Catal. B, **1997**. 11(3-4), 365-382
- [66] Neri, G., G. Rizzo, S. Galvagno, M.G. Musolino, A. Donato, and R. Pietropaolo, *Thermal analysis characterisation of promoted vanadium oxide-based catalysts*. Thermochem. acta, **2002**. 381(2), 165-172
- [67] Palmisano, P., N. Russo, P. Fino, D. Fino, and C. Badini, *High catalytic activity of SCS-synthesized ceria towards diesel soot combustion*. Appl. Catal. B, **2006**. 69, 85-92

- [68] Boaro, M., M. Vicario, C. Leitenburg, G. Dolcetti, and A. Trovarelli, *The use of temperature-programmed and dynamic/transient methods in catalysis: characterization of ceria-based, model three-way catalysts* *Cat. Today*, **2003**. 77(4), 407-417
- [69] Flouty, R., E. Abi-Aad, S. Siffert, and A. Aboukaïs, *Role of molybdenum against ceria sulphur poisoning in the combustion of soot particles and the oxidation of propene* *Appl. Catal. B*, **2003**. 46(1), 145-153
- [70] Twua, J., C.J. Chuanga, K.I. Changa, C.H. Yanga, and K.H. Chenb, *Raman spectroscopic studies on the sulfation of cerium oxide*. *Appl. Catal. B* **1997**. 12(4), 309-324
- [71] Luo, T., J.M. Vohs, and R.J. Gorte, *An examination of sulfur poisoning on Pd/Ceria catalysts*. *J. Catal.*, **2002**. 210(2), 397-404
- [72] Tikhomirov, K., O. Kröcher, M. Elsener, and A. Wokaun, *MnO_x-CeO₂ mixed oxides for the low-temperature oxidation of diesel soot*. *Appl. Catal. B*, **2006**. 64, 72-78
- [73] Peralta, M.A., V.G. Milt, L.M. Cornaglia, and C.A. Querini, *Stability of Ba,K/CeO₂ catalyst during diesel soot combustion: Effect of temperature, water, and sulfur dioxide*. *J. Catal.*, **2006**. 242(1), 118-130
- [74] Fridell, E., H. Persson, B. Westerberg, L. Olsson, and M. Skoglundh, *The mechanism for NO_x storage* *Catal. Lett.*, **2000**. 66(1-2), 71-74
- [75] Fridell, E., M. Skoglundh, S. Johansson, B. Westerberg, A. Törnecrona, and G. Smedler, *Investigations of NO_x storage catalysts*. *Stud. Surf. Sci. Catal.*, **1998**. 116, 537-547
- [76] Fridell, E., M. Skoglundh, B. Westerberg, S. Johansson, and G. Smedler, *NO_x Storage in barium-containing catalysts* *J. Catal.*, **1999**. 183(2), 196-209
- [77] Miró, E.E., F. Ravelli, M.A. Ulla, L.M. Cornaglia, and C.A. Querini, *Catalytic combustion of diesel soot on Co, K supported catalysts*. *Catal. Today*, **1999**. 53, 631-638
- [78] Pisarello, M.L., V. Milt, M.A. Peralta, C.A. Querini, and E.E. Miró, *Simultaneous removal soot and nitrogen oxides from diesel engine exhausts*. *Catal. Today*, **2002**. 75, 645-470
- [79] Querini, C.A., L.M. Cornaglia, M.A. Ulla, and E.E. Miró, *Catalytic combustion of diesel soot on Co, K/MgO catalysts. Effect of the potassium loading on activity and stability*. *Appl. Catal. B*, **1999**. 20, 165-177
- [80] Querini, C.A., M.A. Ulla, F. Requejo, J. Soria, U.A. Sedrán, and E.E. Miró, *Catalytic combustion of diesel soot particles. Activity and characterization of Co/MgO and Co, K/MgO catalysts*. *Appl. Catal. B*, **1998**. 15, 5-19

- [81] Laversin, H., D. Courcot, E.A. Zhilinskaya, R. Cousin, and A. Aboukais, *Study of active species of Cu-K/ZrO₂ catalysts involved in the oxidation of soot*. J. Catal., **2006**. 241, 456-464
- [82] Reichenbach, H.M., H. An, and P.J. McGinn, *Combinatorial synthesis and characteriyation of mixed metal oxides for soot combustion*. Appl. Catal. B, **2003**. 44, 347-354
- [83] Milt, V.G., C.A. Querini, and E.E. Miró, *Thermal analysis of K(x)/La₂O₃, active catalysts for the abatement of diesel exhaust contaminants*. Thermochim. Acta, **2003**. 404, 177-186
- [84] Yuan, S., P. Meriaudeau, and V. Perrichon, *Catalytic combustion of diesel soot particles on copper catalysts supported on TiO₂. Effect of potassium promoter on the activity*. Appl. Catal. B, **1994**. 3, 319-333
- [85] Badini, C., G. Saracco, V. Serra, and V. Specchia, *Suitability of some promising soot combustion catalysts for application in diesel exhaust treatment* App. Cat. B, **1998**. 18(1-2), 137-150
- [86] Saracco, G., V. Serra, C. Badini, and V. Specchia, *Potential of mixed halides and vanadates as catalysts for soot combustion*. Ind. Eng. Chem. Res., **1996**. 36(6), 2051-2058
- [87] McKee, D.W., C.L. Spiro, P.G. Kosky, and E.J. Lamby, *Eutectic salt catalysts for graphite and coal char gasification*. Fuel, **1985**. 64(6), 805-809
- [88] Saracco, G., C. Baldini, N. Russo, and V. Specchia, *Development of catalysts based on pyrovanadates for diesel soot combustion*. Appl. Catal. B, **1999**. 21, 233-242
- [89] Jelles, S.J., J.P.A. Neeft, B.A.A.L.v. Setten, M. Makkee, and J.A. Moulijn, *Improved soot oxidation by fuel adittives and molten salt catalysts*. Stud. Surf. Sci. Catal., **1998**. 116, 621-623
- [90] Jelles, S.J., B.A.A.L.v. Setten, M. Makkee, and J.A. Moulijn, *Molten salts as promising catalysts for oxidation of diesel soot: importance of experimental conditions in testing procedures*. Appl. Catal. B, **1999**. 21, 35-49
- [91] Setten, B.A.A.L.v., J. Bremmer, S.J. Jelles, M. Makkee, and J.A. Moulijn, *Ceramic foam as a potential molten salt oxidation catalyst support in the removal of soot from diesel exhaust gas*. Cat. Today, **1999**. 53, 613-621
- [92] Setten, B.A.A.L.v., R.v. Dijk, S.J. Jelles, M. Makkee, and J.A. Moulijn, *The potential of supported molten salts in the removal of soot from diesel exhaust gas*. Appl. Catal. B, **1999**. 21, 51-61
- [93] Setten, B.A.A.L.V., C.G.M. Spitters, J. Bremmer, A.M.M. Mulders, M. Makkee, and J.A. Moulijn, *Stability of catalytic foam diesel-soot filters based on Cs₂O, MoO₃ and Cs₂SO₄ molten-salt catalysts*. Appl. Catal. B, **2003**. 42, 337-347

- [94] Fino, D., N. Russo, G. Saracco, and V. Specchia, *Cs-V catalysts for the combustion of diesel particulate*. Top. Catal., **2004**. 30/31, 251-255
- [95] Watabe, Y., K. Irako, T. Miyajima, and T. Yoshimoto, "*Traples*" Trap - A catalytic combustion system of diesel particulates using ceramic foam. Diesel particulate emission control, SAE 830082 SP-537, **1983**, 45-59
- [96] Murphy, M.J., L.J. Hillenbrand, D.A. Trayser, and J.H. Wasser, *Assessment of diesel particulate control - direct and catalytic oxidation*. SAE 810112, **1981**
- [97] Hillenbrand, L.J. and D.A. Trayser, *A concept for catalyzedignition of diesel soot*. SAE 811236, **1981**
- [98] Mul, G., F. Kapteijn, and J.A. Moulijn, *Catalytic oxidation of model soot by metal chlorides*. App. Cat. B, **1997**. 12, 33-47
- [99] Mul, G., J.P.A. Neeft, M. Makkee, F. Kapteijn, and J.A. Moulijn, *Catalytic oxidation of model soot by chlorine based catalysts*. Stud. Surf. Sci. Catal. , **1998**. 116, 645-654
- [100] *Compression ignition engine and exhasut system therefor*. WO 2004/025093 A1, Johnson Mathey Public limited company, **2004**
- [101] Dang, Z., Y. Huang, and A. Bar-Ilan, *Oxidation catalyst on a substrate utilized for the purification of exhaust gases*. US 2006/0211569 A1, Sud-Chemie Inc., **2006**
- [102] Pfeifer, M., M. Kögel, R. Staab, P. Adolph, Y. Demel, T. Kuhl, E. Lox, T. Kreuzer, and F.W. Schütze, *Katalytisch beschichtetes Partikelfilter und Verfahren zu seiner Herstellung sowie seine Verwendung*. DE 10 2004 040 549 A1, Umicore AG & Co. KG, **2006**
- [103] Cooper, B.J. and J.E. Thoss, *Role of NO in diesel particulate emission control*. Developments in diesel particulate control systems, SAE 890404 SP-775, **1989**, 171-183
- [104] Setiabudi, A., B.A.A.L.v. Setten, M. Makkee, and J.A. Moulijn, *The influence of NO_x on soot oxidation rate: molten salt versus platinum*. Appl. Catal. B, **2002**. 35, 159-166
- [105] Neri, G., L. Bonaccorsi, A. Donato, C. Milone, M.G. Musolino, and A.M. Visco, *Catalytic combustion of diesel soot over metal oxide catalysts*. Appl. Catal. B, **1997**. 11, 217-231
- [106] Dettling, J.C. and R. Skomoroski, *Catalyzed diesel exhaust particulate filter*. US Patent 5,100,632, Engelhard Corporation, **1992**
- [107] Uchisawa, J.O., A. Obuchi, Z. Zhao, and S. Kushiyama, *Carbon oxidation with platinum supported catalysts*. Appl. Catal. B, **1998**. 18, 183-187

- [108] Uchisawa, J.O., A. Obuchi, R. Enomoto, S. Liu, T. Nanba, and S. Kushiyama, *Catalytic performance of Pt supported on various metal oxides in the oxidation of carbon black*. Appl. Catal. B, **2000**. 26, 17-24
- [109] Uchisawa, J.O., A. Obuchi, R. Enomoto, J. Xu, T. Nanba, S. Liu, and S. Kushiyama, *Oxidation of carbon black over various Pt/MO_x/SiC catalysts*. Appl. Catal. B, **2001**. 32, 257-268
- [110] Uchisawa, J.O., A. Obuchi, S. Wang, T. Nanba, and A. Ohi, *Catalytic performance of Pt/MO_x loaded over SiC-DPF for soot oxidation*. Appl. Catal. B, **2003**. 43, 117-129
- [111] Uchisawa, J.O., S. Wang, T. Nanba, A. Ohi, and A. Obuchi, *Improvement of Pt catalyst for soot oxidation using mixed oxide as a support*. Appl. Catal. B, **2003**. 44, 207-215
- [112] Kim, M.R., D.H. Kim, and S.I. Woo, *Effect of V₂O₅ on the catalytic activity of Pt-based diesel oxidation catalyst*. Appl. Catal. B, **2003**(45), 269-279
- [113] Liu, S., A. Obuchi, J. Oi-Uchisawa, T. Nanba, and S. Kushiyama, *Synergistic catalysis of carbon black oxidation by Pt with MoO₃ or V₂O₅*. Appl. Catal. B, **2001**. 30, 259-265
- [114] Huang, Y., D. Zhongyuan, and B. Amiram, *Catalyzed diesel particulate matter with improved thermal stability*. US Patent 2004/0116285 A1, Süd-Chemie, **2004**
- [115] Davies, M.J., D.C.W. Blaikley, N. Jorgensen, D.E. Webster, and A.J.J. Wilkins, *Catalytic control of diesel particulate emissions*. Worldwide engine emission standards and how to meet them, London, **1993**, pp. 111-121
- [116] Doyle, P.M., *Combinatorial chemistry in the discovery and development of drugs*. J. Chem. Tech. Biotechnol., **1995**. 64(4), 317-324
- [117] Gordon, E.M., R.W. Barrett, W.J. Dower, P.A. Fodor, and M.A. Gallop, *Applications of combinatorial technologies to drug discovery. 2. Combinatorial organic synthesis, library screening strategies, and future directions* J. Med. Chem., **1994**. 37(9), 1385-1401
- [118] Frank, R., *Simultaneous and combinatorial chemical synthesis technique for the generation and screening of molecular diversity*. J. Biotechnol., **1995**. 41(2-3), 259-272
- [119] Gordon, K. and S. Balasubramanian, *Solid phase synthesis - designer linkers for combinatorial chemistry: a review*. J. Chem. Tech. Biotechnol., **1999**. 74(9), 835-851
- [120] Kim, D.K. and W.F. Maier, *Combinatorial discovery of new autoreduction catalysts for the CO₂ reforming of methane*. J. Catal., **2006**. 238, 142-152

- [121] Paul, J.S., J. Urschey, P.A. Jacobs, W.F. Maier, and F. Verpoort, *Combinatorial screening and conventional testing of antimony-rich selective oxidation catalysts*. *J. Catal.*, **2003**. 220, 136-145
- [122] Jandeleit, B., D.J. Schaefer, T.S. Powers, H.W. Turner, and W.H. Weinberg, *Combinatorial Materials Science and Catalysis*. *Angew. Chem. Int. Ed.*, **1999**. 38(17), 2494-2532
- [123] Maier, W.F., *Kombinatorische Chemie - Herausforderung und Chance für die Entwicklung neuer Katalysatoren und Materialien*. *Angew. Chem.*, **1999**. 111(9), 1294-1296
- [124] Sekan, S., *Kombinatorische heterogene Katalyse - ein neuer Weg in einem alten Gebiet*. *Angew. Chem.*, **2001**. 113(2), 322-344
- [125] Farrauto, R.J. and K.E. Voss, *Monolithic diesel oxidation catalysts*. *Appl. Catal. B*, **1996**. 10(1-3), 29-51
- [126] Koebel, M., M. Elsener, and M. Kleemann, *Urea-SCR: a promising technique to reduce NO_x emissions from automotive diesel engines*. *Cat. Today*, **2000**. 59(3-4), 335-345
- [127] Forzatti, P., L. Castoldi, I. Nova, L. Lietti, and E. Tronconi, *NO_x removal catalysis under lean conditions*. *Cat. Today*, **2006**. 117(1-3), 316-320
- [128] Funabiki, M., T. Yamada, and K. Kayano, *Auto exhaust catalysts*. *Cat. Today*, **1991**. 10(1), 33-43
- [129] Twigg, M.V., *Roles of catalytic oxidation in control of vehicle exhaust emissions*. *Cat. Today*, **2007**. 117(4), 407-418
- [130] An, H., C. Kilroy, and P.J. McGinn, *Combinatorial synthesis and characterization of alkali metal doped oxides for diesel soot combustion*. *Cat. Today*, **2004**. 98, 423-429
- [131] An, H. and P.J. McGinn, *Catalytic behavior of potassium containing compounds for diesel soot combustion*. *Appl. Catal. B*, **2006**. 62, 46-56
- [132] Richter, M., M. Langpape, S. Kolf, G. Grubert, R. Eckelt, J. Radnik, M. Schneider, M.-M. Pohl, and R. Fricke, *Combinatorial preparation and high-throughput catalytic tests of multi-component deNO_x catalysts*. *Appl. Catal. B*, **2002**. 36, 261-277
- [133] Schmitz, P.J., R.J. Kudla, A.R. Drews, A.E. Chen, C.K. Lowe-Ma, R.W. McCabe, W.F. Schneider, and C.T.G. Jr., *NO oxidation over supported Pt: Impact of precursor, support, loading, and processing conditions evaluated via high throughput experimentation*. *Appl. Catal. B*, **2006**. 67, 246-256
- [134] Shimizu, Y., T. Hyodo, and M. Egashira, *Mesoporous semiconducting oxides for gas sensor application* *Electroc.*, **2004**. 24(6), 1389-1398

- [135] Maier, W.F., F.M. Bohnen, J. Heilmann, S. Klein, H.C. Ko, M.F. Mark, S. Thorinbert, I.C. Tilgner, and M. Wiedorn, *Sol-Gel for the production of novel catalytic materials*. Applications of Organometallic chemistry in the preparation and processing of advanced materials, **1995**, 27-46
- [136] Klein, S. and W.F. Maier, *Mikroporöse Mischoxide - Katalysatoren mit einstellbarer Oberflächenpolarität*. Angew. Chem., **1996**. 108(19), 2376-2379
- [137] Maier, W.F., J.A. Martens, S. Klein, J. Heilmann, R. Parton, K. Vercruysse, and P.A. Jacobs, *Formselektive Katalyse mit mikroporösen amorphen Mischoxiden*. Angew. Chem., **1995**. 108(2), 222-224
- [138] Corriu, R. and D. Leclercq, *Neue Entwicklung der Molekülchemie für Sol-Gel-Prozesse*. Angew. Chem., **1996**. 108, 1524-1540
- [139] Bradley, D.C., *Metal alkoxide as precursor for electronic and ceramic materials*. Chem. Rev., **1989**. 89, 1317-1322
- [140] Gonzales, R.D., T. Lopez, and R. Gomez, *Sol-Gel preparation of supported metal catalysts*. Cat. Today, **1997**. 35(3), 293-317
- [141] Pajonk, G.M., *Aerogel catalysts*. App. Cat., **1991**. 72(2), 217-266
- [142] Hrubesh, L.W. and J.F. Poco, *Thin aerogel films for optical, thermal, acoustic and electronic applications*. J. Non-Cryst. Solids, **1995**. 188(1-2), 46-53
- [143] Sakka, S. and T. Yoko, *Fibers from gels*. J. Non-Cryst. Solids, **1992**. 147-148, 394-403
- [144] Mukherjee, S.P., D. Suryanarayana, and D.H. Stroppe, *Sol-gel processing in electronic packaging materials*. J. Non-Cryst. Solids, **1992**. 147-148, 783-791
- [145] Hench, L.L. and J.K. West, *The sol-gel process*. Chem. Rev., **1990**. 90, 33-72
- [146] Hasegawa, I. and S. Sakka, *Influence of the type of alkyl group on hydrolysis and polycondensation of tetraalkoxysilane*. J. Non-Cryst. Solids, **1988**. 100(1-3), 201-205
- [147] Scherer, G.W., *Aging and drying of gels*. J. Non-Cryst. Solids, **1988**. 100(1-3), 72-92
- [148] Iler, L.K., *The chemistry of silica*. **1979**: Willey New York
- [149] Yoldas, B.E., *Modification of polymer-gel structures*. J. Non-Cryst. Solids, **1984**. 63(1-2), 145-154
- [150] Brinker, C.J. and G.W. Scherer, *Sol-gel science: the physics and chemistry of sol-gel processing*. **1990**: Academic press, Inc., Boston

- [151] Klein, J., *Konventionelle und kombinatorische Methoden bei der Suche nach hochtemperatur stabilen Mischoxiden*, Ph.D. thesis, Essen Comprehensive University **1999**
- [152] Maier, W.F., *Sol-gel catalysts*. In: B. Cornils, W.A. Hermann, R. Schläogel, C.H. Wong: *Catalysis from A to Z*. **2001**: Wiley-VCH. 534
- [153] Maier, W.F., F.M. Bohnen, J. Heilmann, S. Klein, H.C. Ko, M.F. Mark, S. Thorimbert, I.C. Tilgner, and M. Wiedorn, *Sol-gel methods for the production of novel catalytic materials -Amorphous microporous metal oxides-*. In: J.F. Harrod u. R.M. Laine, *Appl. Organomet. Chem. Prep. Proc. Adv. Mater.*, NATO ASI Ser., *Appl. Sci.* **1995**: Kluwer, Dordrecht. 27-46
- [154] Wachs, I.E., *Recent conceptual advances in the catalysis science of mixed metal oxide catalytic material*. *Catal. Today*, **2005**. 100(1-2), 79-94
- [155] Frenzer, G. and W.F. Maier, *Amorphous porous mixed oxides: Sol-gel ways to a highly versatile class of materials and catalysts*. *Annu. Rev. Mater. Res.* , **2006**. 36, 281-331
- [156] Schwarz, J.A., C. Contescu, and A. Contescu, *Methods for preparation of catalytic materials*. *Chem. Rev.*, **1995**. 95(3), 477-510
- [157] Atkinson, A. and P.T. Moseley, *Thin film electroceramics* *Appl. Surf. Sci.*, **1993**. 65-66, 212-219
- [158] Saukko, S. and V. Lantto, *Influence of electrode material on properties of SnO₂-based gas sensor*. *Thin solid films*, **2003**. 436(1), 137-140
- [159] Lin, H.W., C.P. Chang, W.H. Hwu, and M.D. Ger, *The rheological behaviors of screen-printing pastes*. *J. Mater. Process. Tech.*, **2007**. 197(1-3), 284-291
- [160] Fujimoto, K. and M. Watanabe, *Preparation of pseudo-ternary library by combinatorial robot system based on wet and dry processes*. *Meas. sci. technol.*, **2004**. 16, 41-45
- [161] Evans, J.R.G., M.J. Edirisinghe, P.V. Coveney, and J. Eames, *Combinatorial searches of inorganic materials using the ink-jet printer: science, philosophy and technology*. *J. Eur. Ceram. Soc.*, **2001**. 21, 2291-2299
- [162] Yanase, I., T. Ohtaki, and M. Watanabe, *Combinatorial study on nano-particle mixture prepared by robot system*. *Appl. Surface Science*, **2002**. 189(3-4), 292-299
- [163] Bueno-López, A., K. Krishna, M. Makkee, and J.A. Moulijn, *Enhanced soot oxidation by lattice oxygen via La³⁺-doped CeO₂*. *J. Catal.*, **2005**. 230, 237-248
- [164] Zhang, Y., L. Chen, S. Yang, and J.R.G. Evans, *Control of particle segregation in thick film ceramic combinatorial inkjet printing*. *J. Eur. Ceram. Soc.*, **2007**. 27, 3861-3865

- [165] Liu, J., Z. Zhao, C. Xu, A. Duan, L. Zhu, and X. Wang, *Diesel soot oxidation over supported vanadium oxide and K-promoted vanadium oxide catalysts*. Appl. Catal. B, **2005**. 61, 36-46
- [166] Setiabudi, A., M. Makkee, and J.A. Moulijn, *The role of NO₂ and O₂ in the accelerated combustion of soot in diesel exhaust gases*. Appl. Catal. B, **2004**. 50, 185-194
- [167] Uner, D., M.K. Demirkol, and B. Dernaika, *A novel catalyst for diesel soot oxidation*. Appl. Catal. B, **2005**. 61, 334-345
- [168] Guimon, C., A. Auroux, E. Romero, and A. Monzon, *Acetylene hydrogenation over Ni-Si-Al mixed oxides prepared by sol-gel technique*. App. Cat. A, **2003**. 251(1), 199-214
- [169] Setiabudi, A., J. Chen, G. Mul, M. Makkee, and J.A. Moulijn, *CeO₂ catalysed soot oxidation, The role of active oxygen to accelerate the oxidation conversion*. Appl. Catal. B, **2004**. 51, 9-19
- [170] Kawamura, H., *Diesel particulate filter apparatus*. European Patent 0742352, Isuzu ceramics research institute, **1996**
- [171] Krumme, K.H., *Russfilterkerze für Dieselmotoren*. European Patent 0515776, Ernst-Apparatebau GmbH, **1992**
- [172] Hill, C.A., *Thermally bonded fibrous product*. US Patent 4,650,775, The Babcock & Wilcox Company, **1987**
- [173] Schumann, B., J. Jockel, and M. Kruse, *Verfahren zur Herstellung eines Filterelements und einer Trägerstruktur für einen Katalysator mit verbesserter Temperaturbeständigkeit*. Deutsches Patent 10 2005 042209, Robert Bosch GmbH, **2007**
- [174] Reinsch, B., U. Alkemade, D. Elbe, I. Ullmann, J. Jockel, T. Komori, L. Thuener, and M. Kruse, *Vorrichtung zur Reinigung von Gasgemischen und Verfahren zu deren Herstellung*. European Patent 1600200, Robert Bosch GmbH, **2005**
- [175] Gamel, F. and S. Kany, *Exhaust gas purification device for internal combustion engines*. WO 96/24755, **1996**
- [176] Ciambelli, P., V. Palma, P. Russo, and S. Vaccaro, *The role of NO in the regeneration of catalytic ceramic filters for soot removal from exhaust gases*. Cat. Today, **2000**. 60, 43-49
- [177] Löwe, A. and C. Mendoza-Frohn, *Zum Problem der Dieselruß-Verbrennung auf einem Katalysatorbeschichteten Filter - Der Kontakt zwischen Katalysator und Feststoff*. Chem. Ing. Tech., **1990**. 62(9), 759-762

- [178] Clague, A.D.H., J.B. Donnet, T.K. Wang, and J.C.M. Peng, *A comparison of diesel engine soot with carbon black*. Carbon, **1999**. 37, 1553-1565
- [179] Neeft, J.P.A., O.P.v. Pruisen, M. Makkee, and J.A. Moulijn, *Catalytic oxidation of diesel soot: Catalyst development*. Stud. Surf. Sci. Catal., **1995**. 96, 549-561
- [180] McKee, D.W., *Rare earth oxides as carbon oxidation catalysts*. Carbon, **1985**. 23(6), 707-713
- [181] Schüth, F., C. Hoffmann, A. Wolf, S. Schunk, W. Stichert, and A. Brenner, *in Combinatorial chemistry, High throughput experimentation in catalysis*. **1999**, Weinheim: Wiley-VCH. 463-477
- [182] Olong, N., *No published work*, Ph.D. thesis, Saarland University,
- [183] Harrison, P.G., I.K. Ball, W. Daniell, P. Lukinskas, M. Céspedes, E.E. Miró, and M.A. Ulla, *Cobalt catalysts for the oxidation of diesel soot particulate*. Chem. Eng., **2003**. 95, 47-55
- [184] Grillo, F., M.M. Natile, and A. Glisenti, *Low temperature of carbon monoxide: the influence of water and oxygen on the reactivity of a Co_3O_4 powder surface*. App. Cat. B, **2003**. 48, 267-274
- [185] Saalfrank, J.W. and W.F. Maier, *Directed evolution of noble-metal-free catalysts for the oxidation of CO at room temperature*. Angew. Chem. Int., **2004**. 43, 2028-2031
- [186] Otto, K., C. Lehmann, L. Bartosiewicz, and M. Shelef, *Carbon oxidation catalyzed by lead*. Carbon, **1982**. 20(3), 243-251
- [187] Indra, F., *Partikelfilter für PkW-Dieselmotoren*. VDI-Bericht, **1988**, 327-351
- [188] Holzwarth, A., H.W. Schmidt, and W.F. Maier, *IR-Thermographische Erkennung katalytischer Aktivitäten in kombinatorischen Bibliotheken heterogener Katalyse*. Angew. Chem., **1998**. 110(19), 2788-2792
- [189] THERMOSENSORIK GmbH, Operating manual, *Software MPS 5*, **2004**
- [190] Scheidtmann, J., *Entwicklung und Anwendung kombinatorischer Methoden zur Entdeckung resistiver Gassensoren*, Ph.D. thesis, Saarland University, **2003**
- [191] SETARAM, Brochure, *Setsys evolution state of the art*
- [192] Schmidt, T., *Maßgeschneiderte Katalysatoren für die Verbrennung flüchtiger organischer Kohlenwasserstoffe in Abluftströmen*, Ph.D. thesis, Saarland University **2005**

List of figures

Figure 1.1 Effect of NO _x – PM trade-off and emission control for diesel engines	2
Figure 1.2 Schematic of DPM composition.....	3
Figure 1.3 Diesel particle size distribution	5
Figure 1.4 Catalytic attacks on carbon sheets.....	10
Figure 1.5 Oxidation mechanism of soot in the presence of NO _x and O ₂	11
Figure 1.6 Relationship between mobility temperature and bulk melting point	12
Figure 1.7 Main mechanism of sol-gel process	24
Figure 1.8 Mechanism of acid catalyzed sol-gel process	25
Figure 3.1 Exploded view of reactor	31
Figure 3.2 EDS spectra of coating film surface.....	32
Figure 3.3 ecIRT image of steel	33
Figure 3.4 Schematic of gas flow within gas distribution frame	34
Figure 3.5 Reactor flow profile.....	35
Figure 3.6 Linear regression of current temperature	36
Figure 3.7 Reactor temperature profile.....	37
Figure 3.8 Automated paste robotic system.....	40
Figure 3.9 Schematic of library slate plates.....	45
Figure 3.10 ecIRT image of Pt _y K _z Ce _{100-y-z} O _x catalysts	46
Figure 3.11 Schematic of composition spread of Pt _y K _z Ce _{100-y-z} O _x catalysts.....	47
Figure 3.12 Heat increase ΔT of Pt _y K _z Ce _{100-y-z} O _x catalysts.....	47
Figure 3.13 Reproducibility of the model soot oxidation.....	48
Figure 3.14 BJH pore size distribution of Saffil ceramic fibers	53
Figure 3.15 XRD patterns of Saffil CG ceramic fibres	54
Figure 3.16 XRD patterns of Saffil HX ceramic fibers	55
Figure 3.17 SEM micrographs of alumina supports	56
Figure 3.18 Concentration influence on the T ₅₀ -value	58
Figure 3.19 TEM micrograph of used model soot PrintexU	63
Figure 3.20 Schematic diagram of screening process.....	67
Figure 3.21 ecIRT image of soot oxidation of Co/La and Ce/La	69
Figure 3.22 Temperature T ₅₀ as a function of concentration of Co/La.....	70
Figure 3.23 Temperature T ₅₀ as a function of La ₅ Co ₉₅ O _x to soot ratio	71

Figure 3.24 ecIRT image of soot oxidation of Mn/Ce, Mn/La, and Mn/Ca.....	72
Figure 3.25 Temperature T_{50} as a funktion of concentration of Mn/Ca	73
Figure 3.26 ecIRT image of soot oxidation of Ce/Fe, Ce/Ag , and Ce/Zn.....	74
Figure 3.27 Temperature T_{50} as a function of concentration of Ce/Ag	75
Figure 3.28 Temperature T_{50} of $Pt_yCo_{95-y}La_5O_x$ and of $Pt_yMn_{95-y}Ca_5O_x$	76
Figure 3.29 Temperature T_{50} as a function of BET surface area.....	81
Figure 3.30 XRD patterns of $La_5Co_{95}O_x$	82
Figure 3.31 SEM micrographs of $La_5Co_{95}O_x$	83
Figure 3.32 SEM micrographs of $Pt_2La_5Co_{93}O_x$	84
Figure 3.33 XRD patterns of $Ca_5Mn_{95}O_x$	85
Figure 3.34 SEM micrographs of $Ca_5Mn_{95}O_x$	86
Figure 3.35 SEM micrographs of $Pt_{0.2}Ca_5Mn_{94.8}O_x$	87
Figure 4.1 Setup of IR thermography	90
Figure 4.2 Sectional view of the reactor and its gas line	92
Figure 4.3 The starting position of holesdrilled into the steel block	94
Figure 4.4 Setup of the automated soot coating system	96
Figure 4.5 Plot of soot conversion as a function of temperature	98
Figure 4.6 TG-DTA schematic	99
Figure 4.7 Tecan pipetting robot.....	100
Figure 7.1 Overview of SEM micrographs of $La_5Co_{95}O_x$	141
Figure 7.2 Overview of SEM micrographs of $Pt_2La_5Co_{93}O_x$	142
Figure 7.3 Overview of SEM micrographs of $Ca_5Mn_{95}O_x$	143
Figure 7.4 Overview of SEM micrographs of $Pt_{0.2}Ca_5Mn_{94.8}O_x$	144

List of table

Table 1.1 EU emission standards for diesel passenger cars	7
Table 3.1 Comparison of features of different synthesis procedures	42
Table 3.2 Comparison of activity order of catalysts	49
Table 3.3 BET surface area and pore size distribution of alumina supports	52
Table 3.4 Temperature T_{50} of model soot and alumina fibers	57
Table 3.5 Elemental analysis of 0.2 molar stock solutions.....	59
Table 3.6 Elemental analysis of 0.55 molar $Pt_5K_{10}Ce_{85}O_x$ catalyst composition	60
Table 3.7 BET surface area and primary particle diameter of model soot PrintexU.....	62
Table 3.8 Elemental analysis of model soot PrintexU and of diesel engine soot.....	63
Table 3.9 Combination of base element with selected secondary element	68
Table 3.10 Temperature T_{50} at different catalyst to soot ratios	70
Table 3.11 BET surface area of freshly prepared and treated catalysts.....	79
Table 3.12 Temperature T_{50} of freshly prepared and treated catalysts.....	80
Table 7.1 Precursor used for sol-gel and impregnation approach	136
Table 7.2 Polymers used for paste approach	136
Table 7.3 Metal oxide powders used for paste approach.....	137
Table 7.4 Composition of polymers for CeO_2 paste.....	137
Table 7.5 Composition of polymers for V_2O_5 paste	137
Table 7.6 Composition of polymers for MoO_3 paste.....	137
Table 7.7 Composition of $Pt_yK_zCe_{100-y-z}O_x$ compound	138
Table 7.8 Binary composition.....	139
Table 7.9 Composition of doped binary compound	140

7. Appendix

7.1 Nomenclature

Abbreviations

BET	Brunauer-Emmet-Teller
BJH	Barrett-Joyner-Halenda
CAA	Clean Air Act
CCD	Charge Coupled Device
CEM	Controlled Evaporation and Mixing
CG	Catalytic Grade
CP-MS	Cone Plate Measurement System
DOC	Diesel Oxidation Catalyst
DoE	Design of Experiments
DPF	Diesel Particulate Filter
DPM	Diesel Particulate Matter
ecIRT	emissivity corrected Infrared Thermography
EDS	Energy Dispersive Spectroscopy
EGR	Exhaust Gas Recirculation
EU	European Union
FPA	Focal Plane Array
FPS	frames per Second
GC	Gas Chromatography GPIB General Purpose Interface Bus
HTE	High Throughput Experiments
HTT	High Throughput Technology
ICP-OES	Inductively Coupled Plasma Optical Emission Spectrometry
IP	Injection Pressure
IR	Infrared
LVE	Linear Viscoelastic
MPS	Multi Purpose Software
MWIR	Middle Wavelength Infrared

NIOSCH	National Institute for Occupational Safety and Health
OSC	Oxygen Storage Capacity
PAH	Polycyclic Aromatic Hydrocarbons
PCM	Polymerizable-Complex Method
PM	Particulate Matter
ROI	Region of Interest
SCR ₁	Selective Catalytic Reduction
SCR ₂	Shear Controlled Rate
SEM	Scanning Electron Microscopy
SF	Solid Fraction
SOF	Soluble Organic Fraction
TEM	Transmission Electron Microscopy
TEOS	Tetraethyl Orthosilicate
TGA	Thermogravimetric Analyses
TG-DTA	Thermogravimetric and Differential Thermal Analysis
TOF-MS	Time-of-Flight Mass Spectrometer
TPO	Temperature Programmed Oxidation
TWC	Three Way Catalyst
UPA	Ultra Fine Particle Analyzer
XRD	X-Ray Diffractometer

7.2 Chemical list

Table 7.1 Precursor used for sol-gel and impregnation approach

Chemical	Purity (%)	Supplier
Calcium nitrate tetrahydrate	99	Merck
Cerium (III) nitrate hexahydrate	99.80	Fluka
Cobalt (II) nitrate hexahydrate	99	Merck
Hafnium (IV) chlorid	98	Aldrich
Iron (III) nitrate nonahydrate	98	Fluka
Lanthanum nitrate hexahydrate	99.0	Fluka
Manganese (II) nitrate tetrahydrate	97	Merck
Molybdenum (V) isopropoxide	99	Alfa Aesar
Platinum (II) nitrate	57.74	ChemPUR
Potassium nitrate	99.5	Fluka
Silver nitrate	99.8	Merck
Strontium nitrate	99.97	Alfa Aesar
Zinc nitrate hexahydrate	99.0	Fluka

Table 7.2 Polymers used for paste approach

Chemical	Purity (%)	Supplier
α -Terpineol	98	Merck
Benzyl alcohol	99.5	Merck
Dibutyl sebacate	95	Fluka
Diethylene glycol monobutyl ether	99.2	Aldrich
Ethylcellulose 7N and 22N	-	Hercules Doel B.D.
Glycerol anhydrous 1.26	pure	Merck
Polyvinylbutyral BL-1	-	Sekisui
2-Propanol	99.8	Merck

Table 7.3 Metal oxide powders used for paste approach

Chemical	Purity (%)	Supplier
Cerium (IV) oxide	99.9	ChemPUR
Lanthanum oxide	99.9	ChemPUR
Molybdenum (VI) oxide	99.5	Merck
Vanadium (V) oxide	99.9	ChemPUR

7.3 Compound composition

Table 7.4 Composition of polymers for CeO₂ paste

Substance	Description	Amount (wt%)
Polyvinylbutyral BL-1	binder	20.5
Dibutyl sebacate	softener	10.25
Diethylene glycol monobutyl ether	solvent	69.25
2-propanol	solvent	50

Table 7.5 Composition of polymers for V₂O₅ paste

Substance	Description	Amount (wt%)
Ethylcellulose N 7	binder	5
Benzyl alkohol	softener	2.8
α -terpineol	solvent	92.2

Table 7.6 Composition of polymers for MoO₃ paste

Substance	Description	Amount (wt%)
Ethylcellulose N 22	binder	5
Benzylalkohol	softener	1.4
Diethylene glycol monobutyl ether	solvent	96.1

Table 7.7 Composition of $\text{Pt}_y\text{K}_z\text{Ce}_{100-y-z}\text{O}_x$ compound

Sample order	Pt (mol%)	K (mol%)	Ce (mol%)
1	0	5	95
2	0	10	90
3	0	15	85
4	0	20	80
5	5	0	95
6	5	5	90
7	5	10	85
8	5	15	80
9	5	20	75
10	10	0	90
11	10	5	85
12	10	10	80
13	10	15	75
14	10	20	70
15	15	0	85
16	15	5	80
17	15	10	75
18	15	15	70
19	15	20	65
20	20	0	80
21	20	5	75
22	20	10	70
23	20	15	65
24	20	20	60

Table 7.8 Binary composition

Sample order	A (mol%)	B (mol%)
1	5	95
2	10	90
3	15	85
4	20	80
5	25	75
6	30	70
7	35	65
8	40	60
9	45	55
10	50	50
11	55	45
12	60	40
13	65	35
14	70	30
15	75	25
16	80	20
17	85	15
18	90	10
19	95	5

Table 7.9 Composition of doped binary compound

Sample order	A (mol%)	B (mol%)	Pt (mol%)
1	94.8	5	0.2
2	94.6	5	0.4
3	94.4	5	0.6
4	94.2	5	0.8
5	94	5	1
6	93.8	5	1.2
7	93.6	5	1.4
8	93.4	5	1.6
9	93.2	5	1.8
10	93	5	2

7.4 SEM micrographs

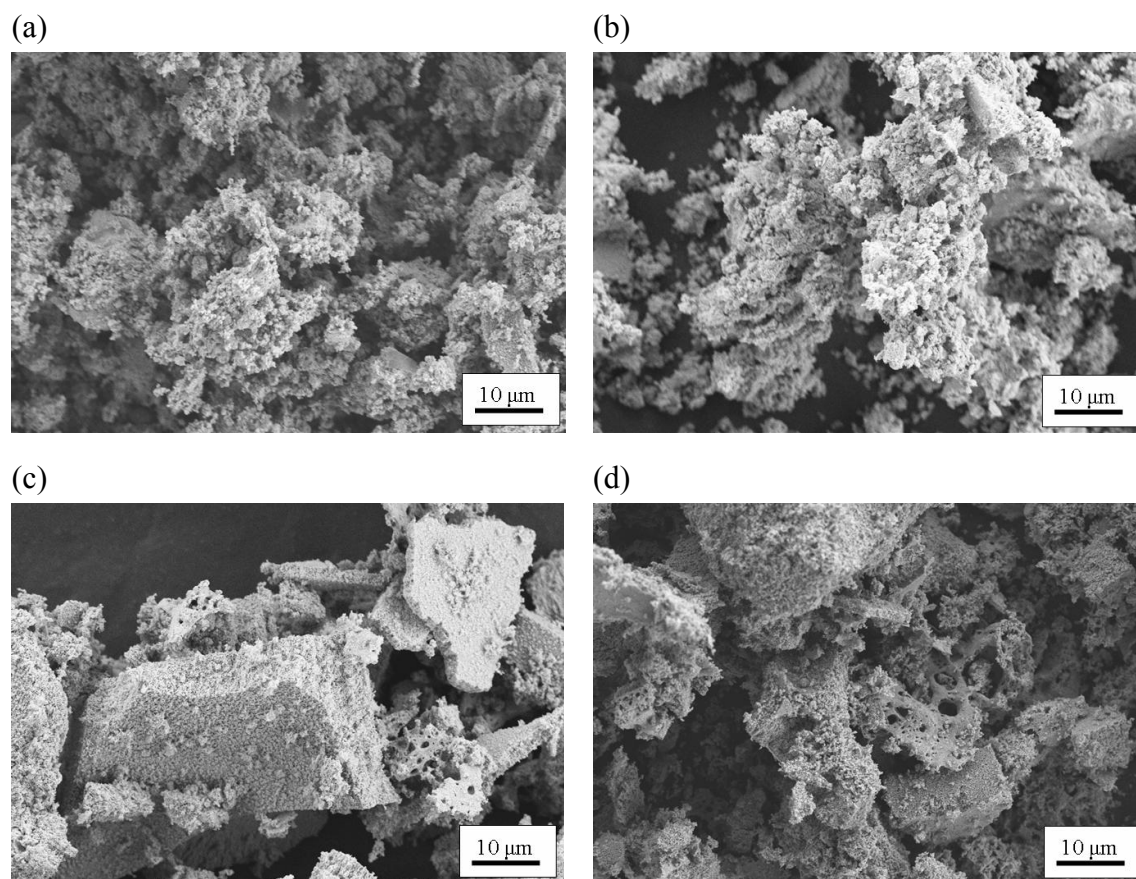


Figure 7.1 Overview of SEM micrographs of $\text{La}_5\text{Co}_{95}\text{O}_x$; freshly prepared (a), thermal (b), hydrothermal (c), hydrothermal & SO_2/NO_2 treated (d)

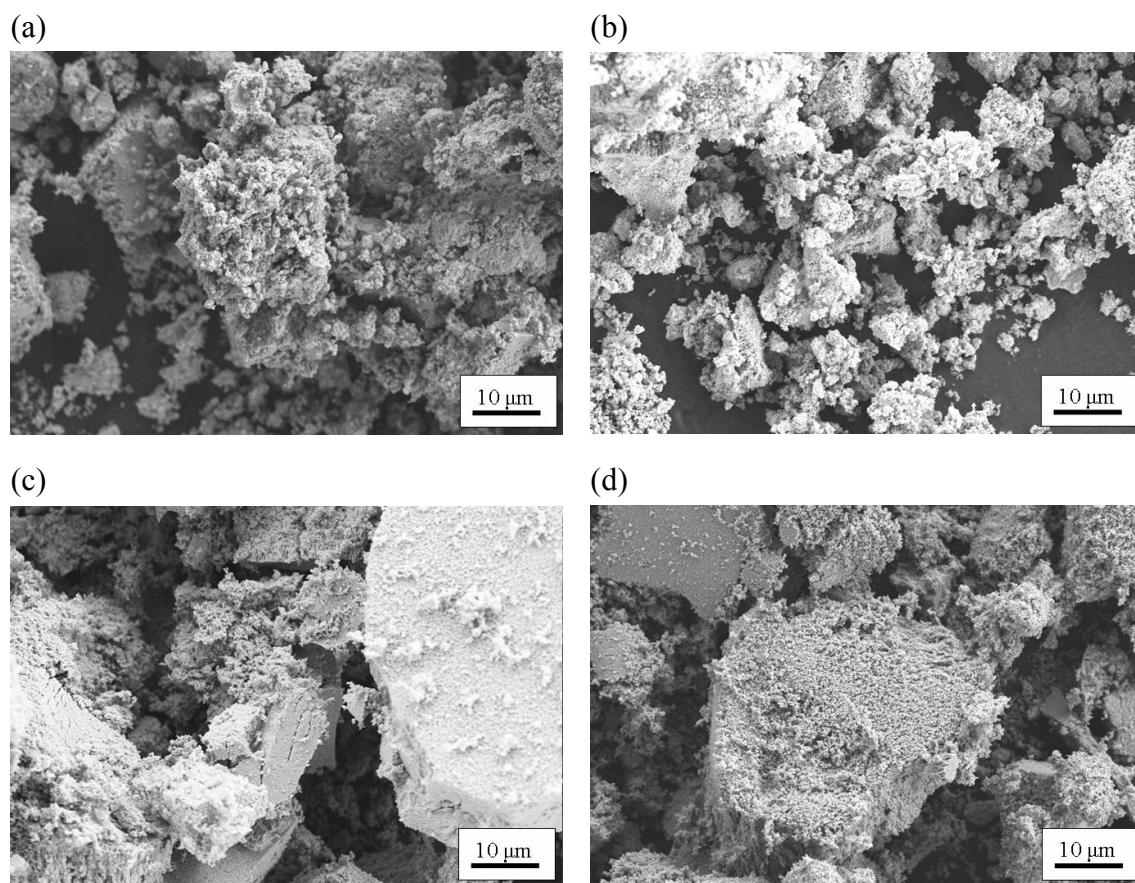


Figure 7.2 Overview of SEM micrographs of $\text{Pt}_2\text{La}_5\text{Co}_{93}\text{O}_x$; freshly prepared (a), thermal (b), hydrothermal (c), hydrothermal & SO_2/NO_2 treated (d)

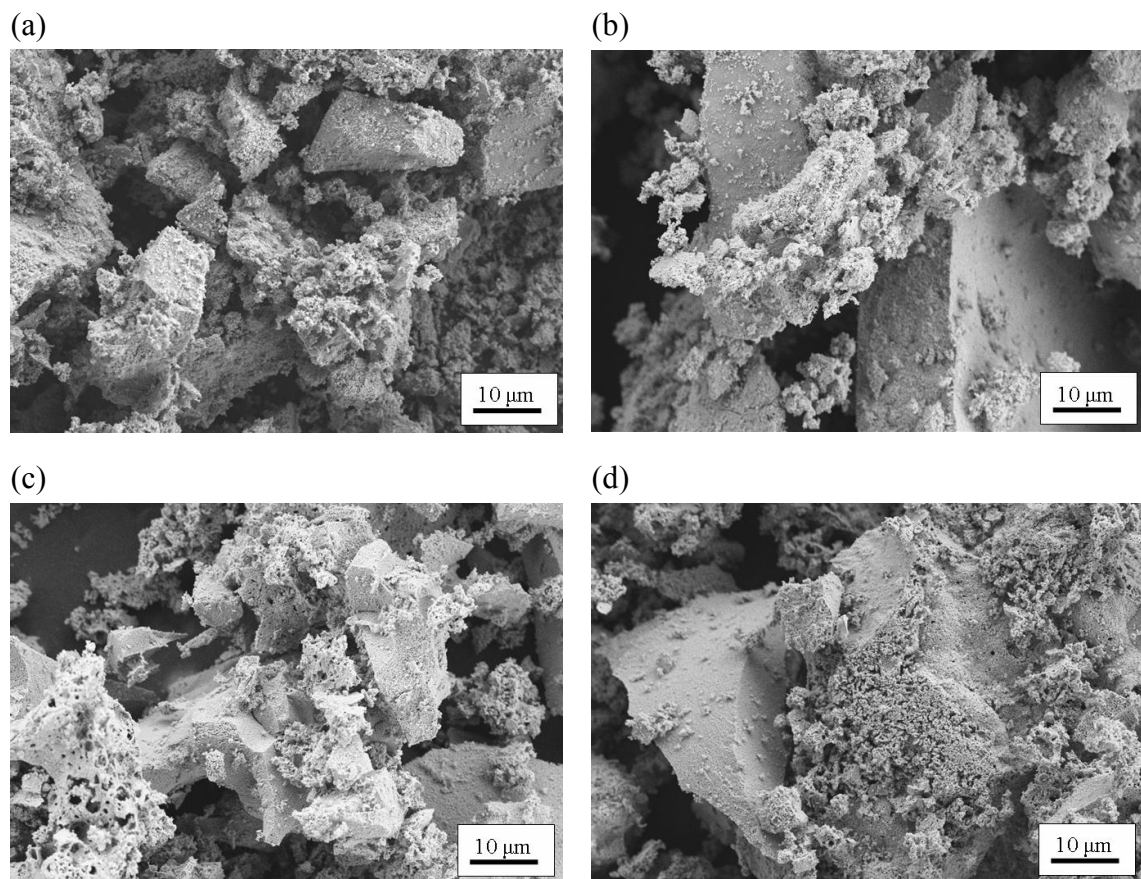


Figure 7.3 Overview of SEM micrographs of $\text{Ca}_5\text{Mn}_{95}\text{O}_x$; freshly prepared (a), thermal (b), hydrothermal (c), hydrothermal & SO_2/NO_2 treated (d)

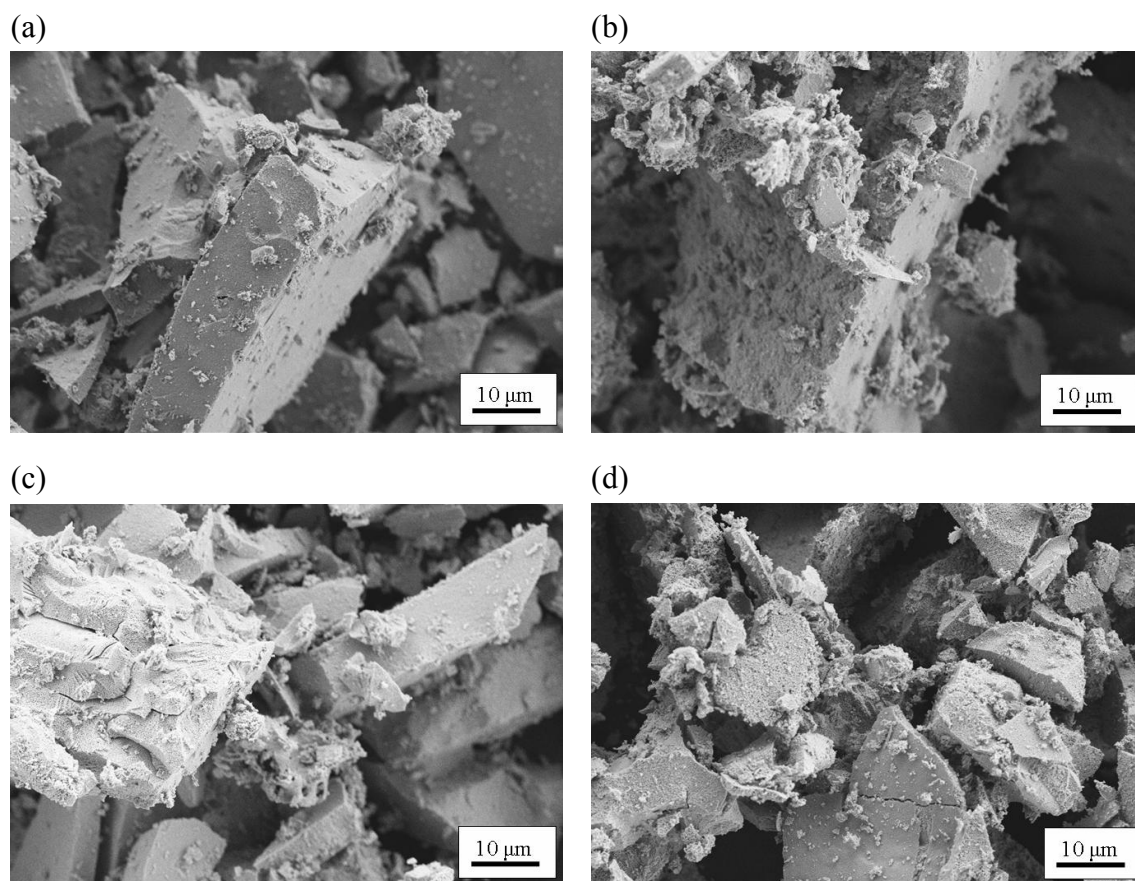


Figure 7.4 Overview of SEM micrographs of $\text{Pt}_{0.2}\text{Ca}_5\text{Mn}_{94.8}\text{O}_x$; freshly prepared (a), thermal (b), hydrothermal (c), hydrothermal & SO_2/NO_2 treated (d)